

Microwave Electronics

**NON-METALLIC CONDUCTORS IN
ANTENNAS AND ABSORBERS FOR
WIDEBAND MICROWAVE
APPLICATIONS**

Thesis submitted by

PAULBERT THOMAS

in partial fulfilment of the requirements

for the award of the degree of

DOCTOR OF PHILOSOPHY

Under the guidance of

Prof. C. K. AANANDAN



Department of Electronics
Faculty of Technology
Cochin University of Science and Technology
Cochin - 682 022, Kerala, India

September 2019

**NON-METALLIC CONDUCTORS IN ANTENNAS AND
ABSORBERS FOR WIDEBAND MICROWAVE
APPLICATIONS**

Ph.D. Thesis under the Faculty of Technology

Author:

PAULBERT THOMAS

Register Number: 3721

Department of Electronics

Cochin University of Science and Technology

Cochin - 682 022, Kerala, India.

Email: paulbertthomas@gmail.com

Supervisor:

Dr. C. K. Aanandan

Emeritus Professor

Department of Electronics

Cochin University of Science and Technology

Cochin - 682 022, Kerala, India.

Email:aanandan@gmail.com

Department of Electronics

Cochin University of Science and Technology

Cochin - 682 022, Kerala, India.

www.doe.cusat.edu

September 2019

NON-METALLIC CONDUCTORS IN ANTENNAS AND ABSORBERS FOR
WIDEBAND MICROWAVE APPLICATIONS

PAULBERT THOMAS

September 25, 2019

Dedication

”What is needed is the scientific approach, the adventurous and yet critical temper of science, the search for truth and new knowledge, the refusal to accept anything without testing and trial, the capacity to change previous conclusions in the face of new evidence, the reliance on observed fact and not on pre-conceived theory, the hard discipline of the mind—all this is necessary, not merely for the application of science but for life itself and the solution of its many problems.”

-Jawaharlal Nehru, *The Discovery of India*, p.512, 1946

Dedicated to those who wish to develop scientific temper, humanism and the spirit of inquiry and reform.

Declaration

I hereby declare that the work presented in the thesis entitled “Non-metallic conductors in antennas and absorbers for wideband microwave applications” is a bonafide record of the research work done by me under the supervision of Prof.C.K.Aanandan, Department of Electronics, Cochin University of Science and Technology, India and that no part thereof has been presented for the award of any other degree.

Kochi - 22
September 25, 2019

Paulbert Thomas

Certificate

Certified that this thesis entitled “Non-metallic conductors in antennas and absorbers for wideband microwave applications” is a bonafide record of the research work carried out by Mr. Paulbert Thomas (Reg.No: 3721) under my supervision in the Microwave Materials Research Laboratory, Department of Electronics, Cochin University of Science and Technology. The results presented in this thesis or part of it has not been presented for the award of any other degree. All the relevant corrections and modifications suggested by the audience during the pre-submission seminar and recommendations by the doctoral committee have been incorporated in this thesis.

Kochi-22
September 25, 2019

Prof.C.K.Aanandan
Dept. of Electronics
Cochin University of Science and Technology
Kochi, India-682022

Acknowledgements

It is my pleasure and honour to thank those whom I met along this journey which realized into this thesis. I would like to thank all the people who contributed in one way or another to the work described in this thesis.

First of all, I would like to thank my dear guide Prof. Aanandan C. K., who is more like a father to me, leaving me bread crumbs in front of my research and personal hurdles, motivating me and bear my faults for such a long period of time. I offer my sincere gratitude to you for keeping your belief in me through to the end. The fruitful discussions with him always helped me to be motivated and to present the research works as clearly as possible. It was a great privilege and honor to work and enjoy his friendship, empathy and considerations offered to me since my post graduation studies at CUSAT.

I started this work with the valuable inputs from Prof. Honey John, Inter University Centre for Nanomaterials and Devices (IUCND). I thank her for extending her helping hands in my work. I am thankful to Prof. P. Mohanan and Prof. K. Vasudevan for their motivational talks and inspiration. I also thank them for their care, advise and support rented throughout the research. The stage of microwave electronics built by them around the department percolates into every person, leading each researcher to a very good career in their field of research. I also thank Prof. James Kurian for providing the best research niche in the department. I am grateful to Prof. Supriya M. H. for her support, company and encouragements. She was the one who encouraged me to take up research shortly after my post graduation.

I thank Prof. K. G. Nair, former Head of the Department for setting up the full fledged microwave laboratories at Department of Electronics, which helped me to utilise the world class facilities for my research.

I thank all other faculty members of department of electronics Mr. Arun. A.

Balakrishnan, Mr. Mithun Haridas T. P, Dr. Bijoy. A. Jose, Dr. Deepti Das Krishna, Dr. Nalesh S., Dr. Tripti. S. Warriar and Mrs. Kumary V. Y. Vidhu for their moral support for my research.

I thank Prof. Jacob Philip, former Director of Sophisticated Test and Instrumentation Centre (STIC) and Prof. V. P. Namboothiri, Department of Photonics for the enlightening classes they delivered during my course work which aided as the walking stick for my research journey.

I thank all the non-teaching staff and technical staff at the Department of Electronics especially Mr. Siraj, Mr. Pradeep, Mr. Padmakumar, Ms. Anitha, Ms. Dhanya, Mr. Russel, Mr. Ibrahim Kutty and the staff at the department of electronics and the administrative section of CUSAT for their cooperation.

There are many faces whom I should thank for their valuable support and friendship. The long list starts with my brother, the one who gave me confidence and the sense of perseverance to not let down self esteem, my dearest Dr. Sreenath S. The current job that I enjoy itself is because of his motivation. Dr. Ullas G. K. is the one who lit up the field of microwave materials before me. The care and friendship he gave me is something that is longstanding. The void created by the absence of Sreenath was completely filled by my dear Neeraj K. P. He is a very good idea generator with whom I could discuss my research problems and life. Perhaps we feel like entangled souls when we start discussing on conducting polymers, for him I am the introducer and for me he is the teacher. There is no one like Nelson K. J. whose critical thinking and confidence has astonished me and even provoked me to rethink about my decisions. My labmate Lindo A. O. was a wonder as far as programming languages were concerned. We always shared a skill sharpening competition mind regarding programming where he was a guide to me. His unparalleled way of thoughts related to Physics has always been a surprise to me which I really miss now. Mr. Sooraj Kamal is a rare mutant of humanity whom I feel was born long before the humanity matured into a constructive coalesce. I was so fortunate to have my research period overlap with his. He is a multi talented reader and active researcher, who guides his fellow researchers to surprising vistas of knowledge without the show-off of his intellectual might. His influence lives through my classes and reaches out to my students and colleagues. Mr. Adrine Antony Correya is my sibling that I have been seeing since my

school days all through under-graduation, post-graduation and Ph.D., as a researcher with variant skill set and enthusiasm. Our imaginative talks related to waste management, agricultural products, and renewable energy were quite awesome. I thank him for proving that regardless of the current state, we can always look forward to the bright side of life. He is the motivation behind my musical part.

Mr. Tony D. was a selfless co-researcher whom I should thank for the doubt clearing sessions regarding anything through brainstorming, even when he was on fire. I was introduced to the field of UWB antennas by Dr. Gopikrishna M. who was always my violin companion in whatever music concerts we had during our time together. I am happy to thank the love and company offered by Dr. Deepti Das Krishna as a co-researcher. It was due to her extensive guidance and different line of thoughts that she shared which led to my first research publications. As a co-researcher, Mr. Cyriac M. O. was a pleasant and funny chatbot who had always something to tell which everyone could laugh upon. It was a great pleasure to have coffee breaks with him. A special thanks to my friend Mrs. Aparna A. S. for her friendship and thought-provoking discussions we had during her post graduation days, on topics like societal impacts of indian caste system on education, importance of science education and rationalist notions of life.

The list never ends and I am indebted to the help and support I received from Mrs. Libimol V. A., Mr. Satheesh, Dr. Nishamol M.S., Dr. Sarin V. P., Dr. Ashkarali P., Dr. Bybi P. C., Dr. Gijo Augustine, Dr. Shameena V. A., Dr. Sujith R., Dr. Jitha B., Dr. Aju John, Dr. Dinesh R., Mr. Abhilash A. P., Mrs. Anju P. M., Dr. Sreejith M. N., Dr. Nijas C. M., Mrs. Sreekala P. S., Mrs. Roshna T. K., Dr. Deepak Unnimadhavan, Mr. Vinesh P.V, Mr. Vivek R., Ms. Sruthi D., Mr. Manoj, Ms. Vinisha C. V., Mr. Aji, Mr. Midhun, Mr. Prasanth P. P. and Mr. Athul.

I thank the University Grants Commission (UGC), Govt. of India for the financial support under Maulana Azad National Fellowship for Minority Students Scheme. I also thank Sophisticated Test and Instrumentation Centre (STIC), Kochi for the support I received on account of material characterization. Words are not enough to thank Dr. Shibu M. Eapen of STIC for the suggestions and friendship I received from him.

My sincere love and wishes to Mr. Denny of Denny signs and Mr. Alex of

Signplus towards a successful business. Without their selfless support for this research, I wouldn't have done it in this manner. Their technical expertise in laser etching and plastic patterning has so much value in this research. I thank Mr. Vinodh at V-Track for being there for PCB fabrication support.

I extend my gratitude towards Cochin Education Society, my colleagues and students at The Cochin College for their love and support. I am in love with my colleagues Dr. Uma S. and Mr. Renjith S., who have been the best part of my life since we met. Their love, constant motivation and strategies were helping me at times when I felt alone. Above all, our trinity league has always been a source of energy, redemption, joy and liveliness to the otherwise dull life of mine. I am so happy to spend the wonderful times ahead with these two beautiful personalities.

I wish to place on record my gratitude to my teachers, mentors and my friends at all stages of my education.

I thank my wife, Neelima, who always supports me in research and in life. It was her support and her complementing character that made it possible to buy more time for research without losing my space in family. Never had I thought of the immeasurable joy of being the father of my son Neil and my daughter Nadine which later on became the driving force towards the successful completion of this work in time. It was the long standing dream of my father Thomas K. P. and my mother Daisy K. T. to see this thesis in real, whom I thank for the support I am receiving since my birth. A special thanks to my sister Livia who was always there beside me as a good friend with a different perspective on the problems faced by me. I am really glad to see her kids - Chris and Christal growing right in front of me under my love and care.

Finally, I would like to thank everybody who was important to the successful realization of this thesis, as well as expressing my apology that I could not mention personally one by one.

Paulbert Thomas

List of Figures

1.1	Classification of non-metallic conductors	4
1.2	Conductivity scaling of different non-metallic conductors . . .	7
1.3	Franck condon excitation diagram of intrinsically conducting polymers	9
1.4	The quasiparticles in conducting polymers	10
1.5	Charge transport types in conducting polymers	11
1.6	A model of HIS structure	15
1.7	An optically transparent microwave absorber (Courtesy: M. Grande, G. V. Bianco, M. A. Vincenti, D. De Ceglia, P. C Apezutto, V. P Etruzzelli, M. S Calora, G. B Runo, and A. D'Orazio)	16
1.8	A flexible UWB antenna (Courtesy: S. Jun, B. Sanz-Izquierdo and M. Summerfield)	17
2.1	Fumehood housing a distillation unit and magnetic stirrer . .	25
2.2	Vacuum filtration unit	27
2.3	Hydraulic pellet press	30
2.4	Two probe method to find sheet resistance	33
2.5	Four probe method to find sheet resistance	33
2.6	Impedance analyzer for low frequency dielectric estimation . .	34
2.7	XRD measurement setup	36
2.8	FTIR measurement setup	37
2.9	Vector network analyzer	38
2.10	Cavity perturbation measurement setup	40
2.11	NRW measurement setup	41
2.12	Pattern measurement setup	43
3.1	Different doping states of PANi	47

3.2	Polyaniline Powder	48
3.3	IUPAC specified route	50
3.4	Low frequency dielectric constant	51
3.5	Low frequency conductivity	52
3.6	Microwave frequency dielectric constant	53
3.7	Proposed synthesis routine	54
3.8	Microwave frequency conductivity	55
3.9	Microwave frequency skin depth	56
3.10	Experimental setup for the verification of measured microwave property	57
3.11	Simulated and measured return loss characteristics of the material	58
3.12	Comparison of return losses for the four samples	59
3.13	SEM images of samples (a) PANi-1, (b) PANi-2, (c) PANi-3, (d) PANi-4	61
3.14	Flake graphite	63
3.15	Highly oriented pyrolytic graphite	64
3.16	Amorphous graphite	65
3.17	Lump graphite	66
3.18	Synthetic graphite	67
3.19	Synthesis steps involved in expanded graphite preparation	73
3.20	FTIR graphs of a) GIC of Sulphate, b) expanded GIC of sulphate, c) GIC of Iron chloride, d) Flake Graphite, e) GIC of Zinc chloride, f) Graphene oxide	75
3.21	XRD graphs of a) GIC of Sulphate, b) expanded GIC of sulphate, c) GIC of Iron chloride, d) Flake Graphite, e) GIC of Zinc chloride, f) Graphene oxide	77
3.22	SEM micrographs of a) GIC of Sulphate, b) expanded GIC of sulphate, c) GIC of Iron chloride, d) Flake Graphite, e) GIC of Zinc chloride, f) Graphene oxide	79
3.23	Microwave complex permittivity of expanded GICs of Sulphate, Iron chloride and Zinc chloride at X band	80
3.24	Synthesis route of Polyaniline-Graphene composite	83
3.25	FTIR spectra of doped and dedoped samples of composite	85
3.26	XRD graph of doped and dedoped samples of composite	86

3.27	SEM images of the graphite, a) after and b) before PANi polymerization reaction	87
3.28	Low frequency complex permittivity of GPAN, GDPAN and NPAN	88
3.29	Microwave frequency complex permittivity of GPAN, GDPAN and NPAN at C band	90
3.30	Comparison of S parameters measured for pellet antenna and other forms	91
4.1	A salisbury screen	95
4.2	A jaumann absorber	96
4.3	A dallenbach absorber	97
4.4	A circuit analog absorber	97
4.5	A pyramidal absorber	98
4.6	A tapered loading absorber	98
4.7	A matching layer absorber	100
4.8	Measured reflection from salisbury screen using graphene sheets at different spacer thickness	102
4.9	Structure of proposed absorber unit cell	103
4.10	Fabricated prototype of the structure	104
4.11	Structure mounted for measurement at anechoic chamber	105
4.12	Measured and simulated reflection from the designed structure	106
4.13	The reflection from a continuous sheet of graded absorber	107
4.14	Mode to mode coupling	108
4.15	Variation of reflectance with layer conductivity	109
4.16	Variation of reflectance with structure thickness	110
4.17	Variation of reflectance with square pellet width	111
4.18	Variation of reflectance with unit cell periodicity	111
4.19	Reflectance variation of TE modes with incident angle	112
4.20	Reflectance variation of TM modes with incident angle	113
4.21	Reflectance variation of TE and TM modes at 11 GHz	113
4.22	Power loss density distribution of the structure at (a)TM-8GHz, (b)TM-11GHz, (c)TM-14GHz, (d)TE-8GHz, (e)TE-11GHz, (f)TE-14GHz	114

4.23	E-field distribution of the structure at (a)TM-8GHz, (b)TM-11GHz, (c)TM-14GHz, (d)TE-8GHz, (e)TE-11GHz, (f)TE-14GHz	114
4.24	H-field distribution of the structure at (a)TM-8GHz, (b)TM-11GHz, (c)TM-14GHz, (d)TE-8GHz, (e)TE-11GHz, (f)TE-14GHz	115
4.25	Surface current distribution on the target at 11GHz	116
4.26	RCS Vertical polarization at 11GHz	116
4.27	RCS Horizontal polarization at 11GHz	117
5.1	Design of the proposed antenna	122
5.2	Measured and simulated S_{11}	123
5.3	Electric field (intensity) and surface current (vector) distributions (dark shade indicates high field intensity) at the three resonances:(a) 3.0 GHz, (b) 5.0 GHz, and (c) 7.0 GHz	123
5.4	Radiation patterns at three resonances	125
5.5	Measured gain of the antenna	126
5.6	Design of the proposed antenna	127
5.7	Measured and simulated S_{11}	128
5.8	Improvement in S parameter by beveling	128
5.9	Improvement in S parameter by impedance transformer	129
5.10	Radiation patterns at three resonances	130
5.11	Gain and efficiency of the antenna	131
5.12	Structure of the proposed antenna with notch	133
5.13	S_{11} of the antenna with and without notch action	134
5.14	Surface current distribution on the antenna	135
5.15	VSWR of the antenna for straight notch and for bend notch	136
5.16	Gain of the antenna with notch on and with notch off states	138
5.17	Radiation pattern at three frequencies	138
5.18	Graphene antenna patterned on PMMA substrate	139
5.19	Graphene based antenna	140
5.20	Comparison of measured return loss of copper-based and graphene-based antennas on FR4 substrate.	141
5.21	Comparison of simulated and measured return loss of graphene-based antenna on PMMA substrate.	142

5.22 Comparison of gain of graphene-based and copper-based antenna on FR4 substrate.	142
5.23 Gain and efficiency	143
5.24 Radiation patterns at three resonances	144

List of Tables

1.1	The microwave frequency bands as per IEEE radar bands . . .	13
3.1	DC conductivity of the synthesized expanded GICs	73
4.1	Comparison of structure thickness in terms of wavelengths . .	109
5.1	Optimized parameter values of the design	124
5.2	Optimized parameter values of the design	131
5.3	Optimized parameter values of the design	137
5.4	Optimized parameter values of the design	145

Contents

List of Figures	xvii
List of Tables	xix
1 Introduction	1
1.1 Rationale behind the study	2
1.2 Material science	3
1.2.1 Synthetic conductors	4
1.2.2 A brief history of conducting polymers	5
1.2.3 Charge transport in conducting polymers	6
1.3 Electromagnetics	12
1.3.1 RADAR technology and countermeasures	13
1.3.2 Ultra wideband communication	16
1.4 Motivation behind the present work	19
1.4.1 Objectives of this study	20
1.5 Organization of the thesis	21
2 Methodology	23
2.1 Synthesis	24
2.1.1 Fumehood	24
2.1.2 Distillation setup	25
2.1.3 Stirrer	26
2.1.4 Ultrasonicator	26
2.1.5 Filtration setup	27
2.1.6 Oven	28
2.1.7 Hydraulic pellet press	29
2.1.8 PCB fabrication	29

2.1.9	Laser patterning setup	31
2.2	Characterization	32
2.2.1	DC conductivity measurement	32
2.2.2	Impedance analysis	34
2.2.3	X-ray diffractometry	36
2.2.4	Fourier transform infrared spectroscopy	37
2.2.5	Scanning electron microscopy	38
2.2.6	Vector network analyzer	38
2.3	Application design	41
2.3.1	Simulation softwares	42
2.3.2	Automatic pattern measurement setup	42
3	Synthesis and characterization of non-metallic conductors	45
3.1	Polyaniline	46
3.1.1	Enhancements possible in PANi	47
3.1.2	Synthesis of Polyaniline via self stabilized dispersion polymerization in agitation free environment	49
3.1.3	Summary	60
3.2	Graphite and its derivatives	61
3.2.1	Graphite Intercalation Compounds	67
3.2.2	Exfoliated graphite	69
3.2.3	Synthesis and characterization of exfoliated graphite	70
3.2.4	Summary	80
3.3	Composites of Polyaniline and Graphite	81
3.3.1	Synthesis and characterization of PANi - graphene com- posite using gelatin as dispersion stabilizer	81
3.3.2	Summary	92
4	Printable non-resonant absorbers using polyaniline-graphene composites	93
4.1	Radar absorbers	94
4.2	Choice of absorbant material	100
4.3	Design of the proposed wideband non-resonant absorber	105
4.4	Results and Discussions	107
4.4.1	Parametrics	109
4.4.2	Angular variation	110

4.4.3	Field distribution and Power loss	112
4.4.4	Bistatic RCS analysis	115
4.5	Conclusion	117
5	Printable antennas based on graphite derivatives	119
5.1	UWB communication and antennas	120
5.2	Design of compact pentagonal Ultra Wideband monopole antenna with microstrip feed	122
5.2.1	Antenna Geometry	124
5.2.2	Results and discussions	124
5.2.3	Summary	126
5.3	Design of compact planar UWB bevelled monopole antenna with CPW feed	127
5.3.1	Antenna Design and Evolution	127
5.3.2	Results and discussions	130
5.3.3	Summary	132
5.4	Design of CPW fed Band-notched Antenna for Portable UWB Applications	132
5.4.1	Antenna design and discussion	133
5.4.2	Results and discussions	134
5.4.3	Summary	138
5.5	Design of printable UWB antenna made of expanded graphite	139
5.5.1	Antenna design and discussion	140
5.5.2	Results and discussion	141
5.5.3	Summary	145
6	Conclusion and Future Scope	147
6.1	Highlights of the current work	148
6.2	Possible future works	150
	References	153
	List of publications	179
	Resume	180

Chapter 1

INTRODUCTION

This chapter describes an overview of synthetic conductors, the history of microwaves, radar technology and UWB antennas. The discussion starts with the introduction of synthetic conductors, their properties and applications. The need for microwave absorbers and the quest for their property enhancement is elucidated in the next session. This is shortly followed by a description of ultra wideband communication and the antennas that are used for it. The motivation towards the present research happens to be the application of synthetic conductors in the fields of wideband absorbers and antennas so as to introduce more robust features into it. The chapter concludes with a description about the organization of the thesis.

Contents

1.1	Rationale behind the study	2
1.2	Material science	3
1.2.1	Synthetic conductors	4
1.2.2	A brief history of conducting polymers	5
1.2.3	Charge transport in conducting polymers	6
1.3	Electromagnetics	12
1.3.1	RADAR technology and countermeasures	13
1.3.2	Ultra wideband communication	16

1.4	Motivation behind the present work	19
1.4.1	Objectives of this study	20
1.5	Organization of the thesis	21

1.1 Rationale behind the study

It has always been and will be the factor of ‘comfort’ that happens to be the driving force of all human development. The singular consciousness of improving the existing system for a better human experience has been working since we started inventing tools. The most stunning example of the impact of such discovery is fire - the alternative source of tamed energy which contributed to the reduction in metabolic energy expenses as required by uncooked raw food. It was from the time since fire, the energy requirements of a large brain was feasible by easing the energy load of the human body with cooked food, as described by the studies of the neuroscientist Dr. Suzana Herculano-Houzel[1].

According to the famous Israeli historian and writer Professor Yuval Noah Harari, the two distinctive features of humans considering other primates are the ability to work in large numbers towards the goal outlined by a common cause and to work with a flexible goal acquisition strategy[2]. These two features lay the baseline of all our innovations. Evidently, this can be witnessed during the world wars when large number of people worked on nationalist basis collectively together to design war strategies, technologies, deploying humanitarian aid etc. each of which demanded newer things in a way to provide comfort. Also we proved that we could radically alter our design strategies as like in the design of Christopher machine by Alan Turing to decipher secret U-boat strike coordinates vomited by the Enigma machines of the Nazi Government. What was evolving in parallel was our science, technology and society, although along that miserable time. The war became a culmination point of all the sciences, their applications and their effects.

It was during this time the discoveries and inventions of Heinrich Hertz, James Clerk Maxwell, Alexander Graham Bell, Jagadish Chandra Bose, Guglielmo Marconi and Claude Elwood Shannon, which were overlooked for a long while, came into picture[3, 4, 5]. It was the start of militarization of these discoveries related to Electromagnetics, Digital communication and Information

theory. The end of the war marked the commercialization of these technological marvels. The technological outcomes of the world war could be summarized into two - the advances in material science and the developments in electromagnetics. It also gave lessons on destructive powers of knowledge and the world nations went into consensus on the wise use of technology, deterrence towards rapid militarization and a need for monitoring such aggressive behaviour. The new world represented responsible military developments respecting each others sovereignty in the light of necessity of national defence. Although the wars between nations have subsided to military show-offs, each state is aware of the threat of terrorism and other post-war ideologies that have the potential to hinder human progress. It is in this context the necessity of research in military technology is justified.

1.2 Material science

Never have we achieved anything without the advancements in our knowledge in the field of material science. Each year newer states and materials are being discovered which start influencing our lives since their inception[6, 7]. The proof of advancements are evident from the remnants of stone age, bronze age, and all the way to the plastic age of modern times with each of these ages being named after the dominant material of use. The discovery of plastics revolutionarized not just the military, commerce and industry globally, but it even touched the lifestyle of every single common man who is least bothered of anything happening around [8]. It is an endless list of applications that plastics are giving us.

Although plastics are notorious for their environmental impact[9], it has grown into this situation just because of its immense applications and necessities in our daily life[10, 11, 12, 13]. Plastic pollution is not to be blamed on plastics, rather it is on our negligence and mismanagement in handling the waste generated from any newer technology. Down the line, we have not yet discovered a more wonderful and utilitarian material than plastics and banning plastics altogether without understanding its positive impact on us is like spitting upwards. Definitely, plastics and the associated technology are here to stay for good.

Until mid 20th century, plastics were considered as electrical insulators and their applications were tailored in that fashion. It was the discovery of

conducting polymers that proved that the next generation of plastics is yet to come - a handful list of polymers which exhibited electrical conductivity[14, 15].

1.2.1 Synthetic conductors

Non-metallic conductors or synthetic conductors are broad class of materials that are not metals but possess electrical conductivity [16, 17, 18, 19]. One reason for the grand success of silicon based technology was its facile planar process through which selective regions in a silicon substrate could be patterned into conducting, insulating or semiconducting regions thereby electrically modifying a single pure crystal of silicon[20]. Synthetic conductors take this to a few more steps further. Just like silicon, they are mostly semiconductors and their conductivity can be modified to suit specific applications. The advantage comes in the fact that they can be tailored as sensors, actuators and with their flexibility and potentials of integration on to conventional plastics, they can spawn a new race of devices and applications. Thus a synthetic conductor is a system which inherits the optical, electrical, electronic and magnetic properties of a metal/semiconductor alongside the mechanical properties and processibility of a polymer.

Synthetic conductors are basically classified into two - Carbon forms and Intrinsically conducting polymers (ICP) (Figure.1.1). Forms of carbon such as carbon nanotubes, graphene, that are electrically conducting belongs to the first group. The second group has polymers that have conjugated backbone. There is a wide list of intrinsically conducting polymers with their own properties. Polyacetylene[21], Polythiophene[22], PEDOT[23], Polypyrrole[24], Polyindoles[25], and Polyaniline[26] are a few promising conducting polymers.

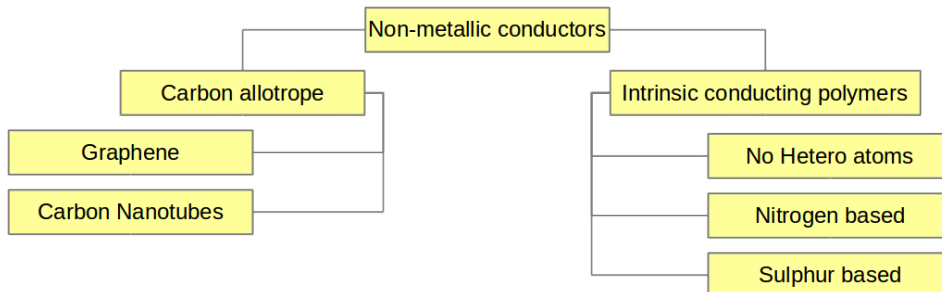


Figure 1.1: Classification of non-metallic conductors

1.2.2 A brief history of conducting polymers

Attempts to create synthetic conductors date back to 1891 when F. Goppelsroeder started synthesizing polyaniline[27]. A semiconducting form of Polyacetylene was first synthesized by Natta et.al in 1958 [28]. A theoretical study by Little indicated the possibility of superconductivity in polymers and put forth the model of a polyene chain with cyanine dye-like substituents. It was with the discovery of superconductivity in crystalline polysulfur nitride by IBM that the research focus on ICP strengthened. During 1974 a serendipity experiment mistakenly performed under Hideki Shirakawa's group produced a silvery thin film of Polyacetylene[21]. Despite its metallic appearance, it was not conducting until in 1977 Shirakawa, MacDiarmid and Heeger discovered that oxidation with chlorine, bromine and iodine vapours resulted in the enhancement of the conductivity of those silvery polyacetylene films by 10 orders of magnitude[29] as shown in the conductivity ladder of Figure.1.2. This procedure of treating polymers with halogens was called doping as analogous to the doping of semiconductors. The process of doping involves the partial addition (reduction) or removal (oxidation) of electrons to or from the π -conjugated system of the polymer backbone. The progress since then was astonishing in this field with Heeger reporting electrical conductivity around 3000 Scm^{-1} for iodine doped films[30]. For the discovery of these materials by Alan J Heeger, Alan G MacDiarmid and Hideki Shirakawa, they were jointly awarded the Nobel Prize in Chemistry in 2000 for their pioneering work related to the discovery and development of conductive polymers. Since then the focus on conducting polymers and other synthetic conductors have skyrocketed. As of now, by virtue of their exotic properties like,

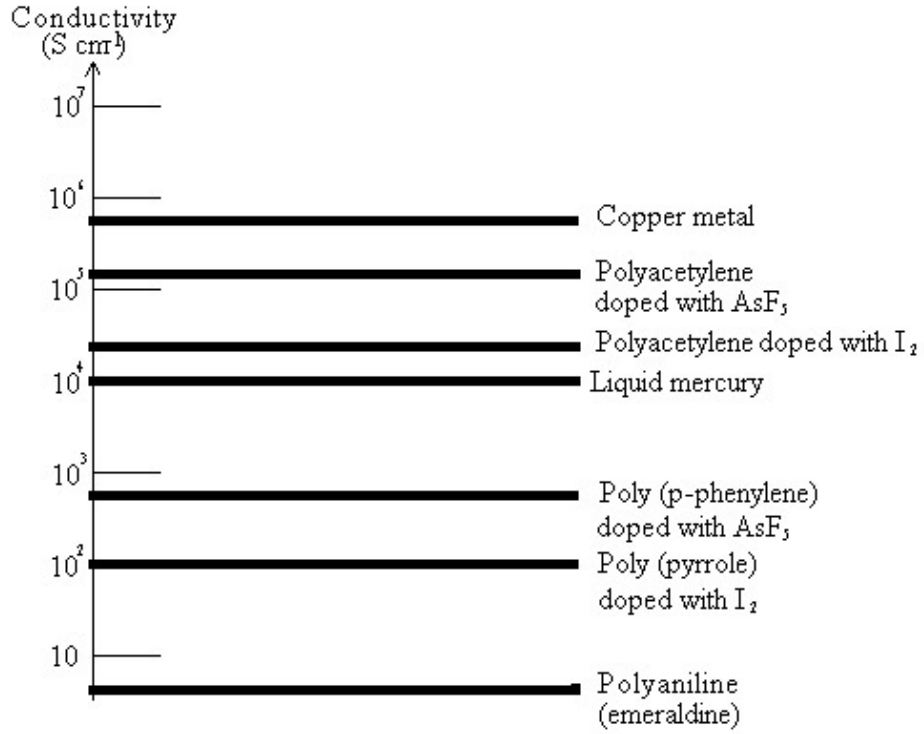
- Light weight[31]
- Corrosion resistance[32]
- Tunable flexibility[33]
- Tunable electrical properties[34, 35]
- Tunable optical properties[36, 37]
- Ease of preparation[15]
- Reversible doping[38, 39]

we have synthetic conductors establishing roles in fields such as,

- EMI shielding[40]
- ESD protection[41]
- Lithography[42]
- Microelectronics[43]
- Corrosion protection[44]
- Opto-electronics[45]
- Field effect transistors[46]
- High density energy storage[47]
- Energy harvesting system[48, 49]
- Display technology[50]
- Interconnection technology[51]
- Paper/plastic based electronics[52]
- Biomedical applications[53]
- Sensors[54, 55]
- High Tc superconductors[56]

1.2.3 Charge transport in conducting polymers

Unlike semiconductors and metals, the charge transport in these materials are not because of electrons and holes, but are mediated by quasiparticles. There are a quite number of views which suggest the formation of quasiparticles and their dynamics in regulating the charge transport in these synthetic conductors[57, 58, 59]. It is worth noting the structures of these materials to better understand their charge transport. Most conducting polymers were initially considered to be of fibrillar systems. But in fact they are like chain bead structures where the beads are of metallic conductivity[60]. These beads



Logarithmic conductivity ladder locating some metals and conducting polymers

Figure 1.2: Conductivity scaling of different non-metallic conductors

are about 9.6 nm in size and they have a core size of 8 nm which shows metal like transport[61]. It is surrounded by a 1.6 nm thick amorphous media of significantly lesser conductivity. The cores of these beads fundamentally behave like metal nanoparticles of the same size and their conductivities are to be modeled on the basis of quantum effects of the bead's size owing to the limited electron wavelengths that can be incorporated in such a small sized particle. The charge carriers are said to hop from one metallic grain to another by quantum tunneling[62]. Assuming that the electron hopping was dependent on the initial and final energy states between which hopping occurred, a Variable Range Hopping (VRH) model was proposed by Mott and coworkers[63]. VRH model predicts that the conductivity as expressed by

$$\sigma = \sigma_0 \exp\left(-\left(\frac{T_0}{T}\right)^{\frac{1}{n+1}}\right) \quad (1.1)$$

$$\text{where } T_0 = \frac{24}{\pi r_0^3 k N(E_f)} \sigma_0 = \frac{9}{4} \sqrt{\frac{3}{2} \pi e^2 \gamma_0} \sqrt{\frac{r_0 N(E_f)}{kT}}$$

n is the dimensionality of the material, r_0 is the localization length, k is the Boltzmann constant, γ_0 is the phonon vibration frequency, e is the electron charge, $N(E_f)$ is the density of states at the Fermi level, and T is the temperature.

Conductivity of any conducting polymer is based on three types of interactions [64, 65] as shown in Figure 1.5

- Intra chain transport

Intra chain conductivity is the intrinsic conductivity of a single polymer chain. It arises due to two reasons:

1. Conjugated backbone
2. Doping

The first reason is not enough for conductivity. It just paves the pathway for making the polymer conductive. The second one is the main contributor of conductivity. It is a process by which a charge is removed from the polymer chain or added to the polymer chain by doping agents. In the case of Polyaniline (PANi), both inorganic and organic acids are found to be the dopants. As mentioned above the process is reversible for PANi. This means that the lost charge or gained charge can be reverted back to its original state (the process of dedoping). Dedoping is done by exposure to bases like Ammonium Hydroxide. This is what is known as reversible doping and dedoping which doesn't have a dope/dedope cycle limit. That is the reason why PANi is used as corrosion resistant agent in paints for protecting metals. It is also the same thing which gives PANi based supercapacitors their 'Pseudo capacitance' alongside 'Electrical Double Layer capacitance'.

The process of doping induces not just charges on the conducting polymer backbone, it causes the polymer chain to have a structural distortion due to the presence of the newly introduced charges around their vicinity. In metals, the valence band and conduction band are separated by the band gap. But in polymers, it is Highest occupied Molecular Orbital (HOMO) and Lowest Unoccupied Molecular Orbital (LUMO) separated by band gap. This bandgap is reduced in the case of ionization of the polymer species by the process of doping. As shown in

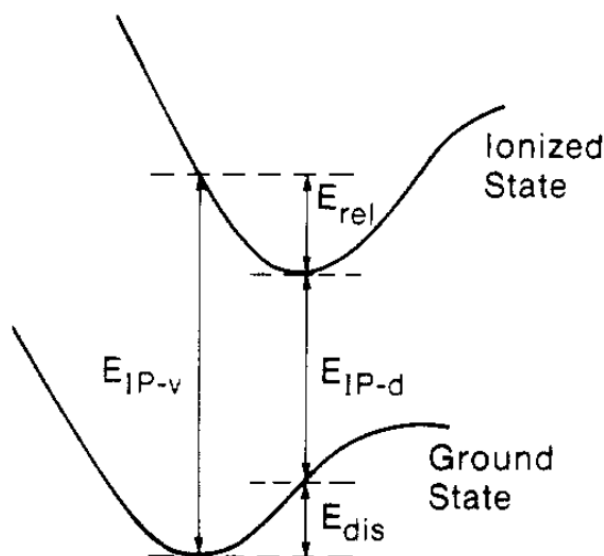


Figure 1.3: Franck condon excitation diagram of intrinsically conducting polymers

Figure 1.3, which is the Franck Condon excitation diagram[66, 67, 68] for conducting polymers, the transition from ground state to the excited state is followed by a relaxation by chain distortion to a new equilibrium position. These structural distortions are a byproduct of doping and when an electric field is applied to such a polymer chain, the charge moves along the chain which causes the distortion also moving[69]. So in the case of conducting polymers, it is not just an electron or a hole that is moving, it is the charge and the lattice distortion caused by it that is moving. Hence, such charge and associated lattice distortion are considered and treated together as a quasi particle. Hence the mobility and drift velocity of these are different than that in metals. The charge transport in conducting polymers is facilitated by quasiparticles like polarons ($\frac{1}{2}$ spin), bipolarons (Spinless) and solitons (Neutral- $\frac{1}{2}$ spin, Charged-Spinless) unlike electrons and holes in inorganic semiconductors. So the conduction mechanism is different as shown in Figure 1.4.

This distortion causes screening of the charge and the mobility is reduced. Consequently it effectively localizes the charge resulting in the formation of a polaron. A polaron is the quasiparticle indicating this phenomenon and consists of an electron/hole along with some phonons

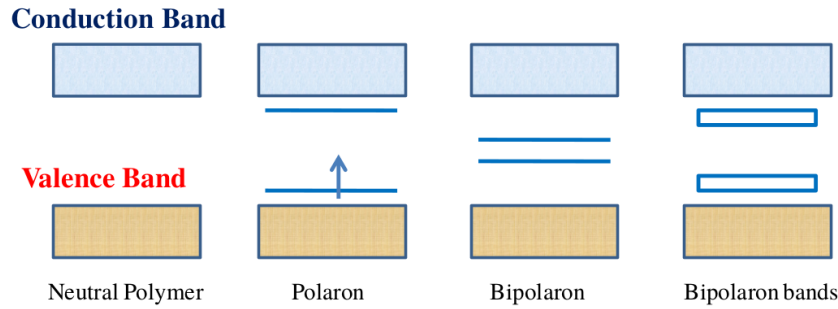


Figure 1.4: The quasiparticles in conducting polymers

manifested by a local structural distortion of the polymer. When further doped, more polarons are induced and they pair up to form bipolarons which are energetically more stable than two separate polarons in a chain. In this case of bipolaron formation, the distortion induced by both the polarons will be constructive and any deviation from this coalesce will be hindered. This means, they travel together or they are locked to each other. Systems like trans-polyacetylene, the ground state is split into two degenerate states of equal probability. Hence the bipolarons will decouple and travel in opposite directions. Each of these are considered as solitons because, they are solutions to a partial differential equation of a dispersive system with slight non-linearity. Thus the wavefunction of a soliton is spread over a long range and it has significant long range stability unlike others.

Thus there are two types of Intrinsically Conducting Polymers (ICP) – one with degenerate ground states (with solitons and polarons) like in polyacetylene and the other with non-degenerate ground states (with polarons and bipolarons) like in polyaniline. Degenerate ones have identical structures in ground state (like in the case of trans-transoid polyacetylene). Non-degenerate ones have non identical structures in the ground state (Benzenoid ring is having lesser energy when compared to quinoid ring as in the case of PANi).

- Inter chain transport

Interchain interactions of a conducting polymer are characterized by chain to chain transport of charges [70]. Although intrachain transport is

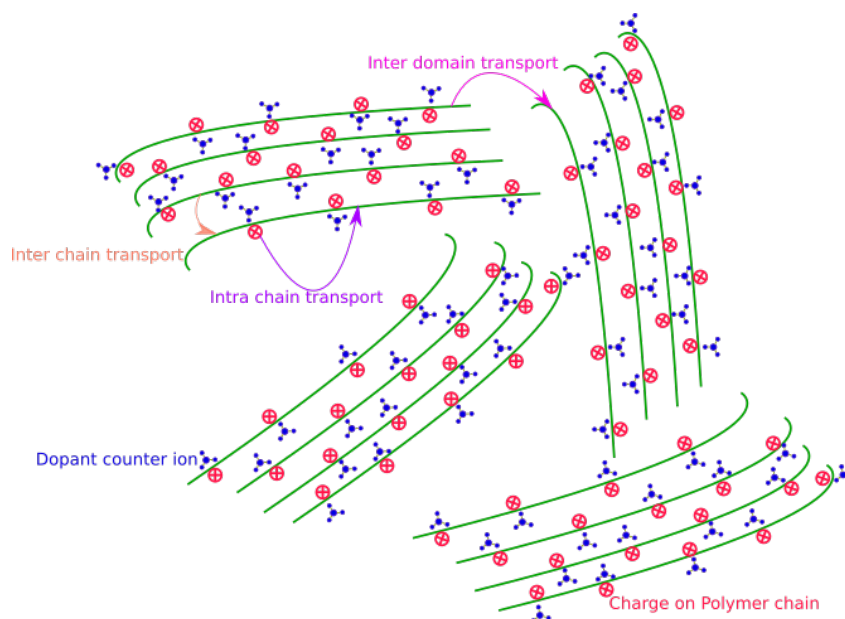


Figure 1.5: Charge transport types in conducting polymers

metallic in nature, the interchain transport is significantly lower because of the high potential wall existing between two adjacent PANi chains. The polarons in adjacent chains are said to hop from one to another with the help of activation energy required for the process being derived from phonons. As phonons are lattice vibrations, this should be viewed as a way of throwing polaron from one chain to another. A polaron reaching the potential barrier oscillates back and forth until it gains energy from the lattice vibrations. This waiting time is around 100 fs. After achieving the required energy, it jumps from one chain to another chain and still if it has sufficient energy, it continues moving in the influence of the external field through the second chain or else it oscillates at the start of the second chain until it obtains enough energy to drift through the chain.

The lowering of activation energy required for this process is a quite interesting phenomenon to be investigated as PANi is being proposed to be alterable by the introduction of ionizable groups at the nitrogen site or at rings leading to new properties without trading the conductivity[15]. Camphor Sulphonic Acid (CSA) doped PANi can be used in combination with solvents like m-cresol/chloroform to introduce conductivity

and solubility enhancement by conformational change through polymer chain uncoiling. In these systems, the entire combination acts as a poly-electrolyte and thereby the chain to chain electron transport can be enhanced significantly[71]. Basically it leads to intrachain and inter-chain ordering in amorphous PANi. It has also been found that metallic nature of conducting polymers results only when it is dispersed in a solution in which it can form three dimensional connected networks by virtue of self organization. Thus interchain interactions can give a lot of exotic properties like water dispersable forms, high conducting forms etc of PANi. The effects of counterions from dopants significantly influence the steric structure and the electron delocalization in the chain as well as between the chains.

- Inter domain transport

The term inter domain conductivity refers to domain regions in the bulk of the polymers between which the conduction takes place[65]. Each of these domains are characterized by similarly aligned conducting polymer chains. The inter domain charge transport suffers more scattering because of the higher potential wall between the domains than that in the case of inter chain interface.

1.3 Electromagnetics

An important milestone during the 20th century science and technology was the awareness of electromagnetic spectrum and the applications of each portion of the spectrum. The electromagnetic spectrum ranges from near DC to very high energy gamma rays. Radio waves, microwaves, millimeter waves, infrared spectrum, visible spectrum, UV rays, X-rays and gamma rays all belong to the same class of electromagnetic waves except that they differ in the amount of energy packed into their photon. Microwaves happen to be the most utilized portion of the electromagnetic spectrum owing to its radiative nature which can be used for both line of sight as well as through-the-wall communications. This is a range of frequencies lying between 300MHz to over 200GHz on the electromagnetic spectrum (Table.1.1). Microwaves are very safe when compared to higher frequency electromagnetic waves such as UV and X rays due to their non-ionizing nature. Hence they are also used in

Band designation	Frequency range (GHz)	Wavelength range (mm)
L	1-2	150-300
S	2-4	75.0-150.0
C	4-8	37.5-75.0
X	8-12	25.0-37.5
Ku	12-18	16.7-25.0
K	18-26.5	11.3-16.7
Ka	26.5-40	5.0-11.3
Q	33-50	6.0-9.0
U	40-60	5.0-7.5
V	50-75	4.0-6.0
W	75-110	2.7-4.0
F	90-110	2.1-3.3
D	110-170	1.8-2.7

Table 1.1: The microwave frequency bands as per IEEE radar bands

microwave imaging and treatment for medical applications. They are used for drying and heating applications. Almost all communication, guidance and navigation systems around the world rely on microwaves. Planetary scans, deep space communication and terrain mapping are based on microwave frequencies.

1.3.1 RADAR technology and countermeasures

One significant product of war was the birth of radio detection and ranging (RADAR) technology. This was a significant step in navigation as well as detection of territorial intrusion. Inevitably it was shortly followed by its counter measures demanded by sheer necessity of survival during the war. The area of radar cross-section (RCS) reduction is a hugely funded research problem after its advent. RCS is a measure of how much detectable a target is under radar surveillance. This detectability comes from the fact that a target when beamed with microwaves tend to reflect, absorb or scatter the incident microwave energy. This causes detectability of the target. Mathematically

RCS is defined as the ratio of reflected power per unit solid angle to the power incident on the target. It has a unit of area and it is expressed in decibel scale as dBsm.

$$\text{RCS, } \sigma = 4\pi \lim_{R \rightarrow \infty} R^2 \frac{|E_s|^2}{|E_i|^2} = 4\pi \lim_{R \rightarrow \infty} R^2 \frac{|H_s|^2}{|H_i|^2} \quad (1.2)$$

Where E_s , E_i are scattered and incident electric field intensities and H_s , H_i are scattered and incident magnetic fields. R is the distance between the detector and the target.

For any target inside a hostile territory, its RCS is detrimental to its own existence and hence reduction of RCS is very important. This is accomplished by reducing the reflected power in the direction of the detector. This can be done by passive methods or active method, the latter being a more expensive and complicated thing to do[72, 73]. Passive means of RCS reduction involves the target remodeling to avoid sharp edges and discontinuities that diffract microwave radiation back to the detector. It is also achieved by scattering the radiation into other angles that can make the target less detectable. Metallic flares can be discharged which can create ambiguity for the attacker to converge on the target which is another way to defy the incoming offense. A strongly adopted technique is the use of radar absorbing materials (RAM) approach. RAM are class of materials or engineered structures which can absorb microwave energy and make the target undetected. They use impedance matching technique to easily guide the incident radiation to an attenuator. An attenuator need not necessarily be a lumped segment, but a distributed effect all over the structure. It offers electric and magnetic losses to the incoming electromagnetic field.

Metamaterials

Metamaterials are artificially engineered materials which has a periodic arrangement of cells which act as engineered atoms in the frequency of interest[74, 75]. The periodicity acts as a crystal lattice and the theories (such as Drude model, Band theory) that explain metallic or semiconducting nature of materials holds for these engineered structures too[76]. Thus it opens up a way to engineer materials which have negative μ and/or ε apart from the naturally occurring materials with positive μ and ε . A special type of metamaterials known as high impedance surfaces (HIS) offers very high surface impedance

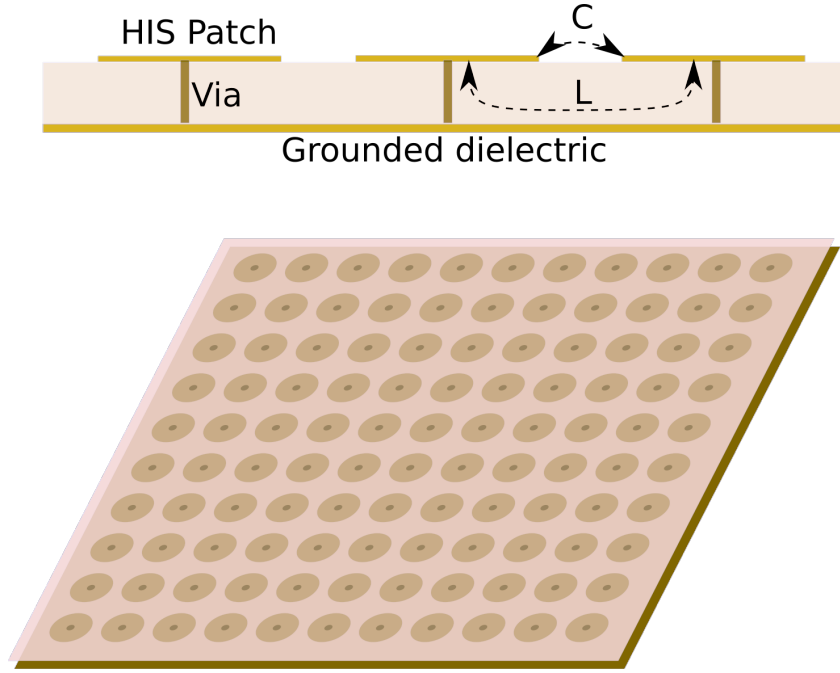


Figure 1.6: A model of HIS structure

to incident waves but induce zero phase shift at reflection. These are periodic array of metallic patches over a grounded dielectric connected to ground using vias (Figure.1.6). They are very good at suppressing surface modes propagating through the interface due to their high impedance. At these suppression frequencies, the capacitive (C) effects between the patches matches the inductive (L) effects of the vias resulting in a resonant condition where it offers high impedance. The impedance (Z) of these structures[77] is represented as

$$Z(\omega) = \frac{j\omega L}{1 - \left(\frac{\omega}{\omega_0}\right)^2} \quad (1.3)$$

$$\text{where the resonant frequency, } \omega_0 = \frac{1}{\sqrt{LC}} \quad (1.4)$$

When the thickness of the grounded dielectric is well below the quarter wavelength of frequency of interest, it acts as a distributed inductor as per equivalent circuit model. This inductance can come parallel to the capacitance of HIS patches patterned over the substrate to act as an artificial magnetic conductor (AMC) even in the absence of vias thereby reducing the complexity

of making HIS surfaces. HIS based structures can be modified to be used as microwave absorbers. If any part of the structure is made lossy, it can cause huge attenuation due to the intense current densities on these structures at resonance. This includes dielectric loss, patterned resistive layers, lumped resistors etc. All these advantages of metamaterials are practically viable when they are able to suit to the custom conformations of the target structures. This requires printable, transparent and/or flexible attributes into these absorber designs[78] (Figure.1.7).

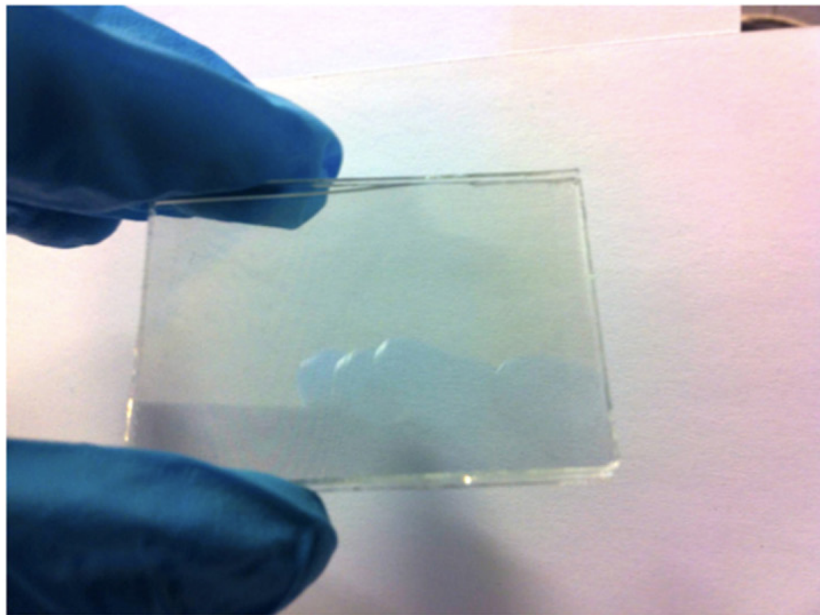


Figure 1.7: An optically transparent microwave absorber (Courtesy: M. Grande, G. V. Bianco, M. A. Vincenti, D. De Ceglia, P. C Apezuto, V. P Etruzzelli, M. S Calora, G. B Runo, and A. D’Orazio)

1.3.2 Ultra wideband communication

In 2002, the Federal Communications Commission (FCC) allocated a spectrum ranging from 3.1GHz to 10.6GHz for Ultra wideband (UWB) communication. This was the onset of UWB based technology for commercial high data rate, short-range communications and imaging systems. A UWB signal is characterized by a fractional bandwidth that is greater than 0.25.

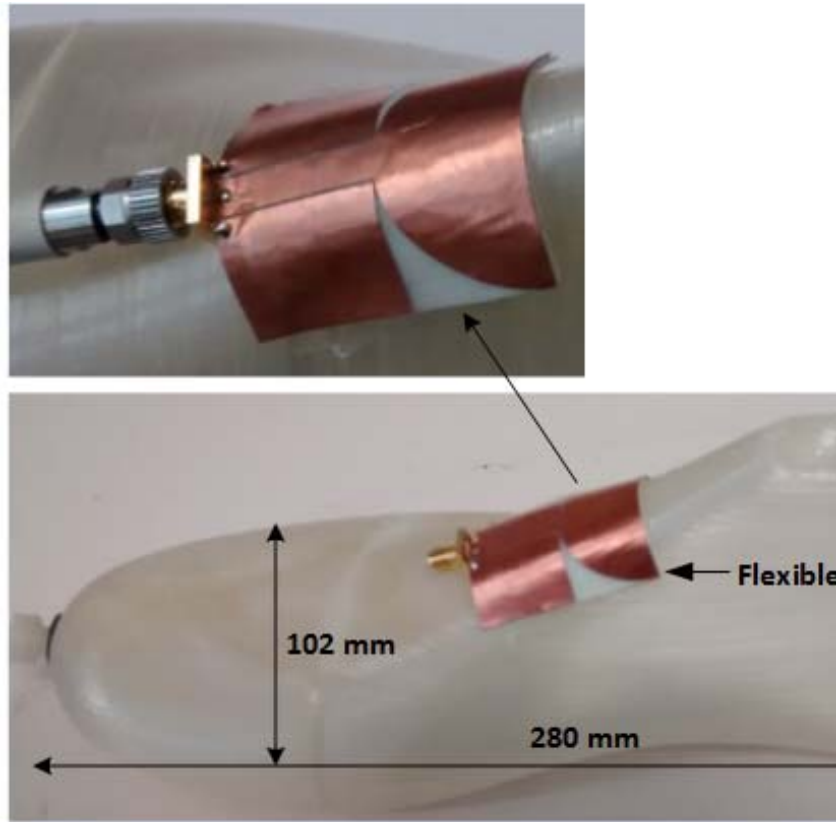


Figure 1.8: A flexible UWB antenna (Courtesy: S. Jun, B. Sanz-Izquierdo and M. Summerfield)

$$B_f = \frac{2(f_h - f_l)}{f_h + f_l} \quad (1.5)$$

The benefits of UWB stems from its wide bandwidth. As per Shannon's theorem[79] on channel capacity ,

$$C = B \cdot \log_2 \left(1 + \frac{S}{N} \right) \quad (1.6)$$

where B is the bandwidth, S and N being signal power and noise power respectively. This means if UWB has more bandwidth, instead of increasing the signal to noise ratio (SNR), by virtue of its wide bandwidth it can deliver the same bit rate well at lower SNR when compared to other narrowband systems.

Therefore the virtue list include high-speed data transfers, large volume audio/video streaming and much more in the consumer electronics sector. The UWB systems were regulated to provide a data speed of 50Mbps through buildings within a range of at least 20m, as well as higher rates (up to 1Gbps) at shorter distances and as a consequence the power demands on UWB circuits were very less even to achieve these fast data rates. This amounts to around one tenth to one hundredth of the power required by other existent wireless devices such as mobile telephones and WLANs for the equivalent data rates, thus making UWB ideal for battery-powered devices.

The power spectral density (PSD), which is a measure of power per bandwidth is so low for UWB since the wide bandwidth and emission power restrictions. Hence UWB emission is much safer in scales of radiation exposure.

$$PSD = \frac{P}{B} \quad (1.7)$$

where P is power expressed in watts, B is bandwidth in hertz. UWB signals are capable of surpassing physical obstacles and hence through the wall communication is possible. This opens up another possibility of UWB ground penetrating radars.

Antennas for UWB

Native method that UWB communication uses are short pulses that occupy the entire spectrum to represent binary data rather than using a carrier for transmission[80]. A yet another scheme is to use multiple bands to communicate which uses a separate carrier modulation for each. Antennas for UWB communication are designed to accommodate both type of signalling schemes, with the former one being the most difficult as it uses entire bandwidth[81]. For portable devices, the demands are high as the structural dimensions for such applications should be as compact as possible. This has the advantage of reduced pulse spreading owing to smaller structures having proximal phase centers for the entire band. Hence for such cases electrically small antennas stand good for transmitting nano second pulses without distortion. A design of electrically small impedance transforming antennas have the advantage of reduced surface current densities due to the presence of travelling waves alongside the absence of sharp resonances associated with standing waves. There is

a recent trend towards the design of such antennas on flexible substrates for applications like BAN and medical monitoring networks (Figure.1.8).

1.4 Motivation behind the present work

The core essence of the work presented in this thesis is the adoption of synthetic conductors into microwave engineering so as to make robust solutions to problems encountered in application areas such as wideband absorbers and wideband antennas. Such conglomeration of synthetic conductors with these microwave applications have the potential to provide flexible, printable and reconfigurable solutions.

Synthetic conductors are a class of materials which exhibit electrical conductivity without being composed of conventional metals. These materials are basically composed of allotropes of carbon such as graphite, fullerene, carbon nanotubes, or it can be another class of materials called intrinsically conducting polymers. Both these materials have a conjugated backbone that gives them their high electrical conductivity. These materials are particularly standing out when compared to metals because of their tunable conductivity, reversible doping, electrochromic properties, optical properties, thermoelectric properties, light weight, flexibility, chemical sensing etc. Hence they have applications in corrosion protection, flexible electronics, printable electronics, body area networks, implantable electronics, brain-computer interconnects, environmental sensors, energy harvesting, high density energy storage, display technologies and much more. However, there exist a lot of engineering challenges that are initially faced by newer technologies like this.

Wideband absorbers are engineered structures used to reduce radar cross section (RCS) of a target so that the target object goes undetected in the normal vicinity range of a radar. Traditionally microwave absorbers were realized by using Salisbury screens, Jaumann absorbers etc which utilize the quarter wavelength resonance absorption mechanism. But they are very narrow band or having thicknesses which hamper its end application. Since then there have been a lot of research regarding thickness reduction and bandwidth enhancement in these absorbers – either together or any of them. Metamaterials were introduced into this for narrow band absorption at significantly reduced thicknesses relative to the wavelength. Lumped resistances or resistive patterns which act as Frequency selective surfaces (FSS) were introduced

so that a wide range of frequencies can be dissipated in these materials and are called circuit analog absorbers. There are another class of structural absorbers called geometric transition absorbers which offer very wideband non resonant absorption by using geometrical modification and material attenuation to reduce the reflected power although at higher thicknesses. Current research in these structures trends towards being flexible, printable and wearable as such structures are now being optimized in terms of ease of production to suit the target shape and mechanical agility.

Ultra wideband (UWB) communication is a wireless standard proposed for short distance high speed data transfer between portable devices using nano second pulses having spectral signature ranging from 3.1 GHz to 10.6 GHz. With the introduction of ultra wideband technology, the requirements for the hardware were made stringent in terms of radiated power, portability, signal distortion etc. An ultra wideband antenna is envisaged to be a component of such system which converts an UWB pulse in the circuit to electromagnetic radiation and vice versa. This is the transmit/receive end node in any UWB system bound to be wireless. An electromagnetic signal in an electronic circuit is said to be ready for radiative transmission only when the impedance of the antenna is matched with that of the surrounding media and is a highly frequency dependent phenomena. Hence the design of UWB antennas offer some level of challenge to achieve wideband matching with less pulse distortion and in a small form factor suitable for portable wireless systems. It is a more demanding research when it comes to making these systems to be built for flexibility and printability so that they can be realized on any substrate. This has potential applications in printable electronics. For those areas where one-time use is intended, trade-offs in radiation efficiency and durability are affordable as in the case of low-power, short range communication for paper-based electronics. In such cases, UWB communication is preferable due to its speed, low power and bandwidth with the additional advantage of its non-resonant type antennas having lower surface current densities when compared to resonant antennas.

1.4.1 Objectives of this study

- To investigate about synthetic conductors, their properties, synthesis methods, processibility etc. and thereby selecting suitable material on

the basis of their microwave properties and ease of fabrication.

- To design wideband microwave absorbers based on lossy materials and high conducting materials so that these have better prospects regarding newer manufacturing processes such as 3D printing, and/or offer mechanical flexibility.
- To design ultra wideband antennas that are portable and printable which can be patterned onto substrates of choice without losing much of its electrical properties.

1.5 Organization of the thesis

The thesis comprises of six chapters.

- Chapter 1: Introduction

This chapter describes an overview of the history of microwaves, antennas, synthetic conductors etc. It also deals with microwave absorbers. The motivation towards the present research is also mentioned. The chapter concludes with a description about the organization of the thesis.

- Chapter 2: Methodology

This chapter presents a brief description of the simulation tools, synthesis/fabrication procedures and experimental techniques used in this research work.

- Chapter 3: Synthesis and characterization of non-metallic conductors

The chapter starts with a brief literature visit on synthetic conductors, their synthesis and characterization. This chapter outlines the important features of synthetic conductors, their types and particularly their synthesis and characterization. Conducting polymer called Polyaniline (PANi) was chosen as one such material and its synthesis routes and properties have been investigated. Another such material is graphite derivatives called expanded graphite which can be used as very good conductors with potential to replace metals in certain applications. The

properties of these materials are also characterized. A composite of Polyaniline and graphene is also investigated in the course of study.

- Chapter 4: Printable non-resonant absorbers using polyaniline-graphene composites

This chapter introduces the various techniques used in the realization of wideband absorbers through a brief literature review. It is followed by the design of wideband absorber using polyaniline-graphene composites. The design is based on non-resonant absorption of microwave energy by conductivity graded layered attenuator structure. This offers good impedance matching and with broadband absorption of microwave power within small thickness. The structure has the potential of 3D printability as the entire system uses only polymers to absorb incident microwave. The fabrication, measurement and analysis of the absorber are described in this chapter.

- Chapter 5: Printable antennas based on graphite derivatives

The essence of this chapter is the design of UWB antennas on any substrate of choice. After a brief review of literature, the chapter begins with UWB antennas of very small sizes designed on standard FR4 substrate with considerations on the wide bandwidth, portability and circuit integration as outlined by FCC specifications. The metallic regions of the optimized structure was replaced with expanded graphite based material so that the pattern can be created on any substrate. The pilot study was done on FR4 substrate. Later on, the fabrication of the structure on more flexible substrate like Poly Methyl Metha Acrylate (PMMA) is done.

- Chapter 6: Conclusion and Future Scope

A summarized account of all the works presented in the previous chapters is highlighted in this chapter along with some directions on the scope for future work in this area.

Thesis also includes the bibliography, list of publications by the author and the resume of the author.

Chapter 2

METHODOLOGY

This chapter presents a brief description of the synthesis/fabrication procedures, experimental techniques and simulation tools used in this research work. The synthesis part is primarily on the chemistry base that is used as part of the work. The measurement and characterization techniques are described afterwards. The chapter ends with a discussion on the simulation environment and the techniques used for the final microwave application design

Contents

2.1	Synthesis	24
2.1.1	Fumehood	24
2.1.2	Distillation setup	25
2.1.3	Stirrer	26
2.1.4	Ultrasonicator	26
2.1.5	Filtration setup	27
2.1.6	Oven	28
2.1.7	Hydraulic pellet press	29
2.1.8	PCB fabrication	29
2.1.9	Laser patterning setup	31
2.2	Characterization	32

2.2.1	DC conductivity measurement	32
2.2.2	Impedance analysis	34
2.2.3	X-ray diffractometry	36
2.2.4	Fourier transform infrared spectroscopy	37
2.2.5	Scanning electron microscopy	38
2.2.6	Vector network analyzer	38
2.3	Application design	41
2.3.1	Simulation softwares	42
2.3.2	Automatic pattern measurement setup	42

2.1 Synthesis

The synthesis part of non-metallic conductors is a series of chemical procedures involving many intricate steps. The practical setup for this is outlined in this section.

2.1.1 Fumehood

A fumehood is an enclosed glass chamber wherein complex chemical reactions involving harsh chemicals can be performed (Figure.2.1). It has an access door to handle the equipments and glasswares inside. The interior of it is well lit and there are adequate number of power connections for equipments housed inside the fumehood. The toxic fumes from the chemical reactions are expelled by a powerful exhaust fan connected to its atmosphere. The setup is quite useful in the synthesis of conducting polymers and its further processing as the monomers of these materials are proven carcinogens especially the aniline which is found to be readily absorbed via skin upon contact. There can be instances where the chemicals can cause nausea, dizziness, blindness, or even explosion due to side reactions which are really harmful. A fumehood gives a significant amount of protection against the harmful effects of chemicals involved in the study.



Figure 2.1: Fumehood housing a distillation unit and magnetic stirrer

2.1.2 Distillation setup

The distillation setup is used for the purification of chemicals prior to reactions. Even though chemicals are stored as per their storage specifications, they get eventually altered due to oxidation and leakage. These have significant consequences in the end product of a reaction. Thus it is desirable that the chemicals are distilled before every use. A distillation setup consists of a heating mantle, a round bottom borosil flask, a condenser assembly, and a collection unit. The chemical to be purified is taken in the round bottom flask and mounted onto the heating mantle. The required temperature for distillation is set on the heating mantle. The round bottom flask is connected to the condenser assembly via bend glass pipes. The condenser has two chambers - an inner chamber and an outer chamber separated by glass partition. The outer chamber has two connections for water inlet and outlet used to cool the vapours which reach the inner chamber from the round bottom flask. These vapours then condense instantly on the walls of the partition and are collected in the collection unit over the course of time.

2.1.3 Stirrer

In any chemical reaction, it is highly desirable that the reactants are perfectly mixed. This ensures that the reactants are efficiently used up and there are no unwanted side reactions caused due to excess or deficit of reactants anywhere in the reaction medium. The first hand technique for achieving this is by stirring. It is also known that for homogeneous nucleation to occur, proper stirring conditions are to be met or otherwise a heterogeneous nucleation results in low quality samples. There are two ways to stir a reaction mixture.

Mechanical stirrer

A mechanical stirrer uses a stirring blade connected to an overhead speed controlled motor which can be set to specified Rotations per Minute (RPM). This blade can be immersed in the reaction medium to evenly mix the reactants. This method of stirring is particularly useful as the stirring power requirement is high when the reactants are highly viscous or form thick precipitates on course of the reaction.

Magnetic stirrer

Magnetic stirrers use rotating magnetic fields to rotate a magnetic fish inside a reaction medium. This kind of stirring is very useful if the reactants are very harsh and needs to be remotely stirred. The magnetic fish, which is a teflon coated chemically inert permanent magnet, is first put inside the reaction mixture. The mixture is enclosed and then kept on the magnetic stirrer's platform underneath which a rotating magnet couples magnetically with the magnetic fish. When the stirrer is turned on, the magnetic fields rotate pushing the fish also in the direction of rotation. Thus the reactants can be stirred in closed containment.

2.1.4 Ultrasonicator

Ultrasonicator is a multipurpose equipment which finds very useful in a chemical laboratory. It has a metallic chamber underneath which it houses a couple of piezoelectric vibrators. These piezoelectric vibrators generate ultrasonic

waves of a few kilo hertz. When the bath is filled with water, the ultrasonic waves generated by the vibrators create cavitations or localized micro vacuums in the water. When these vacuums are instantly filled, it creates a force that tears apart agglomerations of suspended materials and distribute evenly. It is mainly used to create dispersions or suspensions in a medium. Especially, in this study, it was extensively used for creating graphene oxide dispersions and to quickly dissolve salts in solvents. It can also be used to clean stains on glass vessels alongside piranha solution wherein piranha solution is taken in the vessel to be cleaned and then it is carefully sonicated in the water bath without spilling the piranha solution.

2.1.5 Filtration setup

Filtration is an important step in the synthesis of polymer nanoparticles. It is used to separate the reaction products from the solutions. Normally conducting polymers happen to be particulate suspensions in the reaction mixture. These are separated by filtration. There are two ways to filter particulates from the medium.



Figure 2.2: Vacuum filtration unit

Vacuum filtration

Vacuum filtration uses a vacuum chamber connected to a vacuum pump via a pressure controllable needle valve (Figure.2.2). This vacuum chamber has an opening on top of it where a membrane filter assembly can be mounted. The membrane filter assembly has connections to the vacuum chamber which is separated by a membrane filter paper of suitable pore size. The dispersion to be filtered is taken in this membrane filtration assembly. When the vacuum pump is started, the membrane filter paper permits only liquids to pass through to the vacuum chamber and any solid particle who has size greater than the pore size of membrane filter paper is blocked. Thus the particulates can be filtered from the liquid.

Centrifuge machine

Another method to separate dispersions is to use a centrifuge machine. It consists of a metallic rotary housing having an array of glass tube mounts connected to a motor. The dispersion to be separated is taken in glass tubes and kept in the rotary mount. The assembly starts spinning after setting the right RPM and switching it on. This results in very high centrifugal force which forces the particulates to settle down at the bottom of the glass tube. After required rotations, the settled particulates in the glass tubes are separated by easily removing the liquid fraction. This technique is particularly useful when the dispersions are nanoscale. In this work, the polyaniline prepared using gelatin stabilized medium could only be separated from the reaction medium by this method.

2.1.6 Oven

Ovens are useful in heating the materials particularly for drying it. There are a few methods to dry a sample.

Microwave oven

Microwave ovens use the resonant heating of water molecules or any other molecules that have permanent dipolemoment and that responds to 2.4GHz frequency. The heating effect of microwave ovens are not conductive or convective instead they are radiative heaters and they heat the material evenly

throughout its volume. Microwave ovens deliver a lot of power within a short time and can be heated to very high temperatures instantly. In this work, microwave heating was used to exfoliate graphite intercalation compounds.

Hot air oven

Hot air ovens use convective heating to dry samples. It is very useful to dry samples in the presence of air. It is also used for drying wet glasswares. In the present work it was used to dry polyaniline powders and graphite intercalation compounds. The samples can be enclosed in a vacuum container so that the samples can be dried under vacuum which is particularly useful for samples that contain solvents with high boiling points. Such solvents with high boiling point make it difficult to dry as those temperatures can compromise the quality of dried samples. Vacuum drying helps in lowering the boiling point due to lowered vapour pressure in the chamber thereby drying the sample at a much lower temperature.

2.1.7 Hydraulic pellet press

The application development and analysis techniques in microwave requires samples in solid forms. As the conducting polymers are obtained as powders, they are to be machined into pellets. These pellets can be shaped into any forms using suitable hydraulic die. The powder form of the material is taken in a die of required dimension and mounted in the Hydraulic press (Figure.2.3). This equipment applies very high pressure under which the powder is pressed into a solid pellet. In this work, the conducting polymers were pelletized at a pressure of $100\text{kg}/\text{cm}^2$ prior to measurement of their dielectric properties via cavity perturbation, impedance analysis, and application design. Expanded graphite was used with pressure sensitive adhesive to coat onto substrates using hydraulic press.

2.1.8 PCB fabrication

Printed circuit boards were fabricated from raw single side and double copper clad that is commercially available by photolithography technique. The technique involves the following steps:



Figure 2.3: Hydraulic pellet press

1. Preparation of binary mask using computer
This is done by importing the simulated structure into any of the vector graphics editing tool such as Inkscape. The necessary layers are prepared and the final mask design consists of black and white regions where it either blocks UV or allows it to pass thorough. This is printed onto a transparent mask such as oil paper or PET sheet. Thus the mask is generated.
2. Cleaning of the copper surface
The copper surface contains a lot of adsorbed impurities and oxide layer. This is to be removed prior to patterning. Mechanical abrasive scrubs are used to remove oxides and other chemicals are removed by using isopropyl alcohol and acetone.
3. Application of photoresist
A photoresist is a photo sensitive material which either solidifies (Negative photoresist) or coagulates (Positive photoresist) on exposure to

UV light. In this work a negative photoresist was used which solidifies on exposure to UV. It was coated on to the substrate surface by spin coating and dried in air under dark.

4. Mask alignment and UV exposure

The binary mask is aligned with the photoresist coated surface of the copper clad and is exposed to UV light under automatic timer control.

5. Developing

After the exposure to UV, the exposed portions of photoresist solidifies and the unexposed photoresist is removed by using a developer solution. After using developer solution, the underlying copper is exposed in the required pattern for removal.

6. Chemical etching

Chemical etching is the process of removing exposed copper by chemical reagents called etchants. Usually the etchants can be Ammonium peroxo disulphate or Ferric chloride.

7. Cleaning and machining

The structure after etching is cleaned thoroughly using water, acetone and alcohol. This removes the excess etchant and the hardened photoresist from the surface. After this the structure is machined into the adequate dimensions and polished.

2.1.9 Laser patterning setup

Laser patterning is an important tool especially in the fabrication of microwave structures using synthetic conductors. It uses infrared laser to selectively remove portions of a substrate at a predetermined depth. The steps involve the preparation of substrate, pattern generation using vector graphics tool, transfer of pattern to plotter tool of the laser patterner, and final commencement of patterning. Scan gap, power and speed are the principal parameters that determine the depth and resolution of patterning. In a typical patterning, these parameters are first calibrated for the selected substrate by trial and error and the optimum values are used for the actual patterning. It is typically useful for patterning conducting polymers. Metals, which require high power pulsed CO_2 lasers, are not suitable for patterning using infrared lasers.

2.2 Characterization

This section elucidates the methods and characterization performed in this work.

2.2.1 DC conductivity measurement

DC conductivity measurements are performed on thin conductive sheets where probes measure sheet resistance of the samples expressed in Ω/\square . The sheet resistance value when multiplied by thickness gives the resistivity of the material. The inverse of resistivity represents conductivity which is expressed as *siemens/metre*. It is assumed that the material is sufficiently conductive to get accurate values. In a three dimensional conductor, the resistance can be written as ,

$$R = \rho \frac{L}{A} \quad (2.1)$$

$$R = \rho \frac{L}{W \times T} \quad (2.2)$$

$$R = \frac{\rho}{T} \times \frac{L}{W} \quad (2.3)$$

$$R = R_s \times \frac{L}{W} \quad (2.4)$$

Where ρ is the resistivity, L is the length, A is the cross sectional area, W is the width, T is the thickness, and R_s is the sheet resistance of the conductor. Therefore,

$$\text{Bulk resistivity of the material, } \rho = R_s \times T \quad (2.5)$$

In general there are two ways to measure sheet resistance.

Two probe method

In this method, the sheet whose sheet resistance is to be measured is contacted with two planar probes which are printed on a substrate using PCB fabrication technique[82] (figure.2.4). The linear probes will be separated by a distance equal to the length of the probes in such a way that the length will be equal to the width and the area enclosed between the probes become $1unit^2$. Thus a measurement of the resistance between the probes using an impedance meter will directly give the value of sheet resistance of the material.

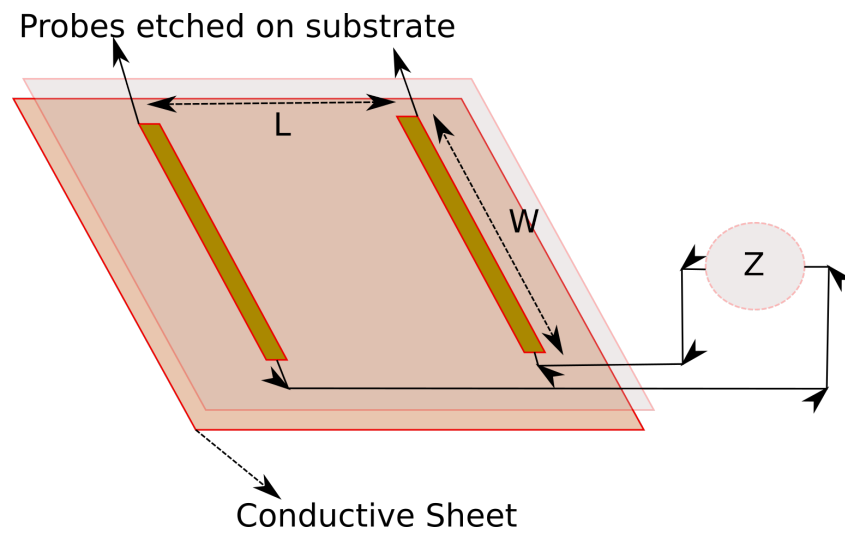


Figure 2.4: Two probe method to find sheet resistance

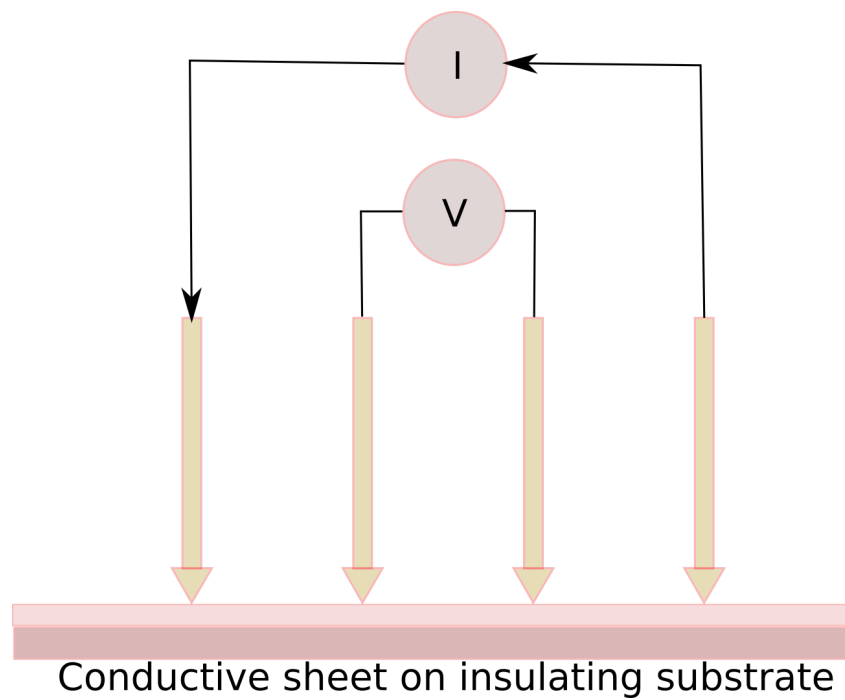


Figure 2.5: Four probe method to find sheet resistance

Four probe method

Four probe method stems from the disadvantage of using a two probe method to measure highly conducting samples[83] (Figure.2.5). For high conducting

samples, the probe resistance will be adding up in series with the sheet resistance during measurement. Hence, to avoid that four probes separated equally are arranged in a linear fashion. A constant current source injects a known amount of current between the outermost two probes. There exists then a voltage gradient between the outermost probes and this voltage gradient is measured by the two innermost probes. The ratio of this voltage to that of the infused current will give the actual sheet resistance of the sample without the probe resistance.

2.2.2 Impedance analysis

The low frequency dielectric parameter extraction of conducting polymers was performed using the Agilent E4980A Precision LCR Meter. This instrument gives the complex impedance of a material connected to its dielectric test fixture in the frequency range 20Hz to 2MHz. The material under test is compressed into pellet form of 13mm diameter and suitable thickness. It was reported in the literature that the dielectric properties such as dielectric constant and loss factor can be computed by Capacitance method as well as Impedance method[84].

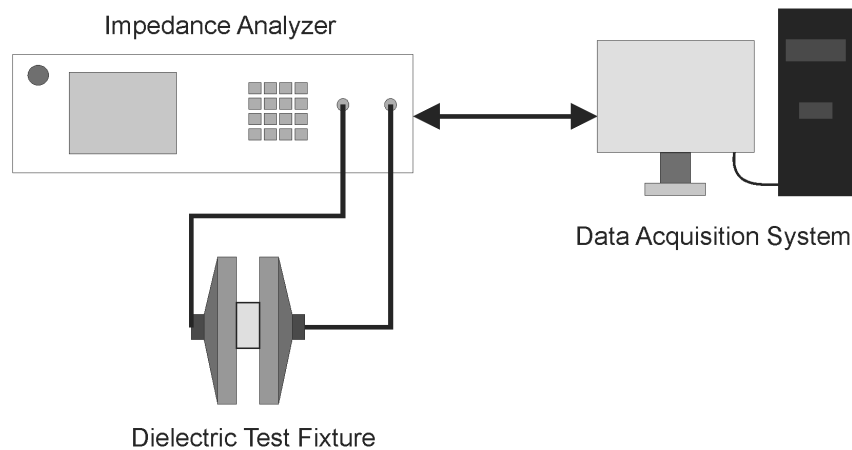


Figure 2.6: Impedance analyzer for low frequency dielectric estimation

- Impedance method

In this method, the resistance and reactance of the pellet is measured.

$$\text{Permittivity Real, } \epsilon'_r = \frac{X}{2\pi f C_0 (R^2 + X^2)} \quad (2.6)$$

$$\text{Permittivity Imaginary, } \varepsilon_r'' = \frac{R}{2\pi f C_0 (R^2 + X^2)} \quad (2.7)$$

- Capacitance method

In this method, the capacitance and loss tangent offered by the pellet is measured.

$$\text{Permittivity Real, } \varepsilon_r' = \frac{C \times t}{8.854 \times 10^{-12} A} \quad (2.8)$$

$$\text{Permittivity Imaginary, } \varepsilon_r'' = \tan(\delta) \times \varepsilon_r' \quad (2.9)$$

Where C_0 =capacitance offered by freespace for the same area and gap offered by the pellet, R=resistance,t=thickness of the pellet, A=area of the pellet, X=reactance, f=frequency, C=capacitance offered by the pellet, $\tan(\delta)$ is the loss tangent of the pellet.

$$\text{Conductivity, } \sigma = 2\pi f \varepsilon_0 \varepsilon_r'' \quad (2.10)$$

$$\text{Skin Depth, } d = \frac{1}{\sqrt{\pi f \mu_0 \sigma}} \quad (2.11)$$

$$\text{Loss Tangent, } \tan(\delta) = \frac{\varepsilon_r''}{\varepsilon_r'} \quad (2.12)$$

It was required that an automated program be setup to measure the various dielectric properties of the material under test kept for measurement in between the dielectric test fixture of the Impedance Analyser. The software code was written in Matlab code which was used to interact with the impedance analyzer remotely via an ethernet or USB interface and to acquire raw data using SCPI command set from which the dielectric properties could be calculated. The software code uses both Capacitance as well as Impedance methods to compute the real and imaginary parts of permittivity of the material under test. This can be used to compute the material's conductivity, skin depth and loss tangent. The block diagram representation is shown in Figure.2.6.

The software computes all these parameters for the entire frequency range of operation and saves the results in csv format files. These files can be used to plot data later.

2.2.3 X-ray diffractometry

X-ray diffractometry is a powerful technique to analyze the crystal structure of a material (Figure.2.7). It is performed on powdered samples and film samples. X-rays which happen to be having wavelengths comparable to the crystal lattice dimensions are beamed onto the sample. This causes diffraction of X-rays from the crystal planes as in the case of a diffraction grating. A surrounding photographic plate captures the scattered radiation. This scattered radiation contains peaks in certain angles. The angular value, wavelength, crystal plane distance are all connected by the famous Bragg's equation.

$$n\lambda = 2d\sin\theta \quad (2.13)$$

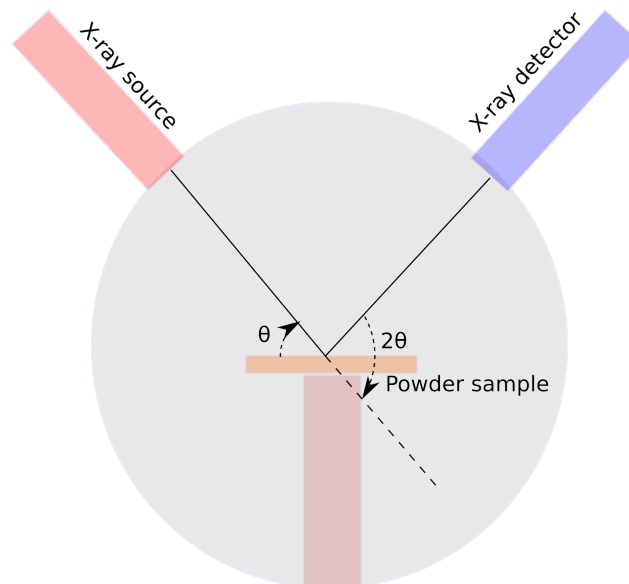


Figure 2.7: XRD measurement setup

XRD graphs are X-ray intensity versus diffraction angle plots which also contains information about the distance between crystal planes for each peak. This plot is very useful in analyzing the efficacy of a tailor-made synthesis method when compared with standard methods in terms of crystallinity and inter-planar distance. In the present work, the powder XRD of the samples were measured using Bruker AXS D8 Advance which gives full-sized goniometer class powder XRD under ambient and non-ambient conditions.

2.2.4 Fourier transform infrared spectroscopy

Fourier transform infrared spectroscopy (FTIR) is a technique used to scan the vibration spectrum of a material under test (Figure.2.8). It gives the information of various chemical bonds and functional groups that are present in the material by analyzing the infrared absorption spectrum of the material. The FTIR analysis of the samples in this work were performed using Thermo Nicolet Avatar 370 FTIR spectrophotometer.

A typical FTIR spectrum is a plot of percentage transmittance versus wavenumber in cm^{-1} . The wavenumber ranges from $4000cm^{-1}$ to $400cm^{-1}$. The IR spectrum can be divided into four regions. The first region which ranges from $4000cm^{-1}$ to $2500cm^{-1}$ represents the peak corresponding to absorption caused by N-H, C-H and O-H single bonds. The second region which ranges from $2500cm^{-1}$ to $2000cm^{-1}$ contains the peaks corresponding to absorption caused by triple bonds. The third region which ranges from $2000cm^{-1}$ to $1500cm^{-1}$ contains the peaks corresponding to absorption caused by double bonds such as C=O, C=N and C=C. The fourth region ranges from $1500cm^{-1}$ to $400cm^{-1}$ and represents a large number of absorption peaks that account for a large variety of single bonds. This region is known as the fingerprint region.

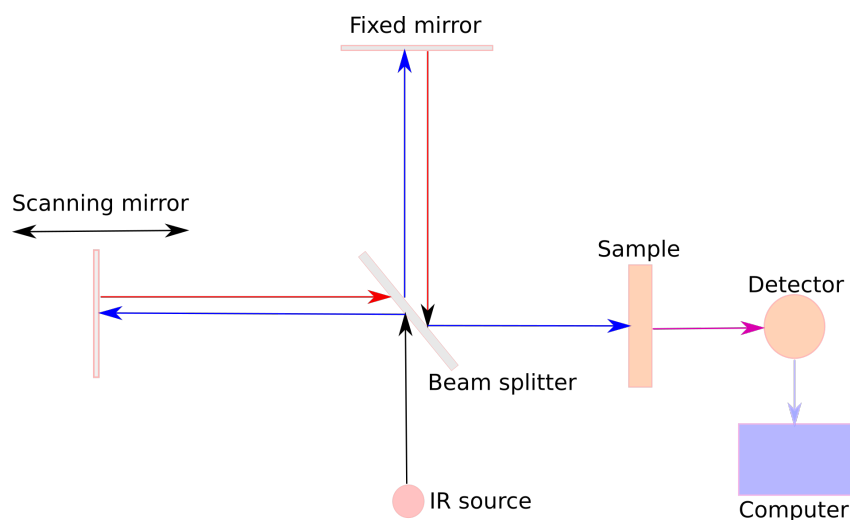


Figure 2.8: FTIR measurement setup

2.2.5 Scanning electron microscopy

Scanning electron microscopy is a imaging technique which can be used to get the micro structural images of a material. It uses powerful electron beams instead of photons to create ther image. The electron beam, which typically has an energy ranging from 0.2 keV to 40 keV, is focused by one or two condenser lenses to a spot about 0.4 nm to 5 nm in diameter to give high resolution images of the material under investigation. The structural and morphological properties of the prepared samples were analyzed using JEOL JSM -6390LV Scanning electron microscope. The technique reaffirms the validity of the analysis performed by FTIR and XRD. It also gives important information regarding the shape of the nano particles that are synthesized.

2.2.6 Vector network analyzer



Figure 2.9: Vector network analyzer

A vector network analyzer (VNA) is a versatile instrument that can be used for various characterization and measurements (Figure.2.9). It is a device which can transmit/receive microwave signals through its ports and measure

the amplitude as well as phase of scattering parameters. Scattering parameter measurement is a common start point for microwave characterization of any material. In the present study, Rohde & Schwarz ZVB20 VNA was used. There are two types of microwave characterization techniques - resonant method, and non-resonant method. In both these methods, the complex permittivity is calculated using measurements from VNA and can be used to calculate the following too:

$$\text{Conductivity, } \sigma_e = \omega \varepsilon'' = 2\pi f \varepsilon_0 \varepsilon_r'' \quad (2.14)$$

$$\text{Loss tangent, } \tan \delta = \frac{\varepsilon_r''}{\varepsilon_r'} \quad (2.15)$$

$$\text{Skin depth, } \delta = \frac{1}{\sqrt{\pi f_s \mu \sigma}} \quad (2.16)$$

$$\text{Microwave heating coefficient, } J = \frac{1}{\varepsilon_r' \tan(\delta)} \quad (2.17)$$

Cavity perturbation technique

Cavity perturbation is a resonant method used to find the complex permittivity of a material under test[85, 86] (Figure.2.10). A precisely machined sample is inserted into a waveguide based resonant cavity which results in the shifting of resonant frequency to lower side due to the perturbation of the maximum electric field point of the standing wave in the cavity by the sample. The frequency shift and the Q-factor change are noted along with the precise sample dimensions to calculate the complex permittivity of the sample as per the following equations.

$$\varepsilon_r' = \frac{f_c - f_s}{2f_s} \left(\frac{V_c}{V_s} \right) + 1 \quad (2.18)$$

$$\varepsilon_r'' = \frac{V_c}{4V_s} \left(\frac{Q_c - Q_s}{Q_c Q_s} \right) \quad (2.19)$$

These equations are derived on the basis of the fact that the sample perturbs the electric field only slightly. Any drastic shift in resonant frequency or Q-factor will leave the result in vain. Also, the volume of the sample should be negligible when compared to the volume of the cavity. It is also required that

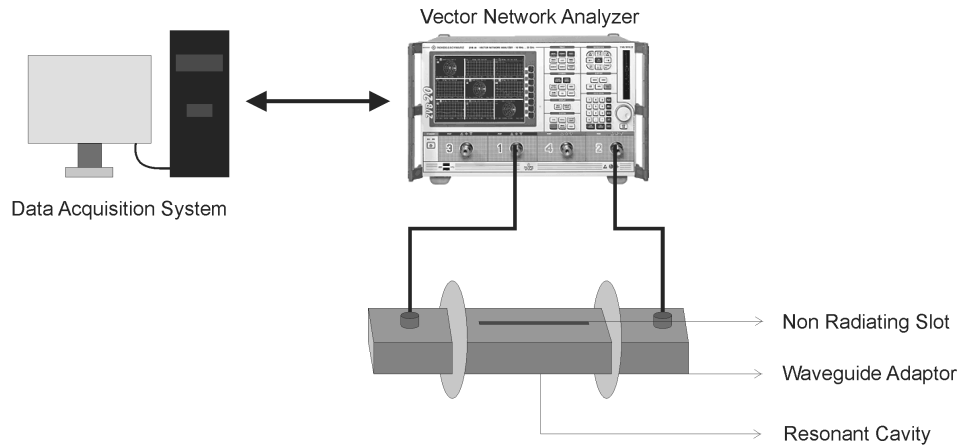


Figure 2.10: Cavity perturbation measurement setup

the cavity is excited in dominant TE_{10} mode. Hence this technique cannot be used for highly lossy materials whose shifts would be way beyond these assumptions. Conducting polymer pellets of nominal conductivity can be microwave characterized by this technique if machined to very small cylindrical volumes.

In this study, a matlab code for performing cavity perturbation was designed. The software code comprises of two modules. First module (autoperturb) is for measuring the resonant frequency shift and Q-factor changes from Rohde & Schwarz ZVB20 Vector Network Analyzer using SCPI commands via ethernet interface. This is the data acquisition part of the software. The second module (modperturb) is for the actual dielectric estimation from the data collected using the first section.

Nicolson-Ross-Weir technique

Nicolson-Ross-Weir (NRW) technique is a non-resonant method of solving for the microwave complex permittivity and permeability of a material under test [87, 88] (Figure.2.11). The method essentially uses two port scattering parameters to calculate the permittivity and permeability of the material. It is a broadband technique which is prone to phase ambiguities and imperfections in the thickness measurement of the sample. This is a fast measurement technique widely used for lossy materials in sheet form with thickness less than quarter wavelength of the probing signal.

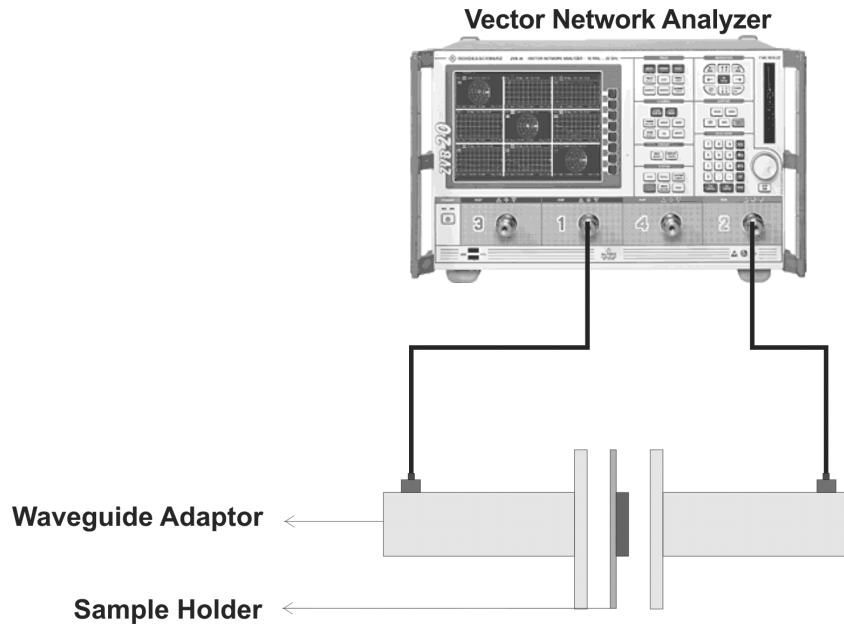


Figure 2.11: NRW measurement setup

The measurement procedure starts with the TRL calibration of waveguide adaptors connected to VNA by means of coaxial cables. The calibration is performed with sample holder also in place so that the effects of sample holder are compensated and the calibration reference plane coincides with the sample. After calibration, the sample is inserted into the sample holder and the two port network parameters are measured and saved into an s2p file. These measured values are used to calculate the complex permittivity and permeability of the samples using the NRW algorithm implemented in matlab code.

2.3 Application design

The prospectives of synthetic conductors in microwave engineering was illustrated in this work through their application side perspective by designing microwave absorbers and antennas based on polymer materials. This section discusses the methodologies adopted in the application part.

2.3.1 Simulation softwares

Before the fabrication of any structure for microwave end application, it is designed, parameter identified and optimized using full wave electromagnetic simulation softwares that are commercially available. In this work, Finite Element Method (FEM) based CST Microwave Studio was used for the simulation studies[89]. This is a fast solver which can simulate planar, multilayer or 3D structures with good accuracy. It has a collection of solvers each tailor-made to suit niche applications. It has complex 3D and 2D structure import and export support which is of use while prototyping an optimized design.

Frequency domain solver in CST is particularly useful in simulating periodic structures whose unit cell is defined as the structure. The periodicity is indicated by applying a periodic boundary condition and the excitation is given by assigning a floquet boundary condition and thereby a floquet port at the required boundary. The metallic ground is assigned with electric boundary condition. The incident angles can be varied using θ and ϕ parameters already allotted in the parameter list. The template has field monitors for monitoring E-field, H-field, surface current, Farfield RCS, power loss density distribution etc. These field monitors can be analyzed along with the scattering parameters to derive conclusions on the performance of periodic structures.

The time domain solver in CST is used in the simulations pertaining to planar antennas and in particular, in this study, UWB antennas. After the geometric drawing of the antenna is done, boundary conditions are imposed on the antenna and is usually open boundary with added space on every direction. A waveguide port is used to excite the antenna. The one port scattering parameter is calculated and the field monitors if allotted will measure the E-field, H-field, surface current, far field radiation pattern, gain and efficiency of the antenna under test.

2.3.2 Automatic pattern measurement setup

This system consists of a wideband horn antenna connected to a VNA via low loss broadband coaxial cables, and a turn table driven by a control system[90] (Figure.2.12). A program running in a computer remotely controls the VNA and coordinates the motor control system to measure the angular variation of radiation from the antenna under test mounted on the turntable. A variant of this setup uses arc mounted broadband T/R antennas for measuring

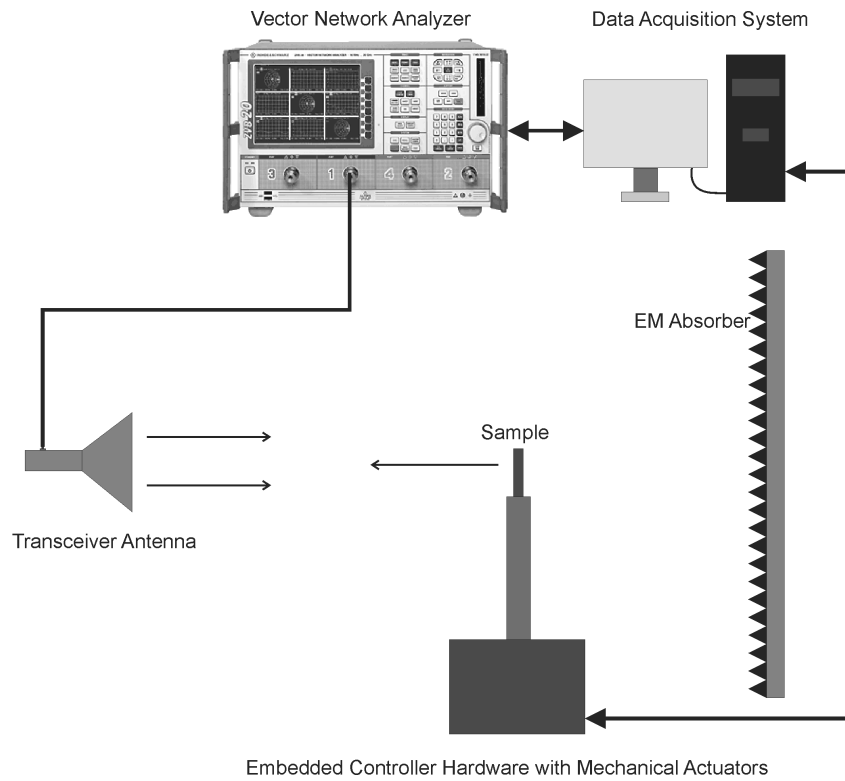


Figure 2.12: Pattern measurement setup

the broadband monostatic and bistatic RCS measurements on a RCS target structure mounted on central turntable. Both these setups are housed in an anechoic chamber which is a big room completely shielded from outside radiations by a layer of metal. The inner walls of the anechoic chamber are covered with pyramidal geometric transition broadband absorbers made from polyurethane foams containing carbon black and ferrite absorbers. This configuration minimizes microwave reflections inside the chamber and avoid multipath interference which would otherwise undermine pattern measurement.

Antenna pattern measurement was an important step in the study of antennas. This was realized by in-house designing the hardware and software required for the task. This consists of a matlab code running in a central computer that interfaces to Rohde & Schwarz ZVB20 VNA. The software sends SCPI commands through a TCP/IP port to communicate with the VNA. The central computer is also connected to a stepper motor control system intended

for controlling the turntable setup. The stepper motor control system was designed using PIC microcontroller which has serial port connectivity with the central computer. The firmware of the PIC microcontroller was written using Hitech C embedded C programming language. This acts as a custom operating system capable of receiving commands from a remote PC through RS232 serial interface as well as driving the motors intelligently to suit the measurement needs. The hardware was designed using Proteus Virtual Simulation Manager tool suite. This custom design has two output stepper motor power drives, an SMPS power supply, a serial port interface, and a control circuitry on board.

Chapter 3

SYNTHESIS AND CHARACTERIZATION OF NON-METALLIC CONDUCTORS

The chapter starts with a brief literature visit on synthetic conductors, their synthesis and characterization. Conducting polymer called Polyaniline (PANi) was chosen as one such material and its synthesis routes and properties have been investigated. Another such synthetic conductor are graphite derivatives called expanded graphite which can be used as very good conductors with potential to replace metals in certain applications. The properties of these materials are also characterized. A composite of polyaniline and graphene is also investigated in the course of study.

Contents

3.1 Polyaniline	46
3.1.1 Enhancements possible in PANi	47
3.1.2 Synthesis of Polyaniline via self stabilized dispersion polymerization in agitation free environment .	49
3.1.3 Summary	60

3.2 Graphite and its derivatives	61
3.2.1 Graphite Intercalation Compounds	67
3.2.2 Exfoliated graphite	69
3.2.3 Synthesis and characterization of exfoliated graphite	70
3.2.4 Summary	80
3.3 Composites of Polyaniline and Graphite	81
3.3.1 Synthesis and characterization of PANi - graphene composite using gelatin as dispersion stabilizer . .	81
3.3.2 Summary	92

3.1 Polyaniline

Polyaniline (PANi) has been identified as a viable conducting polymer that can be used to replace metals in applications like anti-static discharge coatings, Electro-magnetic interference shielding, interconnection technology, charge storage[91, 92, 93, 94] etc. Particularly interesting out of these is the scope of Polyaniline in microwave communication technology, owing to the tunable conductivity, environmental stability, low cost of monomer and simpler preparation methods. Polyaniline exists in three different oxidation states[95] Leukoemeraldine (Fully reduced), Emeraldine (Half Oxidized), and Pernigraniline (Fully Oxidized) as illustrated in Figure. 3.1. Among these, the emeraldine, which is the most beneficial form has promising potentials. The emeraldine base when doped with acid results in an electrically conducting emeraldine salt form (Figure.3.2). To add to this, the change is reversible. i.e., it can be reverted back to its insulating emeraldine base form by chemical or electrical treatment.

As far as microwave electronics is concerned, typical application areas for materials exhibiting such behaviour would be to replace conventional metals and absorbers used in Stealth technology, Radar Absorbing Materials, Radar Cross Section reduction, Frequency selective surfaces, High impedance surfaces, Electro magnetic interference shields, Flexible antennas etc[96, 97, 98, 99]. These applications demand ruggedness, environmental stability, flexibility and temperature resilience. Although such applications are possible,

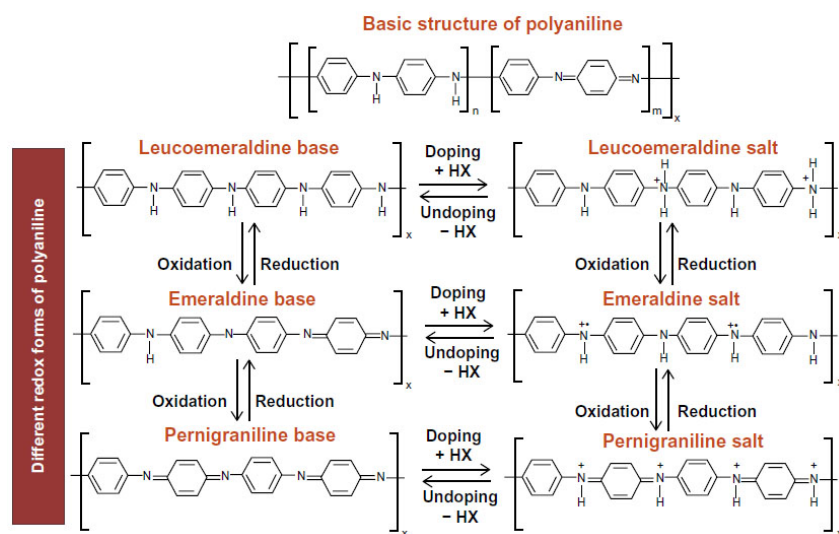


Figure 3.1: Different doping states of PANi

Polyaniline as itself has its own cons. The most annoying being the poor processability of the polymer. Whether it is possible to make Polyaniline compatible with conventional plastics without trading its intrinsic conductivity is still a question. Not just the possibility, but the feasibility of doing so is also something which needs special attention. Plausible solutions for these aspects of Polyaniline are explored in the following section.

3.1.1 Enhancements possible in PANi

The basic nature of PANi being just below the metal to insulator transition in the insulator region, for many practical applications, it is worth having enhanced properties. There are two properties to be enhanced in conducting polymers:

- Bulk conductivity

The conductivity of PANi is determined by the nature of dopant, doping density, relative concentration of reactants, reaction parameters such as temperature, constituents of the reaction environment etc. All these factors are responsible for the intrachain transport. The polymerization process of PANi has two stages: the induction period and the rapid polymerization period[100]. The rings of aniline polymerize in a chain

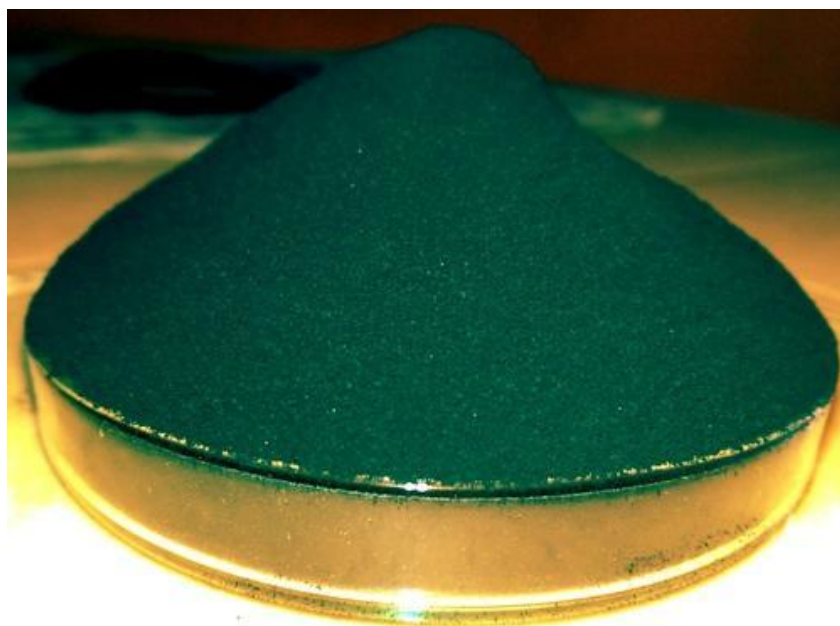


Figure 3.2: Polyaniline Powder

manner to get the final product. This reaction is supposed to happen via the para position of the aniline ring so that there are no side chain reactions that can cause steric hindrance and disorder in the system.

It has been seen that secondary doping, with m-cresol/CSA mix can significantly enhance the conductivity by forming supramolecular structures which act as polyelectrolytes[101]. This happens mainly due to the conformational changes in chain as well as the formation of three dimensional conducting networks of the fundamental polymer constituents using self organization. Also the effect of m-cresol in the orderly arrangement of the benzenoid and quinoid rings will also contribute to better conductivity. The self organization into metallic state is also reported in the case of simpler amorphous PANi when well dispersed in media like Poly methyl metha acrylate (PMMA) above a critical volume concentration[102]. These factors affect the bulk conductivity through both inter chain and inter domain transport.

- Processibility

Chain functionalization is a significant step towards the commercial ap-

plication of any conducting polymer[103]. The rigid backbone with strong inter chain interactions can make PANi less processible. Dispersible forms of PANi can be prepared by using alkoxy side groups on the polymer chains. PANi is readily dispersible in chloroform by use of DBSA alongside tetra butyl ammonium sulphate. By the introduction of more hydrophilic sites on the backbone, PANi can be dispersed in polar solvents like water with the aid of hydrogen bonding. There are solvents such as N-Methyl-2-Pyrrolidone (NMP), N,N Dimethyl Acetamide(DMAc), Hexamethyl phosphoramide (HMPA) which provide more chain-solvent hydrogen bonding than chain-chain hydrogen bonding.

Plasticizers like Poly vinyl chloride (PVC), Poly vinyl alcohol (PVA), N-methyl-2-pyrrolidone (NMP), Poly methyl metha acrylate (PMMA), Polystyrene (PS) can help in obtaining mechanical strength also to films of PANi when the PANi concentration in them are above the critical volume concentration. These materials can act as the host matrix and sometimes interact with the chain structure to enhance even the intra chain transport.

It has also been found that PANi forms thin films on suitable substrates during the polymerization reaction[104]. These substrates when in contact with the reaction medium gets its first coating of PANi during the induction period of the polymerization and seem to grow nanofibres perpendicular to the surface. Thin films of PANi can thus be grown on properly surface treated glass, or PET substrates without the use of a plasticizer or solvent by such insitu polymerization methods. The same technique can be extended to fabrics coated with PANi. Fabrics being porous with a lot of surface area, they offer more sites for the growth of PANi on them which is particularly useful for fabric based electronics.

3.1.2 Synthesis of Polyaniline via self stabilized dispersion polymerization in agitation free environment

Among many Intrinsically Conducting Polymers (ICP), Polyaniline (PANi) became very popular owing to its ease of preparation, reversible electronic

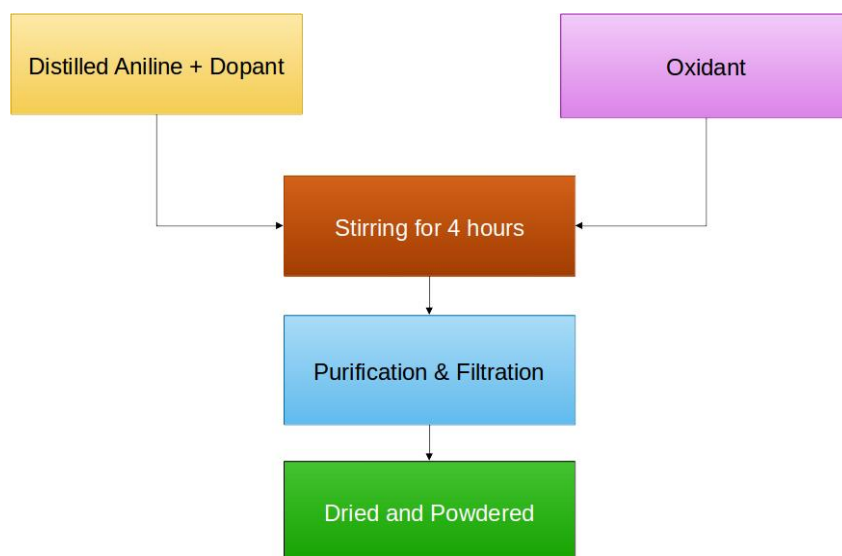


Figure 3.3: IUPAC specified route

characteristics with simple acid/base chemistry and better environmental stability. Since the discovery of PANi, variants of PANi with better properties are being developed[105, 106]. The challenge inherent with PANi is in its conductivity and processability enhancement. The poor processability arises from the reduced degree of freedom resulting from the pi-conjugated polymer backbone of conducting polymers in general. But the pi-conjugation wherein electron probability gets distributed along the polymer backbone is the core of electrical conductivity in these synthetic metals. This delineates a trade-off between conductivity and processability of these materials. The standard method of preparation is as suggested by IUPAC document written by J. Stejskal et al[107]. The paper addresses the preparation of Polyaniline by a radical cation initiated autocatalytic oxidative polymerization of aniline monomer in the presence of hydrochloric acid as dopant. The synthesis route as per this report is shown in Figure. 3.3.

There has been a trend in recent years towards the preparation of PANi in nanoscale form[108, 109, 110]. When compared with bulk conducting polymers, nanoscale conducting polymers display better performance in applications by virtue of the unique properties arising from their size such as high conductivity, large surface area, and light weight[111]. These nanostructures can be synthesized by many methods such as soft-template methods, hard

template methods, controlled solution synthesis, electro-spinning technique, self-assembly etc[112]. Interestingly, there has been quite a lot of research articles which give importance in the synthesis of novel PANi with exotic morphologies. The aim of those are to enhance the product for more surface area, sensing capability and porosity at nanoscale level. Among these work, seminal to the idea of morphology dependance on reaction technique was illustrated by the work of Kaner et.al. who proposed that PANi prefers to grow as nanofibres in aqueous media[113].

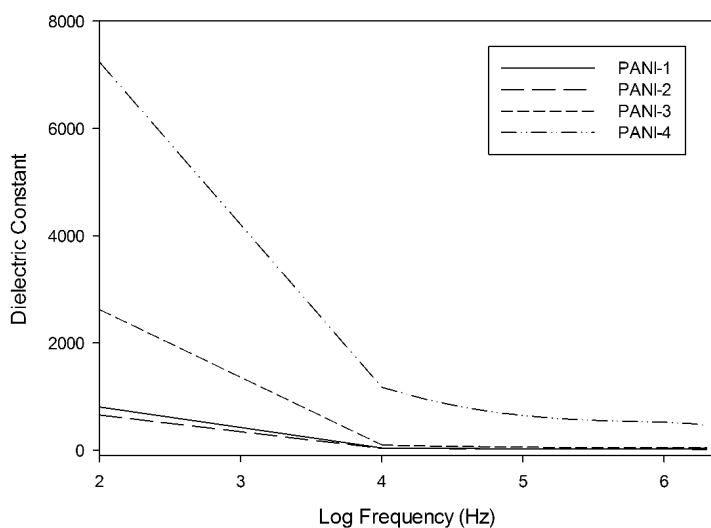


Figure 3.4: Low frequency dielectric constant

It has been reported earlier that stable PANi dispersions in aqueous medium can be made with PANi nanofibres prepared from polymerization of aniline monomer without mechanical agitation[114]. PANi preferentially looks for nanofibre configuration in undisturbed reaction mixtures. In the presence of stirring, the initial nanofibres get agglomerated as stirring induces collision of initial nucleates which act as the reaction centres. This causes heterogeneous nucleation and makes agglomerated particulates of initial nanofibres as the final product. These particulates settle down after reaction and pose difficulty in the solution processing of PANi. When the reaction is not stirred, the PANi nucleates grow radially outwards as nanofibres due to homogeneous nucleation. Such made PANi are easily dispersible into stable suspensions at

high concentrations in aqueous media after purification indicating the absence of stirring induced agglomeration.

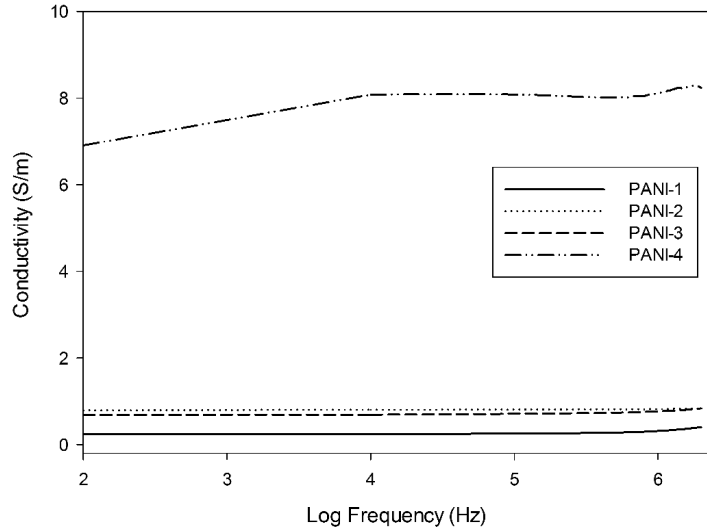


Figure 3.5: Low frequency conductivity

In the standard polymerization reaction it is found that during PANi formation, undesired branching and premature termination can cause poor quality samples containing PANi in composite morphologies. In such cases, ortho-coupling of aniline rings instead of para-coupling cause problems and give way to many low molecular weight oligomers and unwanted crosslinking. S. H. Lee et al has shown that PANi nanofibres can be easily prepared by self-stabilized dispersion polymerization (SSDP) in aqueous-organic heterogeneous mixtures[115, 60]. In such a heterogeneous mixture, anilinium hydrochloride acts as an interfacial stabilizer between the two media. When the reaction proceeds, the organic media isolates the oligomers from the reaction sites in aqueous media, making PANi less vulnerable to side linkages. This in turn helps to reduce agglomeration and improves the quality of samples.

In this work, a comparative study of Polyaniline samples synthesized via different routines is done with an attempt to combine self-stabilized dispersion polymerization and eliminating mechanical agitation of the reaction mixture thereby inhibiting the heterogeneous nucleation of PANi nucleates. This work also attempts to quantify and compare the microwave property variation for

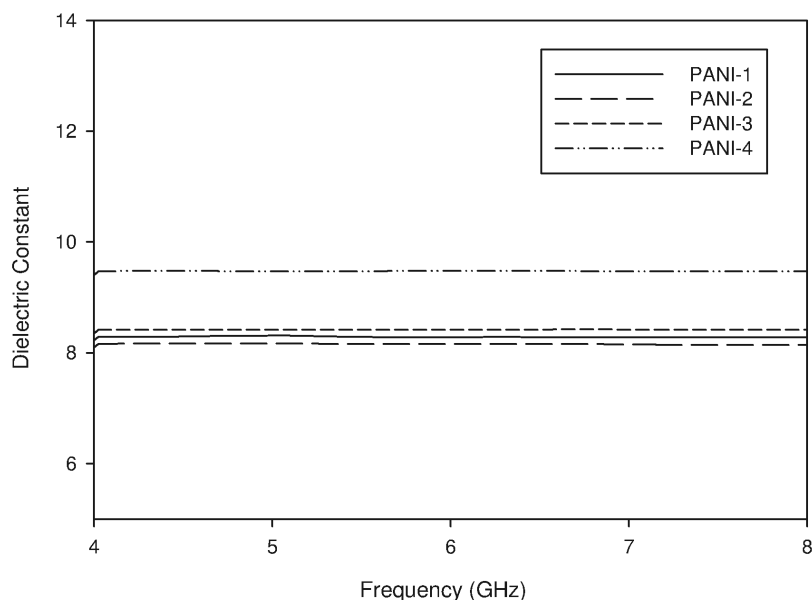


Figure 3.6: Microwave frequency dielectric constant

PANi samples prepared by self stabilized dispersion polymerization in agitation free environment with respect to other synthesis routes. The developed material is investigated for its low frequency and microwave properties and its property dependency on synthesis routine, which is the aim of this study. An attempt to study the radiative properties of such made material for use as polymer antennas is also investigated.

Sample preparation

All chemicals used were of analytical grade from Merck Chemicals. Four samples namely PANi-1 (conventional routine), PANi-2 (without mechanical agitation), PANi-3 (using SSDP), PANi-4 (proposed) were prepared. It has been previously demonstrated that the conductivity of polyaniline with organic acids like Camphor sulphonic acid (CSA) or Naphthalene sulphonic acid (NSA) is many orders higher than that obtained with inorganic acids[116]. For a comparative study between synthesis methods, doping with any inorganic acid would suffice. Hence hydrochloric acid was chosen as the dopant. The reactants were pre-cooled to $0^{\circ}C$. Aniline monomer (5ml) was dissolved

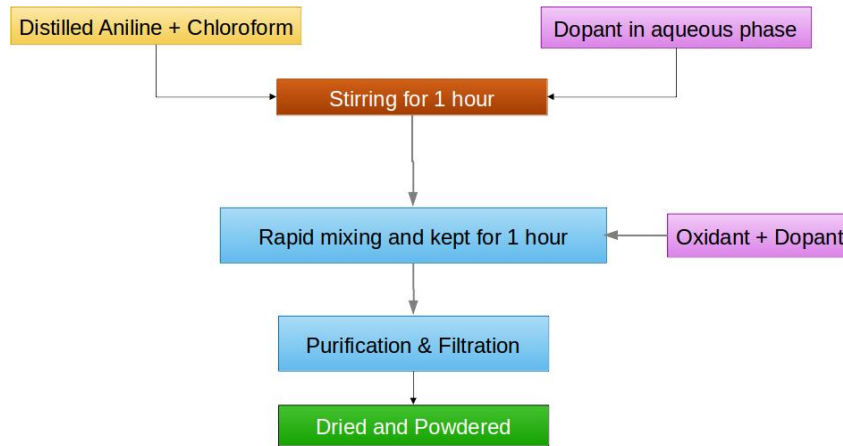


Figure 3.7: Proposed synthesis routine

in 1 Molar aqueous acid (HCl) and mixed with chloroform (aqueous acidic aniline solution: chloroform=2:1). The mixture was kept under constant stirring at 300 RPM in a mechanical stirrer until the mixture became a turbid colloid. The temperature was kept constant at 4°C . Ammonium Persulphate taken in aqueous acidic solution was then added rapidly to the above colloid and stirred for 2 minutes. The mechanical stirring was then stopped and the reaction mixture was allowed to stand for 12 hours. The PANi obtained was filtered, washed with water, dopant acid and acetone. The sample was dried at 50°C in oven for 4 hours, grounded to fine particulates and stored in polyethylene covers. The flowchart in Figure 3.7 shows the steps involved in the proposed synthesis routine.

The powdered samples were pelletized into standard 13 mm diameter cylindrical pellets of height 1.25 mm for low frequency dielectric characterization. Cylindrical samples of average volume= 3.8443mm^3 were prepared from the same 13mm pellet samples for maintaining constancy in packing fraction for microwave dielectric parameter extraction.

Results and discussions

The behaviour of materials towards electromagnetic fields can be entirely attributed to the dependence of dielectric properties over the frequency of incident radiation. A time varying electromagnetic field induces oscillating dipoles in a material composed of permanent dipole moment, upon incidence. Thus

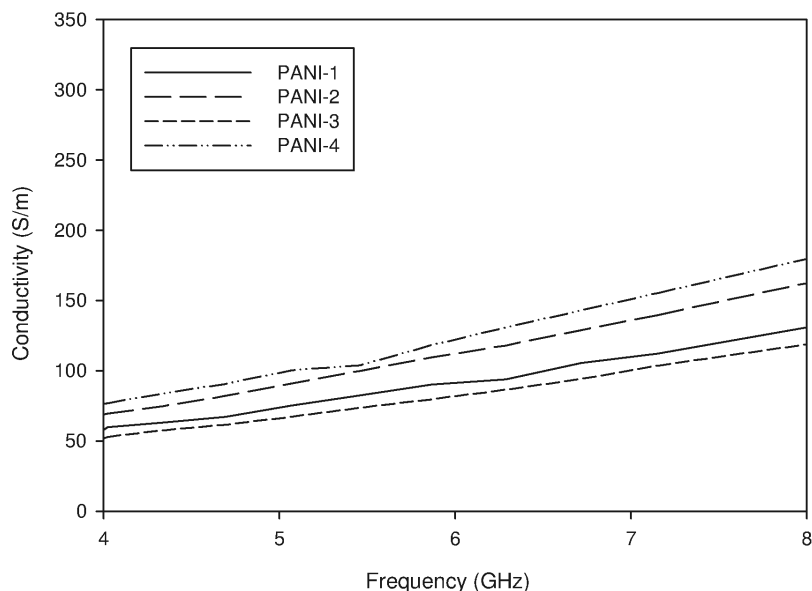


Figure 3.8: Microwave frequency conductivity

the power in the incident radiation propagates through the medium by polarizing the material. Hence the extent to which the medium can be polarized determines the energy storage capacity of the material. Apart from this, a portion of power used to oscillate the dipoles is lost as heat. Radar absorbing materials utilize this property to avoid unnecessary reflections of incident electromagnetic pulse. In the case of conducting polymers, the charge delocalization effect creates free charges. This accumulation of surface charges brings discontinuity in the field induced inside the material. The reduced field strength in the material is accompanied by reflection of a part of incident field from the surface charge sheet present at the conducting polymer boundary. As stated earlier, Polyaniline with HCl dopant contain charges with lesser mobility. Due to this less conductivity of HCl doped PANi samples; they act as lossy material instead of a good electrical conductor, albeit electrical conductivity can be enhanced manifold by dedoping Polyaniline and reprotonating it with CSA or NSA. Thus field do propagate through PANi giving rise to the real part of permittivity in contrast to highly conducting reprotonated PANi samples in which case the constitutive parameters become frequency independent from dc to microwave[117].

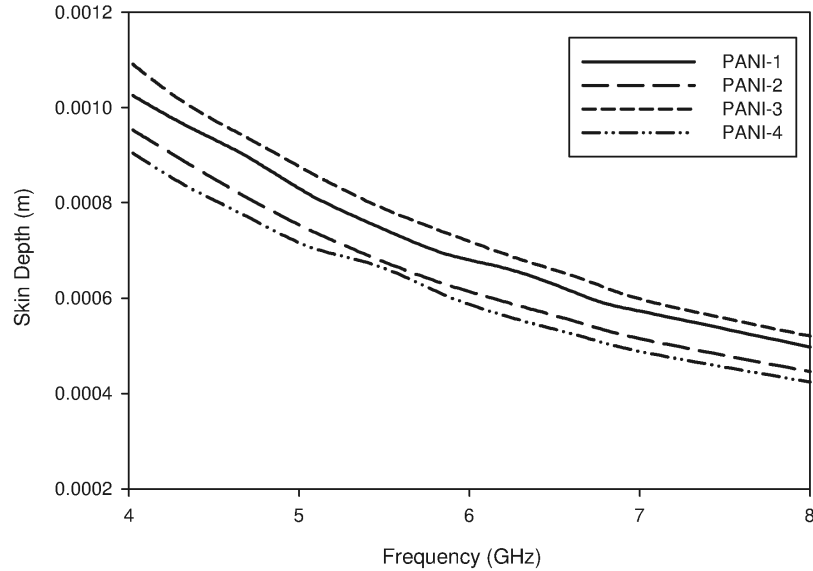


Figure 3.9: Microwave frequency skin depth

1. Dielectric Characteristics

Low Frequency Electronic interactions present in conducting polymers arise out of three processes: intra-chain, inter-chain and inter-domain. A material which is below the percolation threshold contains conductive chains and domains separated by potential barriers. This situation is accompanied by reduced electron hopping probability for chain to chain or for domain to domain transport. In such cases the material under test (MUT) contains a capacitive component and the complex impedance will have a negative imaginary part at the measured frequency. For better conductivity, the material needs to be percolated above the threshold and then the samples will behave inductively. Hence at very low frequencies, it is convenient to measure complex impedance offered by the MUT and then extract the dielectric parameters such as conductivity, dielectric constant, skin depth, loss tangent etc. which are manifestations of the complex permittivity. In short, low frequency dielectric characterization can be expressed in two parameters: conductivity and dielectric constant from the real and imaginary parts of com-

plex impedance respectively. The dielectric constant and conductivity variations against log frequency in the range 20Hz-2MHz are plotted in Figure 3.4 and Figure 3.5 respectively. From Figure 3.5 it is evident that the new method gives very good conductivity at these low frequencies and the material can be considered inductive load which is an indication of better percolation. Also the dielectric constant is greater than that for the other samples. Better dielectric constant indicates better energy storage capacity of the material at these frequencies. It can be seen that the dielectric constant is very high at low frequency. This is because of relaxation process and electrode effects due to polarization between surfaces[118, 119, 120, 121].

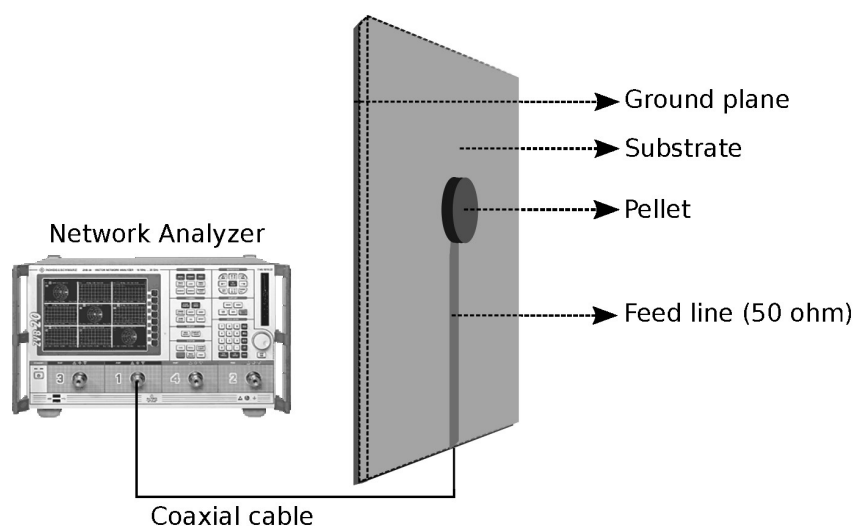


Figure 3.10: Experimental setup for the verification of measured microwave property

Microwave Frequency The microwave material properties evaluated in the C-band indicates that the dielectric constant maintains less variation while the conductivity increases with frequency in the C band as seen from Figure 3.6 and Figure 3.8. This increase can be attributed to the fact that the dipolar oscillations may slip out of phase when the incident field is fast varying. Hence as the frequency increases, the polarization can be resolved into an in-phase component and an out-of-phase component with respect to the incident field, causing thermal

dissipation of microwave energy. The tangent of the angle between these two fields give the loss tangent which is a direct measure of the losses inherent in these materials. In Figure 3.9 the skin depths at C-band for the four samples are compared. It can be seen that it is the lowest for PANi-4. The skin depth decreases with frequency due to the increase in conductive losses alongside dielectric losses.

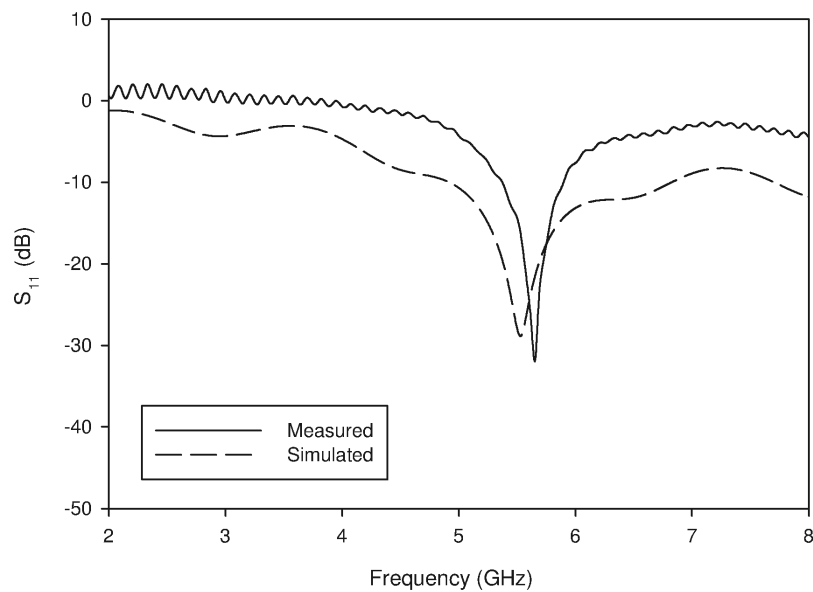


Figure 3.11: Simulated and measured return loss characteristics of the material

2. Absorption Characteristics

The evaluation of material properties thus obtained was done using circuit simulation in CST Microwave Studio. A typical experimental setup consists of a microstrip feed being used to excite a polymer pellet as shown in Figure 3.10. It can be seen from Figure 3.11 that the simulation results are in good congruency with the measurement. For comparison, the return losses of each of the four samples kept on the microstrip feedline are also projected onto Figure 3.12. Apart from the differences in conductivity, the only notable change among these samples is in the dielectric constant. The pellet on the feedline has a resonance at 5.5GHz.

This resonance is at a lower frequency for the sample prepared by new method, when compared with the other three samples. This happens due to an increase in the effective electrical dimensions of the pellet with the increase in the dielectric constant and thus lowering the resonant frequency. From material properties, it has to be noted that the material is not strictly dielectric and that it has some losses. Results indicate that the radiative gain of the polymer pellet on microstrip feed setup is very small (-3.5dB) and that the sharp dip in return loss at 5.5GHz is due to high absorption faced by the coupled field in the lossy dielectric. Thus the power at that particular frequency from the feedline is not radiated to freespace but dissipated in the pellet itself. This proposes applications in the field of radar absorbing materials which selectively absorb power in a desired frequency band.

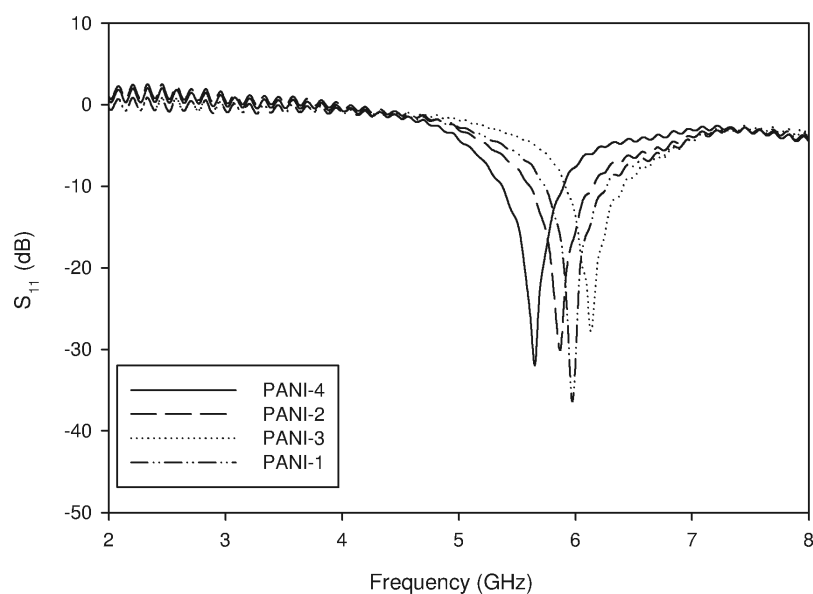


Figure 3.12: Comparison of return losses for the four samples

3. Morphological Characteristics

The morphological properties of a material has significant role in determining its macroscopic properties. In case of conducting polymers, the bulk conductivity is related to the morphology of the material. This

determines the quality of the material. When the particle size decreases, the surface area increases which will significantly improve the inter-chain and inter-domain charge transport. Thus it is required that the particle size be reduced. From Figure 3.13, it can be seen that the size reduction achieved in PANi-4 is better compared to the samples prepared via other methods. This difference will be more prominent in the case of low frequency conductivity. This is because of the fact that the increased surface area aids better conductivity and can be seen in Figure 3.5 which places the new sample well above the others in the conductivity ladder. Also it has to be noted that for the other samples the particle size is large resulting in lesser contact area and increased inter-chain and inter-domain capacitance. Due to high contact area, PANi-4 will exhibit least inter-chain and inter-domain capacitance and was found to exhibit highest inductive reactance. A high inductive reactance is the indication of coiled structure in the particles. But at microwave frequencies, the capacitive impedance of the other samples are reduced and this makes their conductivity appear higher at these frequencies. Conductivity of PANi-4 although ranked highest at these frequencies is slightly reduced which is due to higher inductive impedance offered by the coiled structure. This is not a disadvantage as for use as thin films of polyaniline, a treatment with m-cresol will uncoil the structure and straighten it out, resulting in reduced inductance and higher conductivity.

3.1.3 Summary

The study compares the electromagnetic behaviour of polyaniline samples developed through self-stabilized dispersion polymerization in an agitation-free environment and by other methods. The samples give remarkable property enhancement over the samples prepared via conventional procedures for polymerizing aniline. The C-band material properties such as dielectric constant, conductivity, skin depth etc. are compared with the low frequency spectral characteristics of the samples. The microwave properties are confirmed by simulation studies using microstrip feedline. The material is a lossy dielectric. The morphological studies reveal the cause of better electrical properties obtained in the new method. The PANi samples prepared via this method can be used to develop better processable PANi nanocomposites for various

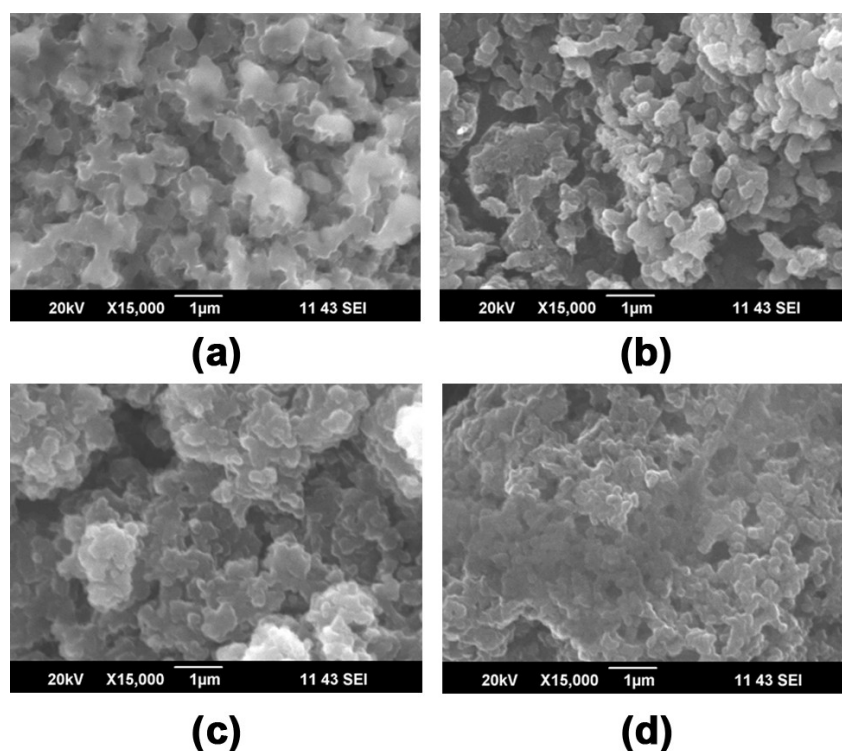


Figure 3.13: SEM images of samples (a) PANi-1, (b) PANi-2, (c) PANi-3, (d) PANi-4

microwave applications like frequency selective surfaces, radar absorbing materials, wave attenuators etc.

3.2 Graphite and its derivatives

Graphite is considered as a wonder material which happens to be an allotrope of carbon. It has a lot of properties which make it stand of as a special status material such as:

- Excellent electrical and thermal conductivity[122]
- Good thermal shock resistance [123]
- High mechanical strength[124]
- Low coefficient of thermal expansion[125]

- Low coefficient of friction[126]
- Superb chemical resistance[127]
- One of the lightest of all reinforcing agents[128]

When in diamond, carbon is SP^3 hybridized, the carbon atoms in graphite are SP^2 hybridized, leaving way for a π bond. Graphite has a layered structure with each layer formed out of a sheet of SP^2 bonded carbon atoms. The individual layers are called graphene. The layers are held together via Van der Waal's forces. Hence the layers slide over each other if applied with shear stress parallel to it. The remarkable property in this is that the electrons in the π bond are free to travel through the material. Hence it is electrically conductive. Because of this high conductivity, it is used in electrodes, batteries and solar cells. There are different types of graphite[129] such as:

- Flake graphite

Flake graphite (Figure.3.14) is found in metamorphic rocks uniformly distributed through the body of the ore or in concentrated lens shaped pockets. Carbon concentrations vary between 5% and 40%. Graphite flake occurs as a scaly or lamella form in certain metamorphic rocks such as limestone, gneisses and schists. Flake graphite is removed by froth flotation. "As floated" graphite contains between 80% and 90% graphite. Flake graphite is produced with $> 98\%$ through chemical beneficiation processes. Flake graphite is a key component of the lithium-ion batteries used in electric vehicles. Flake graphite is also an essential part of vanadium-redox battery technology, with nearly 300 tonnes of flake graphite required per 1,000 megawatts of storage.

- Highly Oriented Pyrolytic Graphite

Highly Oriented Pyrolytic Graphite (HOPG) and Thermoconductive Pyrolytic Graphite (TCPG) are forms of high purity Pyrolytic Graphite (Figure.3.15) annealed under pressure and high temperatures and refers to graphite with an angular spread between the graphite sheets of less than 1° . HOPG specimens are layered polycrystals, similar to mica. Each bulk polycrystal looks like mosaic of microscopic monocrystal grains of different sizes. The structure is columnar, the columns run vertically within the flat slab of the material, and the grain boundaries can be seen



Figure 3.14: Flake graphite

on the lateral surfaces. The grains are slightly disoriented with respect to each other.

- Amorphous graphite

Amorphous graphite (Figure.3.16) is the least graphitic of the natural graphites. However, the term "amorphous" is a misnomer since the material is still crystalline. Amorphous graphite is found as minute particles in beds of mesomorphic rocks such as coal, slate or shale deposits. The graphite content ranges from 25% to 85% dependent on the geological conditions. Amorphous graphite is used in the refractories industry to manufacture crucibles, ladles, molds, nozzles and troughs that can withstand very high temperatures, particularly the casting of steel. Indeed, the electrodes used in many electrical metallurgical furnaces, including the electric arc furnaces used in steel processing, are manufactured from this type of graphite. It is also used to make pencil lead.

- Lump graphite



Figure 3.15: Highly oriented pyrolytic graphite

Crystalline vein graphite (Figure.3.17) is believed to originate from crude oil deposits that through time, temperature and pressure have converted to graphite. Vein graphite fissures are typically between 1cm and 1 m thick, and are typically $> 90\%$ pure. Vein graphite is used in advanced, thermal and high-friction applications such as car brakes and clutches. It can also be used in much the same way as flake graphite as its shows great performance in applications that require high thermal and electrical conductivity.

- Synthetic graphite

Synthetic graphite (Figure.3.18) can be produced from coke and pitch. It tends to be of higher purity though not as crystalline as natural graphite. There are essentially two types of synthetic graphite. The first is electrographite, which is pure carbon produced from calcined



Figure 3.16: Amorphous graphite

petroleum coke and coal tar pitch in an electric furnace. The second type of synthetic graphite is produced by heating calcined petroleum pitch to 2800°C . On the whole synthetic graphite tends to be of a lower density, higher porosity and higher electrical resistance. Its increased porosity makes it unsuitable for refractory applications. Synthetic Graphite consists mainly of graphitic carbon that has been obtained by graphitization, heat treatment of non-graphitic carbon, or by chemical vapour deposition from hydrocarbons at temperatures above 2100K . Synthetic graphite can also be made from high temperature treatment of carborundum (Silicon Carbide) by eradicating silicon from it.

The derivatives of graphite can be classified into three on the basis of their nature of reaction[130]

- Surface compounds



Figure 3.17: Lump graphite

They are formed at the surface atoms of graphite structure because of the reactivity that these regions exhibit owing to the free valence bonds at the edges. An example for this reaction would be oxidation which is involved with the surface and edge carbon atoms.

- Substitutional compounds

They are so named because, these graphite compounds contain foreign atoms in place of the normal SP^2 carbons. It is sometimes considered as doping. An example is the substitution of boron in carbon lattices of graphite.

- Intercalation compounds

The intercalation compounds of graphite are interstitial compounds in which the foreign species is included in the interplanar spaces of the



Figure 3.18: Synthetic graphite

graphite structure. They are very exotic materials which have a lot of enhanced properties suitable for energy storage, energy harvest, superconductivity etc. The next section is a study based on these materials.

3.2.1 Graphite Intercalation Compounds

Graphite intercalation compounds (GIC) are graphite derivatives which are formed by the intercalation of foreign molecular species in between the layers of graphite. As the graphite layers are strongly bonded than that between adjacent layers, any intercalating agent will push apart the layers without breaking the individual layers. The intercalation can be physical or chemical. As per the nature of bonding it can be divided into two[131]

- Covalent or homopolar bonding

In this case, the intercalating species forms covalent bonding with the carbon atom in the plane by converting the trigonal SP^2 hybridization to SP^3 hybridization. As a result, the planes become physically curved and the material loses its inherent electrical conductivity arising from the conjugated double bonds. An example is graphite oxide, tetracarbon monofluoride etc.

- Partially ionic or polar

In these components, the intercalating species involves in an ionic bond with the graphite structure which results in electron donating or accepting in the graphite layers and consequently a shift in Fermi energy. Thus it enhances properties of the graphite and hence is considered as an important class of graphite derivatives. When an excess of these intercalating agents are used, they form ordered interlayer structures or lamellar structures. When this excess concentration is removed, the interlayer structures disappear although a small amount of residue remains. The extent to which the intercalation happens is marked by a stage number. A graphite structure is considered as stage one intercalated if two interlayer structures are separated by one graphene layer. The number of graphene layers between two adjacent interlayers of intercalates define the stage number. If the intercalation agent concentration is more, the stage number becomes less and the number is identified using XRD. There are a collection of this species as listed below:

– Graphite-Halogens

Halogens form ionic bonds by accepting electrons from graphite as they are electronegative. Fluorine and bromine react easily from their vapours whereas iodine and chlorine form compounds by the aid of interhalogens like iodine bromide, iodine monochloride etc. The end products are p-type materials.

– Graphite-Alkali metals

Alkali metals like lithium, sodium, potassium, rubidium, and cesium can intercalate by donating electrons to the graphite layer. This interaction results in the structure becoming an n-type material. These are prepared by heating graphite with any of these metals in an evacuated chamber. The following electric and magnetic changes are to be noted due to this type of ionic intercalation:

1. Decrease in the electrical resistivity in both a and c axes
2. Decrease in anisotropy ratio of electrical resistivity
3. Increase in the positive temperature coefficient of electrical resistivity along both a and c axes

4. Change in sign of the thermoelectric power in both a and c axes,
 5. Decrease in the negative Hall coefficient with increasing intercalate concentration
 6. Anomalies in the electrical conductivity in the temperature range 77 ± 360 K.
 7. Change of the magnetic susceptibility from negative to positive
 8. Changes in the g-shift and the linewidth of the electron spin resonance
 9. Knight shift of the Cesium-133 nuclear magnetic resonance.
- Graphite-Acid compounds

The reaction of graphite with acids like nitric acid, sulfuric acid, perchloric acid, and selenic acid results in the formation of intercalation compounds called acid salts of graphite. This reaction gives the graphite a p-type doping. The most prominent ones are graphite-nitrate and graphite-bisulfate. Graphite-nitrate can be made by intercalating nitric acid directly into graphite. Graphite-bisulfate is a reaction with sulphuric acid in the presence of an oxidizing agent. The stage-1 compounds of these are in blue color and they can be converted to higher stage numbers by dilution with water.

- Graphite-Halide compounds

Graphite-halides are those intercalation compounds formed by the halides like ferric chloride. These halides are electron acceptors which donate holes to the graphite layers. A high temperature treatment of these halides with graphite will make them intercalate into the layers. By varying the reaction temperature, which is above 180°C , different stages can be obtained. The material is a p-type semiconductor.

3.2.2 Exfoliated graphite

With the application of adequate heating graphite intercalation compounds exfoliate due to the expansion of intercalants[132]. The exfoliation involves a large expansion along the c-axis. The process involves the intercalate in the

graphite to vaporize, thus forming gas pockets which burst. The expansion of the gas pockets is made possible by the shear of the graphite layers with respect to one another. If the pockets do not burst and the heating is not excessive, the exfoliation can be reversible upon subsequent cooling. However, excessive heating causes irreversible exfoliation.

Better quality exfoliation is achieved when flake graphite is used to intercalate and then exfoliating it as flakes have parallel layers and the expansion is not hindered by defects along the *c* axis. After exfoliation the flake is much longer along the *c*-axis than in the in-plane direction, which is why it is referred to as a worm. Due to the cellular structure of each worm, the compression of a collection of worms without a binder results in mechanical interlocking among the worms. This results in a sheet form called flexible graphite. This sheet can be cut to any shape and hence it finds application as a gasket material for harsh environments as graphite is inert and temperature-resilient and also for electro-magnetic interference shielding due to its electrical conductivity and high specific surface area enhance the reflection of high-frequency electromagnetic radiation.

Exfoliated graphite has a viscous and elastomeric features because of the ease of sliding of the graphite layers relative to one another in the cell wall of the cellular structure of exfoliated graphite. As a consequence of this viscous character, exfoliated graphite is an attractive component for formulating materials for vibration damping. Because of its resiliency and connectivity, exfoliated graphite is an attractive component for formulating thermal interface materials, which are needed for improving thermal contacts, such as the contacts between a microprocessor and a heat sink in an electronic package. Furthermore, exfoliated graphite is attractive as electrochemical electrode materials, because it provides handleability and excellent volumetric and interfacial conductivities. Exfoliated graphite may even be disintegrated mechanically to form graphene.

3.2.3 Synthesis and characterization of exfoliated graphite

Exfoliated graphite is prepared from intercalated graphite. Hence it is necessary to intercalate any of the forms of graphite with suitable intercalation compounds to get exfoliated graphite powder. In this section, the preparation of exfoliated graphite is discussed. It has been seen that the intercalation

of graphite is based on the same methods for the preparation of graphene oxide (GO), except the temperature constraints and the relative amount of the reactants used. The common method by which the graphene oxide is prepared happens to be the Hummer's method[133] and its modifications[134]. In this method, flake graphite or natural graphite is used as the precursor. It is treated with sulphuric acid, Sodium nitrate and Potassium permanganate in the presence of Hydrogen peroxide. This results in the formation of Dimanganese heptoxide which is a powerful oxidant[135]. It causes oxidation of the layer edges of graphite causing the edges to puff up a bit due to the presence of hydroxyl group. This aids in the intercalation process as now under sufficient conditions, it eases the diffusion of intercalants through these edges. If the concentration of the intercalants is much higher, at above a particular temperature, the vapor pressure of the intercalant becomes sufficient to overcome the threshold potential for intercalation. So at times when the GO preparation happens to be at a significantly higher concentration, rather than oxidation, the prominent reaction will be intercalation. In these reactions the amount of graphite taken is much higher than that is used in the preparation of GO. The oxidation reaction preferentially happens at the edge defects in the graphite flakes as they happen to be the most reactive sites in graphite. Hence, when the amount of graphite is taken in excess, then the oxidation happens only at the edges and paves way for the intercalants to intercalate into the layers. This is then washed and filtered to remove excess intercalants and oven dried to obtain the intercalated samples. Such made samples are to be rapidly heated so that the intercalants expand due to the excessive heating and are released by shearing apart the stacked graphene layers[136]. This results in the rapid expansion of intercalated graphite in the c axis direction giving the expanded graphite its worm-like morphology. The process can be done with microwave irradiation and is known as microwave assisted exfoliation[137] of intercalated graphite.

It has been demonstrated that there are other methods to achieve exfoliation of graphite such as those by liquid phase exfoliation[138], solvent interface trapping[139], ultrasound assisted exfoliation in supercritical CO₂[140], stirring induced shear exfoliation in surfactant media[141], electrochemical exfoliation[142] etc. Among these, the scope for mass production in a time critical method happens to be the microwave exfoliation and the electrochem-

ical method. Due to its simplicity, microwave assisted exfoliation was selected for this study.

An improvement of Hummers method proposed by Tour's group at Rice University is the basis of this synthesis[143]. The advantage of the Tour method consists in a production of graphene oxide having a higher hydrophilic degree, in contrast with GO produced by Hummers method. Hence, this graphene oxide results more oxidized and soluble. It is also possible to intercalate graphite using the Tour's method although it was proposed as a method for GO preparation. In this, flake graphite is treated with a combination of sulphuric acid, phosphoric acid and potassium permanganate. The method involves the use of H_2SO_4/H_3PO_4 in a ratio of 9:1 with an increased amount of $KMnO_4$. The advantage of this method consists in no generation of toxic gases, such as NO_2 or ClO_2 , in the reaction and an easy temperature control. The presence of phosphoric acid generates a more intact graphitic basal plane. In this work, exfoliated graphite was prepared by microwave irradiation and as such prepared powder sample was characterized in the microwave frequency range. The material is tested for its potential use as flexible conductors in microwave frequency.

Sample preparation

All chemicals used were of synthesis grade from Merck Chemicals. Redundant samples were prepared for testing and verification of properties. The intercalation is performed by Tour's method with excess graphite. A typical synthesis via this method is elucidated in the Figure.3.19. Flake graphite of mesh size 150 is used as the start material. A treatment of 5g of flake graphite with 8ml sulfuric acid, 2ml phosphoric acid and 1.8g of potassium permanganate at 10°C for four hours will allow the intercalation of sulphuric acid into the graphite structure. A miniscule of such made sulfuric acid intercalated graphite is kept in a ceramic crucible and irradiated with microwave. This expands the graphite into large volume due to the release of trapped gases in the interplanar layers and is performed in a well ventilated area as the evolving gases are corrosive. Such made expanded graphite are stored in containers. For FTIR, SEM and XRD measurements, the powder samples are used as such. For measuring the dielectric properties at microwave frequencies, the powder sample was coated onto PMMA substrates with the aid of

Sample	Thickness (mm)	DC conductivity (S/m)
Graphene-1	0.35165	10156.20
Graphene-2	0.34845	8968.29
Graphene-3	0.26865	15509.65

Table 3.1: DC conductivity of the synthesized expanded GICs

hydrolic press. The binder used was commercially available spray pressure sensitive adhesive (PSA) from Molyduval[144]. The substrate is sprayed with a layer of PSA. Then the substrate is inserted into the die over which 0.1g of the expanded graphite is evenly distributed. The die is then subjected to a pressure of 100 kg/cm^2 which results in the adhesion of expanded graphite as a silvery foil onto the substrate with the aid of PSA. These foils are highly electrically conducting and the resistance happens to be less than an ohm per square. These samples are named as Graphene-1 (expanded graphite intercalated with sulphate), Graphene-2 (expanded graphite intercalated with iron chloride), and Graphene-3 (expanded graphite intercalated with zinc chloride).

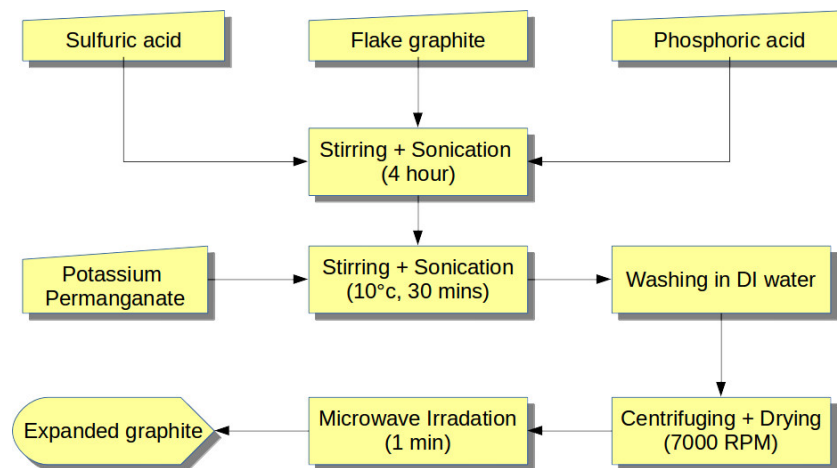


Figure 3.19: Synthesis steps involved in expanded graphite preparation

Results and discussions

1. DC conductivity

The DC conductivity of the samples were calculated from sheet resistance using the formula $\sigma = 1/(R_s \times t)$. This tabulated in Table.3.1. It can be seen that the the Zinc chloride intercalated sample has better conductivity among the three.

2. Fourier transform infrared spectroscopy

The FTIR spectra of the samples are shown in the Figure.3.20. Oxidation peak around 3468cm^{-1} is not prominent for sulfuric acid GIC (Figure.3.20a). It can be seen that the sulfuric acid GIC exhibits O-H bending at 1366cm^{-1} , C-O stretching at 1218cm^{-1} , C=O stretching at 1739cm^{-1} , C=C stretching at 1633cm^{-1} , C-H deformation vibration at 1442cm^{-1} , C-C skeleton vibration at 538cm^{-1} and 432cm^{-1} . It is to be noted that the iron chloride GIC (Figure.3.20c) shows the characteristic oxidation signal at 3468cm^{-1} due to the stretching of -OH (hydroxyl) groups. There are also signals corresponding to C=O stretching at 1736cm^{-1} , C=C stretching at 1641cm^{-1} , O-H bending at 1367cm^{-1} , C-O stretching at 1219cm^{-1} , C-C skeleton vibration at 536cm^{-1} and 449cm^{-1} . In the case of zinc chloride GIC (Figure.3.20e), the oxidation signal is very prominent at 3462cm^{-1} . Other absorptions are at 1738cm^{-1} due to C=O stretching vibration, 1633cm^{-1} due to C=C stretching vibration, 1366cm^{-1} due to C-H deformation vibration, 1217cm^{-1} due to C-O stretching, C-C skeleton vibration at 532cm^{-1} and 449cm^{-1} . The FTIR of exfoliated product (Figure.3.20b) is also measured. In this, 2919cm^{-1} and 2850cm^{-1} happens to be C-H stretching vibrations, 1730cm^{-1} due to C=C stretching vibration, 1365cm^{-1} due to C-H deformation vibration, 541cm^{-1} and 408cm^{-1} due to C-C skeletal vibrations. In this case, the skeletal vibrations become prominent after exfoliation because of the more degree of freedom gained after expansion along the c-axis of GIC. For comparison, the FTIR of graphene oxide prepared via Tour's method is given in Figure.3.20f. It can be distinguished that GO and GIC differs at the peak at 3486cm^{-1} , wherein, GO exhibits a broader peak due to the excessive amount of oxidation while, GICs have lesser peaks in the region.

3. X-Ray diffraction study

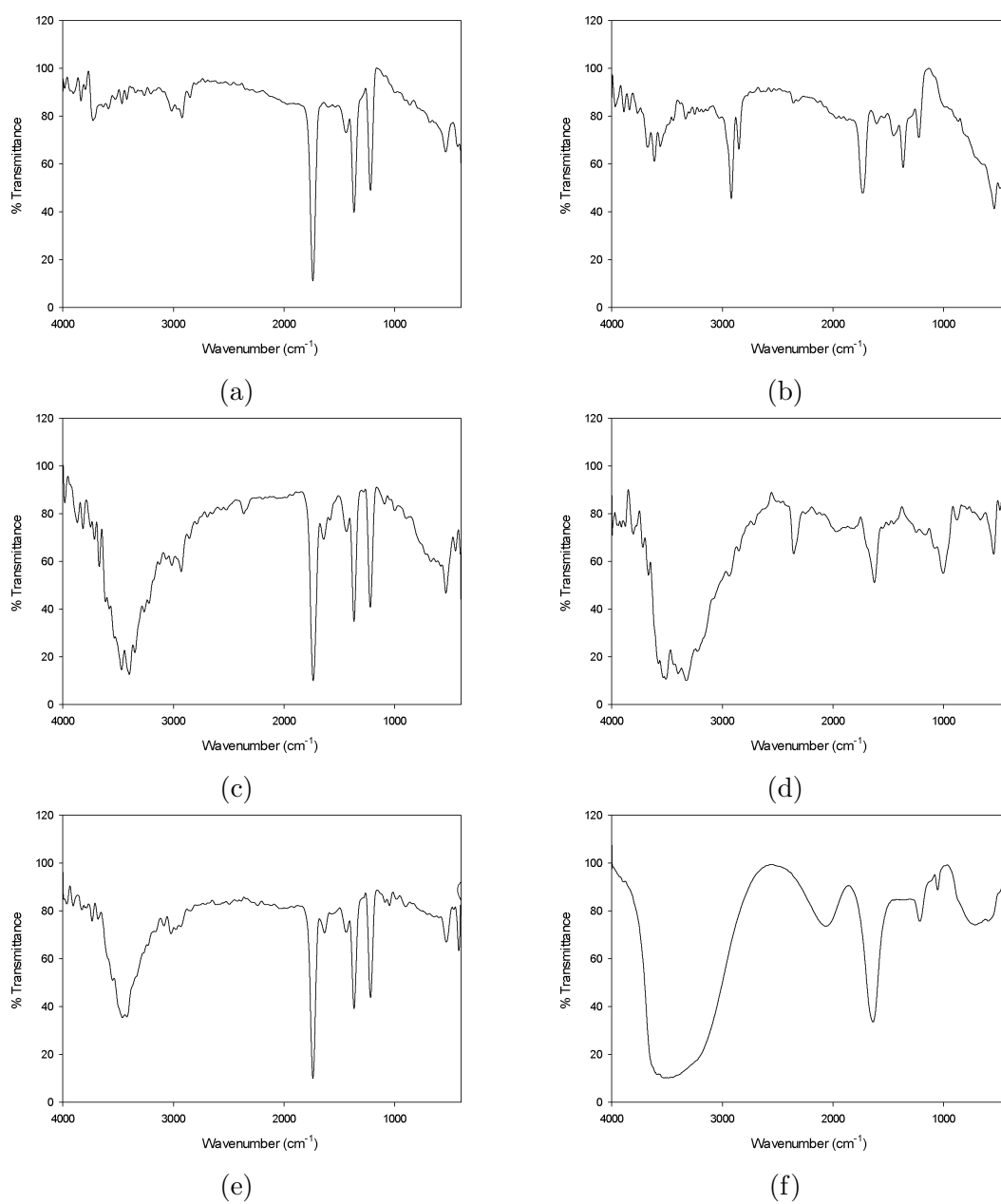


Figure 3.20: FTIR graphs of a) GIC of Sulphate, b) expanded GIC of sulphate, c) GIC of Iron chloride, d) Flake Graphite, e) GIC of Zinc chloride, f) Graphene oxide

The X-ray diffraction curves are shown in the Figure.3.21. The stan-

standard flake graphite (Figure.3.21d) has two peaks at angles $2\theta = 26.6^\circ$ corresponding to the (002) plane with an interlayer spacing of 3.34nm and at $2\theta = 54.7^\circ$ corresponding to the (004) plane having an interlayer distance of 1.37nm. The intensity of these peaks are very high due to the large number of stacked graphene layers in flake graphite from which the X rays are reflected. In the case of sulfuric acid GIC (Figure.3.21a), the intensity of reflection is so high for (002) plane at $2\theta = 25.87^\circ$. The (004) layer also is a prominent peak. The graphene oxide (Figure.3.21f) has a peak at $2\theta = 11.64^\circ$ which is typical of GO with a comparatively higher interlayer spacing of 7.596nm due to intercalation of water molecule and other species. The peak at $2\theta = 26.6^\circ$ and that at $2\theta = 54.7^\circ$ has vanished completely due to complete conversion into oxidized state. It is of significant importance the fact that the reflections from microwave exfoliated GIC (Figure.3.21b) observed at $2\theta = 26.6^\circ$ is much lesser than that of its parent sulfuric acid GIC. This shows that the layers have been expanded significantly resulting in lesser reflections at $2\theta = 26.6^\circ$ without any change in interplanar distance and virtually no peak at $2\theta = 54.7^\circ$. As was predicted from the FTIR analysis, the iron chloride GIC (Figure.3.21c) has some amount of oxidation leading to the appearance of a broad peak at $2\theta = 11.64^\circ$. But the intensity of $2\theta = 26.6^\circ$ peak happens to be significantly lower than that for sulfuric acid GIC. This is of importance as the expansion of such a material can be volumetrically more. Similarly the intensity values of $2\theta = 54.7^\circ$ is also lesser. The case of zinc chloride GIC (Figure.3.21e) is also the same as that in the case of iron chloride GIC with the presence of GO indicated by the peak at $2\theta = 11.64^\circ$ although at a lesser intensity. The intensity of the $2\theta = 26.6^\circ$ peak is lesser than the iron chloride GIC which proposes better exfoliation for zinc chloride GIC during exfoliation and was found so during microwave exfoliation of it.

4. Morphological characteristics

Scanning electron microscopy (SEM) images of the samples are taken for further insight into their structures and to confirm the quality expected from FTIR and XRD results (Figure.3.22). In flake graphite, the graphite sheets will have a large number of layers which can be viewed

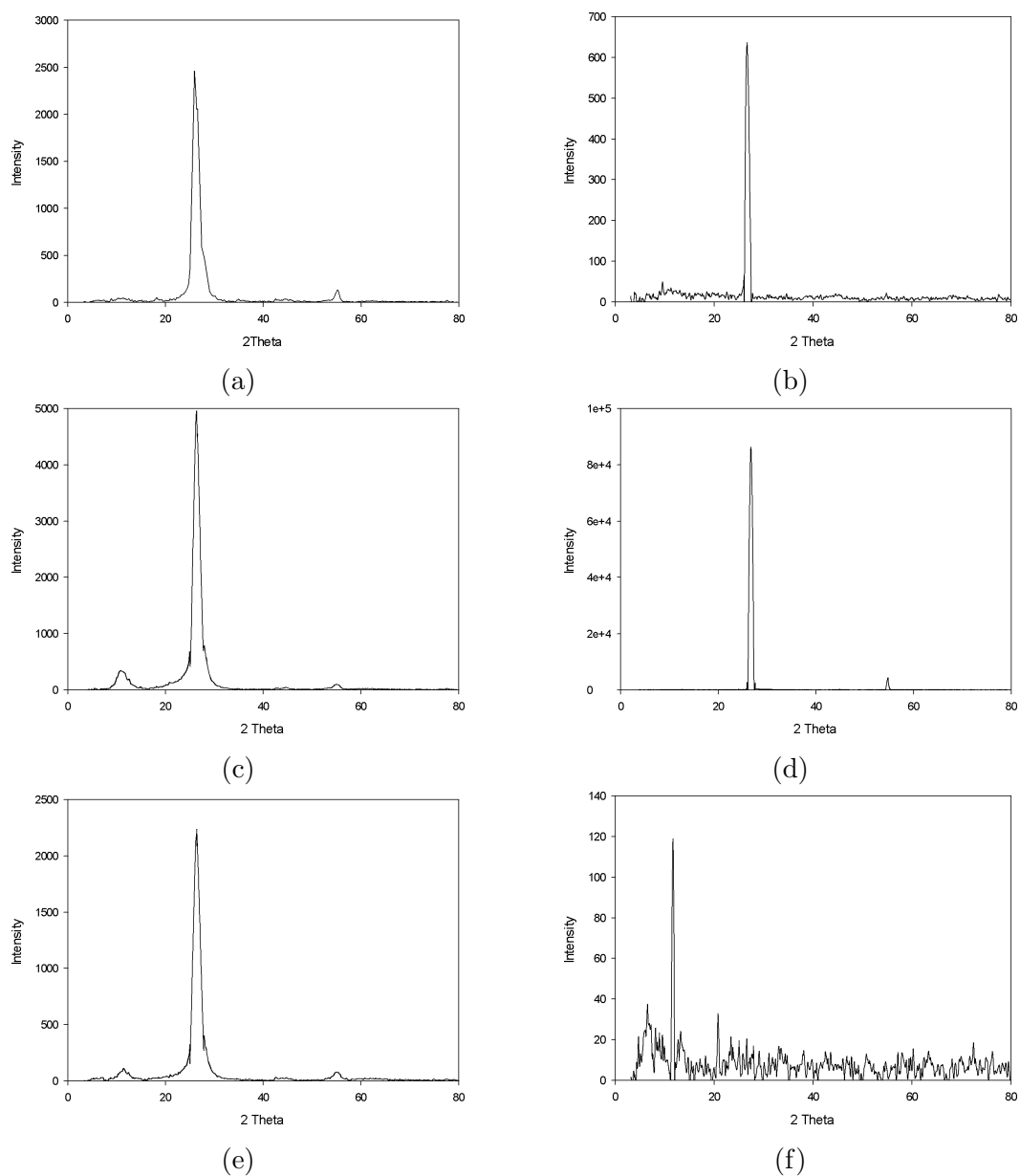


Figure 3.21: XRD graphs of a) GIC of Sulphate, b) expanded GIC of sulphate, c) GIC of Iron chloride, d) Flake Graphite, e) GIC of Zinc chloride, f) Graphene oxide

as bright spots as seen in Figure.3.22d. In the case of GICs, this bright regions disappear and only puffed up layers are viewed. This is due to

the intercalation of foreign species into the interlayer spacing which is evident from the SEM images of sulfuric acid (Figure.3.22a), iron chloride (Figure.3.22c) and zinc chloride (Figure.3.22e) GICs. If any of these GICs are stressed under microwave irradiation, the intercalants in the interlayer spaces are excited and the energy received from microwaves is used to push apart the layers forming thinner layers with very large expansion in the c axis. This is evident in the SEM image of exfoliated graphite (Figure.3.22b) derived from sulfuric acid GIC. It can be seen that the SEM of GO (Figure.3.22f) consists of very thin exfoliated layers of oxidized sheets. Owing to the higher degree of oxidation in this sample, the layers are easily peeled off by mechanical shear applied by ultrasonic cavitation or even by a magnetic stirrer.

5. Microwave complex permittivity

The three GICs were microwave exfoliated into their corresponding expanded forms which are the end products that are to be used in various applications proposed in Chapters 4 and 5. As a result, now the sample set consists of three exfoliated GICs - sulphate GIC (Graphene-1), Iron chloride GIC (Graphene-2), Zinc chloride GIC (Graphene-3). The reflection and transmission 2 port S-parameters are measured for the samples using Vector Network Analyzer (VNA) and the microwave complex permittivity as calculated by Nicolson-Ross-Weir method is shown in Figure.3.23.

It is to be noted that all the three samples exhibit very high real part of permittivity (Figure.3.23a). The imaginary part (Figure.3.23b) happens to be very high for Graphene-3. This was expected from the fact that better exfoliation was obtained in the case of Zinc chloride GIC. Graphene is usually considered as a weakly magnetic or diamagnetic material with permeability less than 1. But when intercalated with foreign species, its permeability changes accordingly and they can achieve ferromagnetic or ferrimagnetic states. For Graphene-1, the real permeability (Figure.3.23c) is the highest whereas for the samples Graphene-2 and Graphene-3, the real values are almost similar as they are of the category of metal halide GICs. The magnetic losses are manifested in the imaginary part of the permeability which indicates higher magnetic losses for Graphene-1 as shown in the Figure.3.23d.

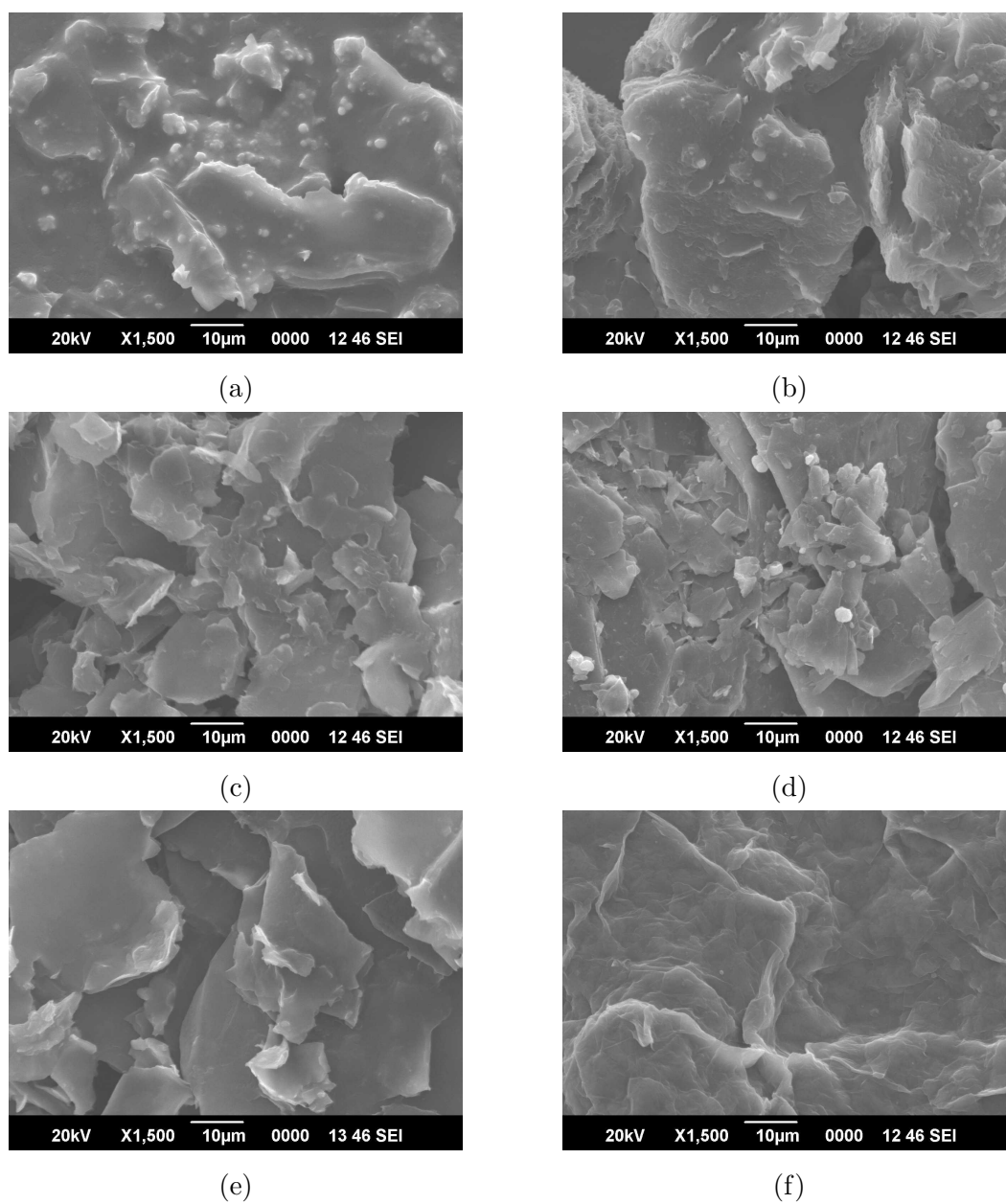


Figure 3.22: SEM micrographs of a) GIC of Sulphate, b) expanded GIC of sulphate, c) GIC of Iron chloride, d) Flake Graphite, e) GIC of Zinc chloride, f) Graphene oxide

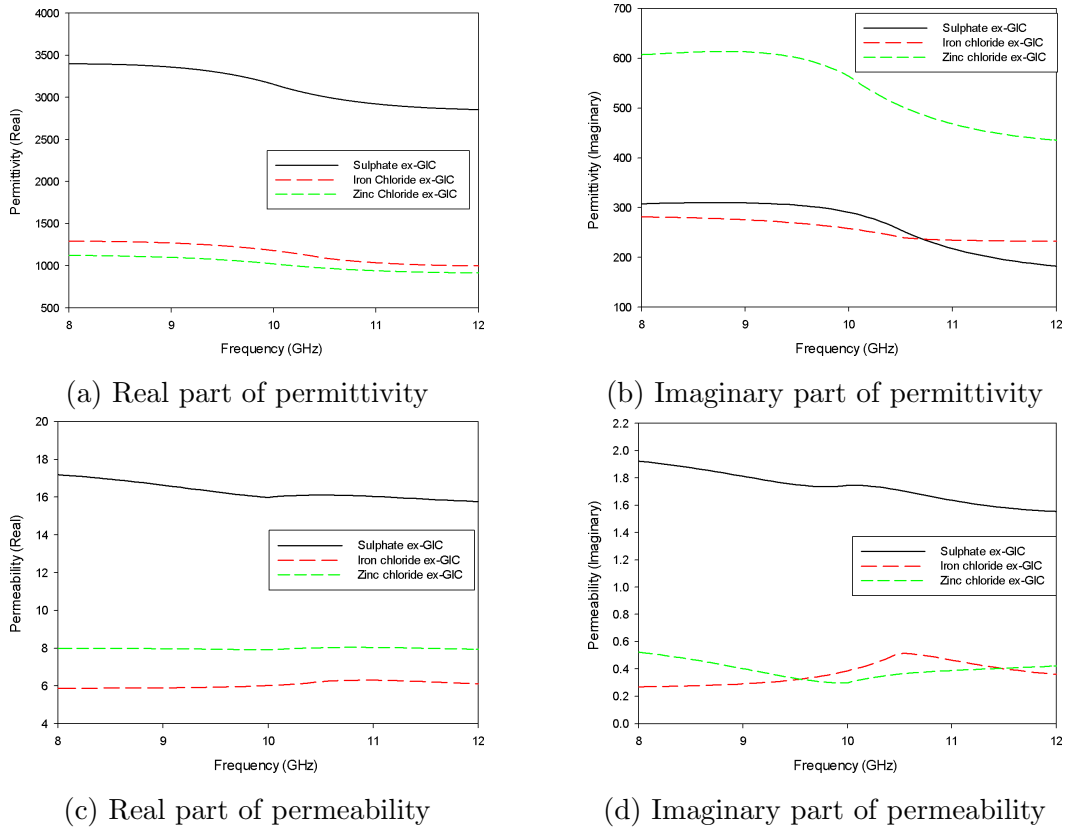


Figure 3.23: Microwave complex permittivity of expanded GICs of Sulphate, Iron chloride and Zinc chloride at X band

3.2.4 Summary

This section discusses the different forms of graphite, especially the graphite intercalated compounds of it which are of significant importance in the light of tuning electrical parameters that differ from the parent material. The material properties have been studied by analyzing DC conductivity, FTIR spectra, XRD, SEM and they are characterized in microwave X band for their complex permittivity and permeability. The synthesized materials offer very good conductivity and hence a potential candidate for replacing metallic structures in printable electronics.

3.3 Composites of Polyaniline and Graphite

In this section, an attempt is made to synthesize a composite of Polyaniline and expanded graphite. Pure PANi is often modelled as metallic islands dispersed in a pool of insulator which determine the bulk conductivity apart from doping density. Despite the good conductivity of PANi, the processibility of these materials pose a difficulty in enhancing the conductivity. Hence it is difficult to have PANi with very high conductivity without the need for secondary dopants and dispersive organic solvents such as m-cresol and NMP. Such enhanced forms of PANi require removal of excess solvents which have high boiling points. Graphene being a zero band gap material, it has many attractive features when combined with non-zero band gap materials like PANi in applications like charge storage, sensors, tunable conductivity, tunable optical properties, electronically switchable bandgap etc[145, 146, 147, 148]. But dispersions of graphene are difficult to stabilize and hence it takes significant chemical treatments prior to application-level implementation which might reduce the conductivity. Being a layered structure of carbon atoms in SP² hybridized state, graphene has very high planar conductivity due to charge delocalization all over a single layer of graphene sheet, although the interplanar electron hopping is lesser comparatively. This high planar conductivity can be utilized to bridge the metallic islands in PANi. The conductivity of PANi can be increased by grafting them onto graphene sheets. The composite acts to bridge the metallic islands by complementing each other in a way that wherever PANi has lesser conductivity, graphene sheets would compensate and vice versa. It is a potential candidate for microwave applications such as wearable antennas. The following work reports the synthesis and characterization of Polyaniline – microwave exfoliated graphene (PANi-Graphene) composites for microwave applications.

3.3.1 Synthesis and characterization of PANi - graphene composite using gelatin as dispersion stabilizer

PANi or graphene cannot form solutions in any of the solvents, but very good dispersions of them can be made using certain organic solvents in which the resultant supermolecular structure is solution processible. However, graphene solutions are made using oxidation of graphene into graphene oxide (GO),

which form good solutions in water and other solvents. But the conductivity of GO is much less in its oxidized state than for making solutions and films, it is of less importance in electronics. The GO solutions can be converted back to graphene by strong reducing agents like hydrazine[149, 150, 151] or by microwave irradiation[152]. The preparation of PANi is done usually in aqueous media with acidic dopants. But at such lower pH values, graphene particulates into micrometer sizes due to van der Waal interaction and due to its inherent hydrophobic nature. Thus the nucleation sites of PANi becomes heterogeneous. This is why most prefer a GO PANi composite rather than graphene in the synthesis of PANi-graphene composites[153]. The complexity of the reducing GO back to graphene haunts such preparation methods. For better conductivity, the graphene layers should be well dispersed in the reaction medium. Researchers have overcome the problem of agglomeration in lower pH media by using dispersion stabilizing agents such as Polystyrene Sulfonate (PSS)[151, 154] and also by hydrazine/microwave reduction of GO solutions with simultaneous ultrasonication[155] prior to chemical oxidative polymerization of aniline monomers. These methods involve corrosive and exotic chemicals.

In this work the PANi-Graphene composite is prepared in stable pH value in the presence of gelatin as dispersion stabilizer. Gelatin is a protein biopolymer derived from the hydrolysis of collagen fibres in animal tissue. It is considered as an amphiphilic molecule with affinity towards both polar and non polar molecules[156]. Such molecules exhibit surfactant like behaviour in forming aqueous-oil emulsions. The authors have stabilized the microwave exfoliated graphene by using gelatin as dispersion stabilizer with anilinium camphorsulfonate. Anilinium camphorsulfonate acts as a secondary stabilizer and as the PANi precursor. Thus a stable emulsion is obtained with no sediments of graphene agglomerations. It has been found that water soluble PANi can assist in the dispersion stability of graphene in acidic media[157]. Thus as the polymerization progresses, the dispersions are more stabilized by the reaction products itself. Such made PANi-graphene composites were used for microwave characterization and for the fabrication of polymer antenna. The low frequency impedance analysis is also done to evaluate the superior property of the material. The PANi-Graphene polymer antenna is fabricated. The S_{11} and S_{21} are measured and compared with a similar antenna made in copper and another in pure PANi.

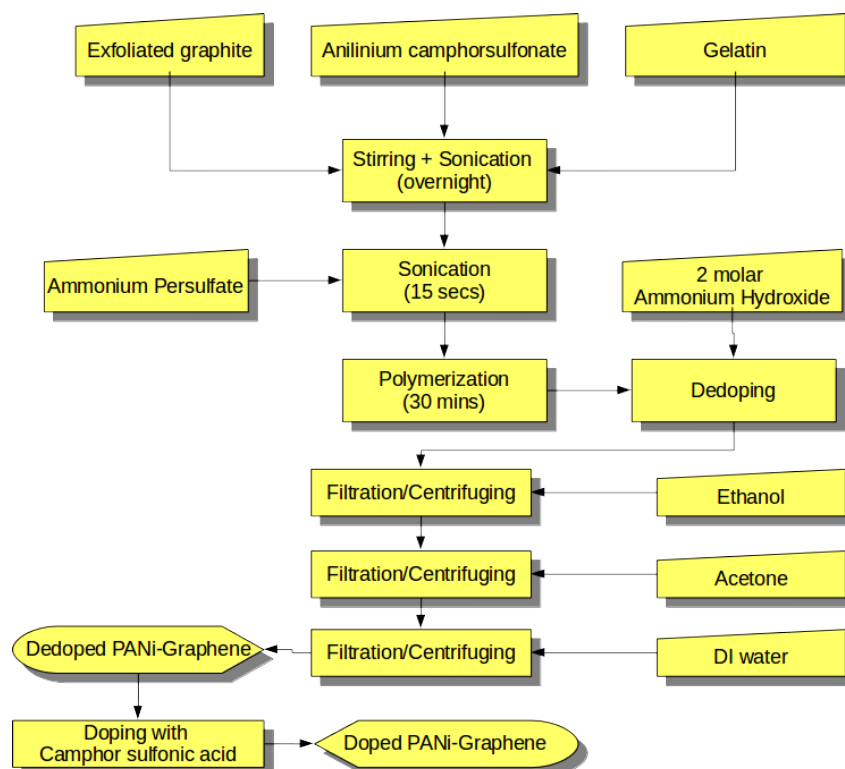


Figure 3.24: Synthesis route of Polyaniline-Graphene composite

Sample preparation

- **Materials:** Flake graphite of mesh size 60, Aniline monomer, 99% Sulfuric acid, 78% Phosphoric acid, Potassium permanganate, deionized water (DI), Ammonium persulfate, Ammonium Hydroxide, Gelatin powder, Ethanol and Acetone were purchased from Merck Limited, India.
- **Preparation of Exfoliated graphene:** Flake graphite was intercalated with sulfuric acid using the Tour's method[157, 143] with excess amount of graphite. The reaction is as follows: 5g of graphite is mixed with 8ml sulfuric acid and 2ml phosphoric acid. The mixture was stirred vigorously and sonicated for 1 hour. Then 1.8g of potassium permanganate was added to it with vigorous stirring and sonication for 30 minutes. The mixture was then transferred to excess DI water and stirred and sonicated. The graphene intercalation compound (GIC) was sedi-

mented by centrifuging at 7000rpm. A small portion of GIC was microwave irradiated for 1 minute in a ceramic crucible to finally exfoliate the graphene. The exfoliation resulted in very large volume to mass ratio in the exfoliated graphene.

- **Preparation of PANi-Graphene composite:** The microwave exfoliated graphene was then dispersed in gelatin dissolved in 1M anilinium camphorsulfonate to which Ammonium persulfate solution was rapidly mixed. The oxidative polymerization was allowed to progress until 30 minutes after which the reaction mixture was transferred into 2M ammonium hydroxide to dedope the polymer and stop the reaction. The residue of filtration was then washed with ethanol, acetone and excess DI water. This sample is the dedoped sample designated as GDPAN. A portion of GDPAN was washed with 1M camphorsulfonic acid (CSA) to make the doped sample designated as GPAN. Both samples were oven dried at $40^{\circ}c$. Pellets of 13mm diameter of both samples were made by applying a pressure of $150kg/m^2$ for 10 minutes to the corresponding powder forms. Doped pure PANi (NPAN) was prepared using standard IUPAC synthesis routine[107] for reference. The entire sequence of synthesis is illustrated in Figure.3.24.

Results and Discussions

- **Fourier transform infrared spectroscopy** The FTIR spectra of the doped and dedoped samples are shown in Figure.3.25. The characteristic peaks due to PANi are as follows: 1580 and 1492 due to C=N and C=C stretching vibrations of quinoid and benzenoid rings; band from 1294 to 1240 due to C-N stretching. The peak at 795 indicates $\pi - \pi$ interaction and hydrogen bonding between graphene sheets and PANi. It is evident that the transmittance peak at $3453cm^{-1}$ changes reversibly due to the differences in interaction of PANi with graphene in its doped and dedoped states. Thus it can be seen that the reversible doping process alters the entire spectrum of the material.
- **X-ray diffraction study** The XRD graph of doped and dedoped samples were taken to analyze the crystallinity and other aspects. The presence of crystalline regions of expanded graphite is indicated by the

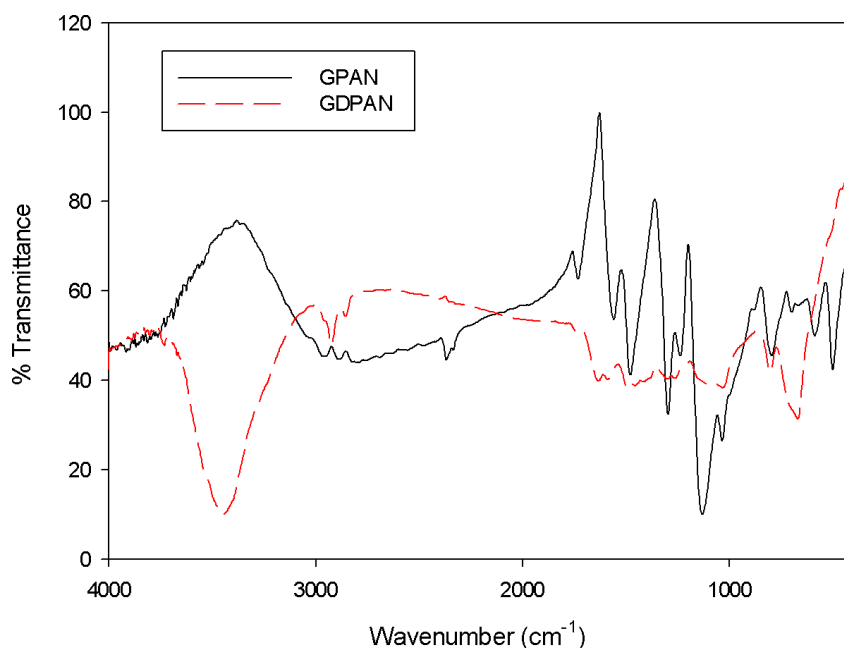


Figure 3.25: FTIR spectra of doped and dedoped samples of composite

sharp peak found at $2\theta = 26.52^\circ$. The intensity count of the expanded graphite peak is comparatively lower than Figure.3.21d pointing out to the possibility of PANi induced exfoliation due to interlayer and inter-domain growth of PANi on graphene. It is also seen that the intensity count of dedoped state is larger than that of doped state. This indicates the reversible exfoliation of graphite domains due to the coiling of PANi chains connecting those graphite domains. One interesting finding is that presence of doped state of PANi is distinguished by the peak at $2\theta = 14.9^\circ$ from the dedoped state. In the case of dedoped state, this peak is shifted to $2\theta = 19.31^\circ$ probably due to the conformational change in PANi chains induced by dedoping. The peak at $2\theta = 11.51^\circ$ is due to the presence of a few amount of graphene oxide.

- Morphological study** The morphology of the product before and after the reaction was recorded by Scanning Electron Microscopy images. The Polymerized sample and the graphite before polymerization is shown in Figure.3.27. It can be seen that the polymerization reaction was successful in covering the surface of graphene sheets with PANi nanofibres.

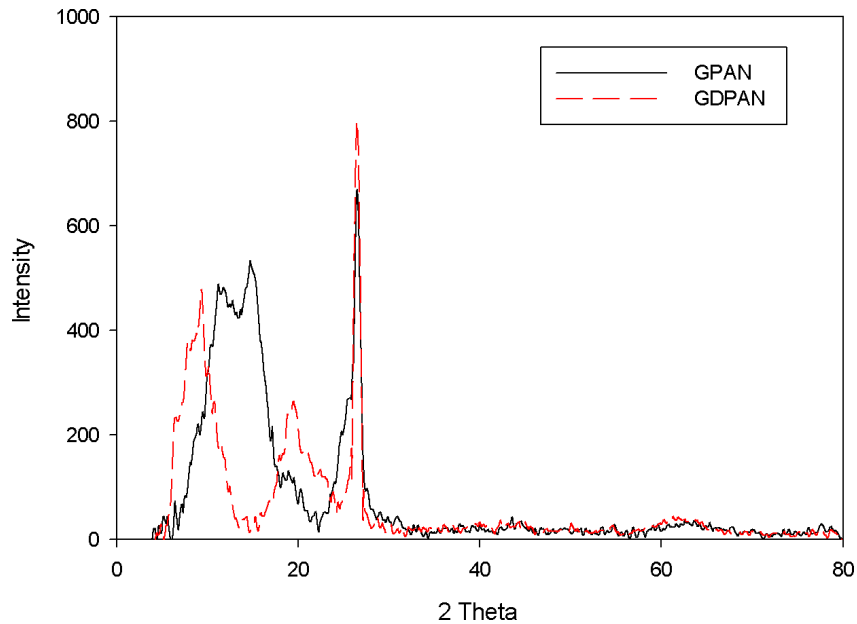
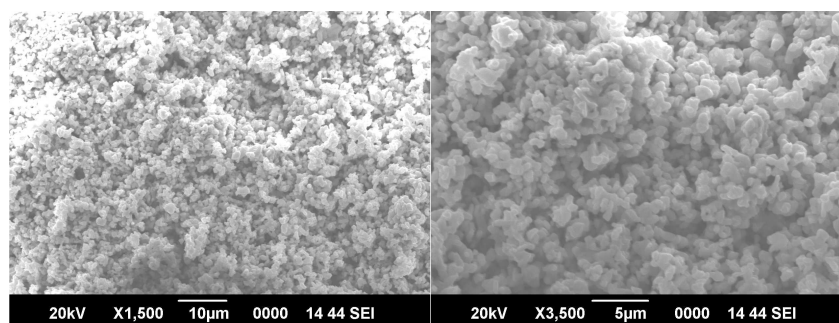


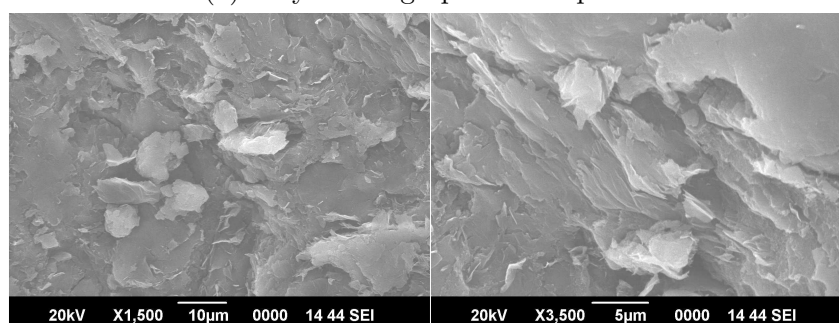
Figure 3.26: XRD graph of doped and dedoped samples of composite

The graphite after exfoliation contains a few layers of graphene are also visible in the imagery.

- **Low frequency dielectric properties** The complex impedance of the samples in the 20Hz-2MHz spectrum was analyzed using Agilent E4980 Precision LCR meter. Standard 13mm diameter pellets were held in the sample holder while the computer controlled measurement system evaluates the material properties – dielectric constant and conductivity of the three samples. The system evaluates the material properties as projected in the literature. It can be seen from the Figure.3.28 that the GPAN exhibits a better conductivity around one order higher when compared to that of GDPAN. It can also be seen that both GPAN and GDPAN are exhibiting a conductivity which is three orders higher than NPAN.
- **Microwave characterization** The pellet samples were machined into precise small cylindrical shapes using laser etching and microwave characterization is performed using Rohde & Schwarz ZVB20 Vector Network Analyzer (VNA). Resonant cavity perturbation method was used



(a) Polyaniline graphene composite



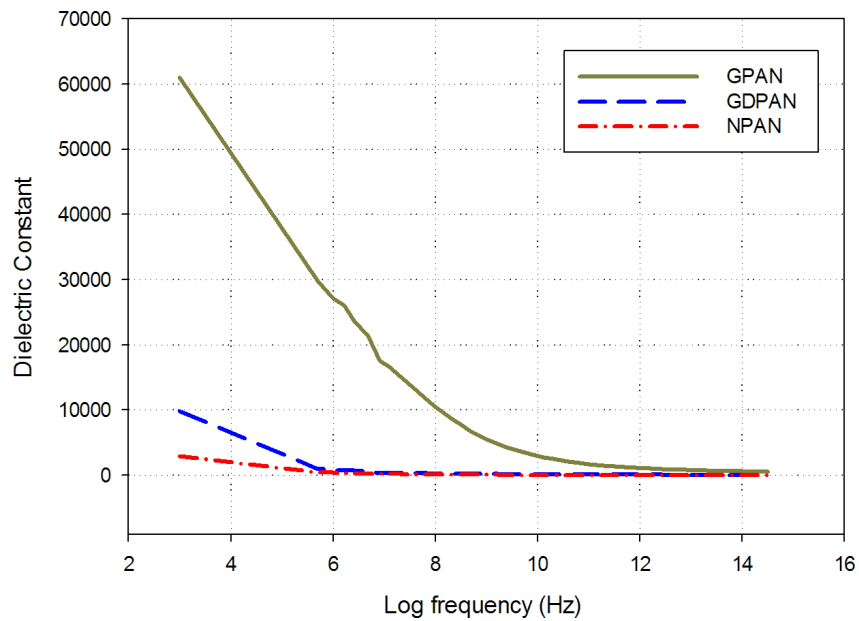
(b) Expanded graphite before the polymerization

Figure 3.27: SEM images of the graphite, a) after and b) before PANi polymerization reaction

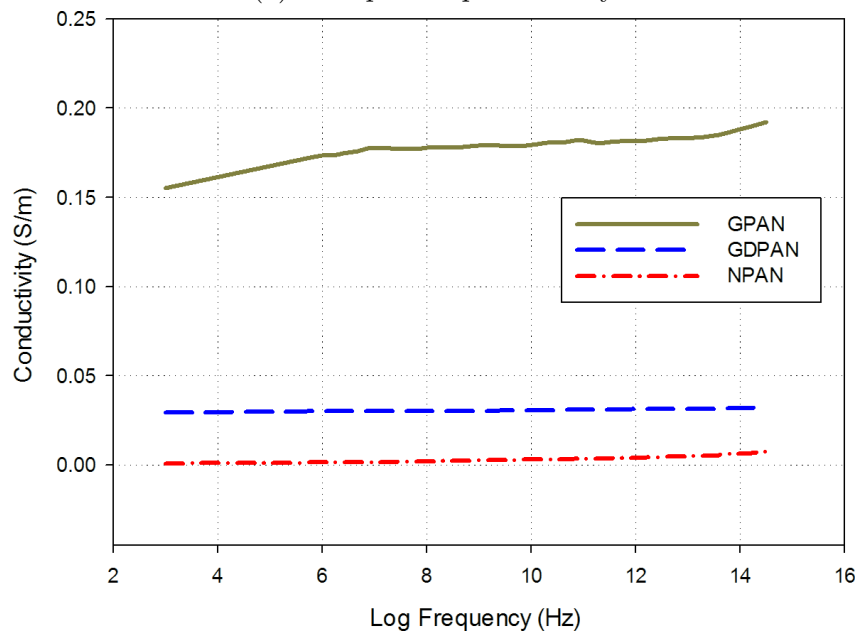
to estimate the material properties at C band. The dielectric constant, conductivity and skin depth were measured and calculated by the computer controlled experiment setup implementing the method as described in the literature. It can be seen from Figure.3.29a that the dielectric constant of the GPAN is greater than that for GDPAN. This can be attributed to the bulky counter ion introduced in the polymer chain during doping with CSA. The conductivity (Figure.3.29b) is also significantly enhanced in the case of doped sample.

- **Antenna fabrication**

Polymer antennas were fabricated by properly placing 13mm diameter pellet on a microstrip feedline of 50Ω input impedance. A full two port TOSM calibration was performed on VNA. The S_{11} and S_{21} of GPAN, GDPAN, NPAN and metal are plotted in Fig. It can be seen that the antenna has a higher S_{21} during cross polarization over the 5-6GHz



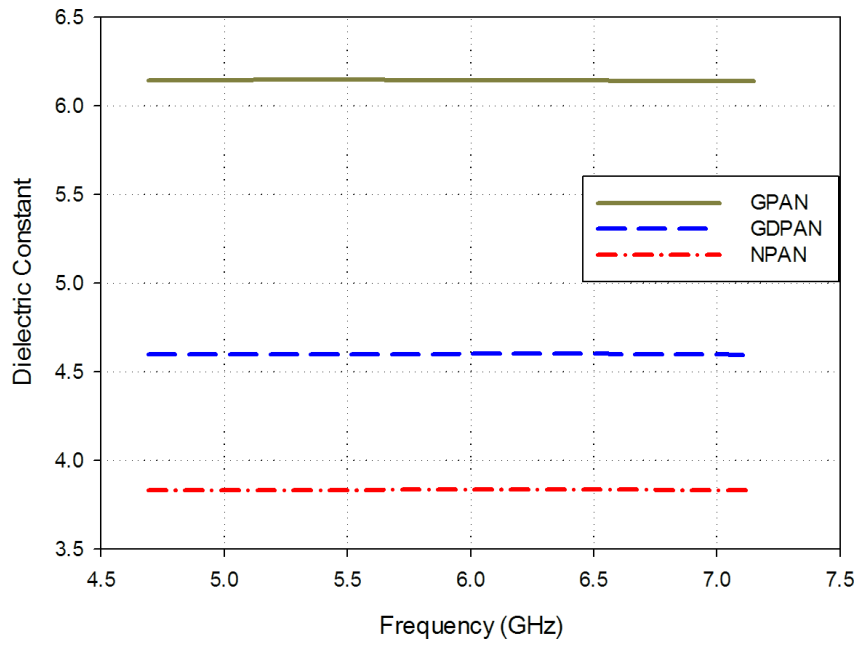
(a) Real part of permittivity



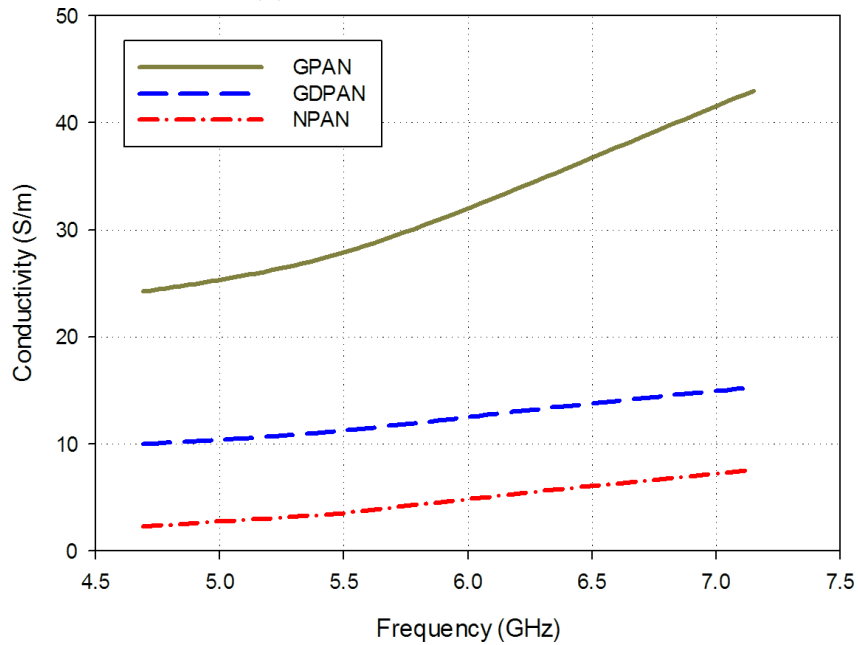
(b) Imaginary part of permittivity

Figure 3.28: Low frequency complex permittivity of GPAN, GDPAN and NPAN

band. From the S_{21} of metal antenna, it can be seen that the circular patch of 13mm diameter exhibits a resonance in this frequency band and the corresponding S_{21} is high relative to other bands. This is a resonant band where the radiation is due to resonant currents which are maximum. As depicted in Fig.5, it can be seen that the polymer antenna exhibits wideband impedance matching. This impedance matching does not necessarily guarantee radiation efficiency. Especially at bands which are matched by resonance, the high currents can have some attenuation due to the loss tangent. To increase the radiation efficiency of a resonant antenna the electrical conductivity should be maximized so that the electric fields are screened by the delocalized charge carriers in the PANi-Graphene composites. It can be seen from Fig.6 that the S_{21} is more for GPAN than that for GDPAN or NPAN. For non-resonant antennas, the antenna currents will be much less and the power loss will not be as prominent as that for resonant antennas.

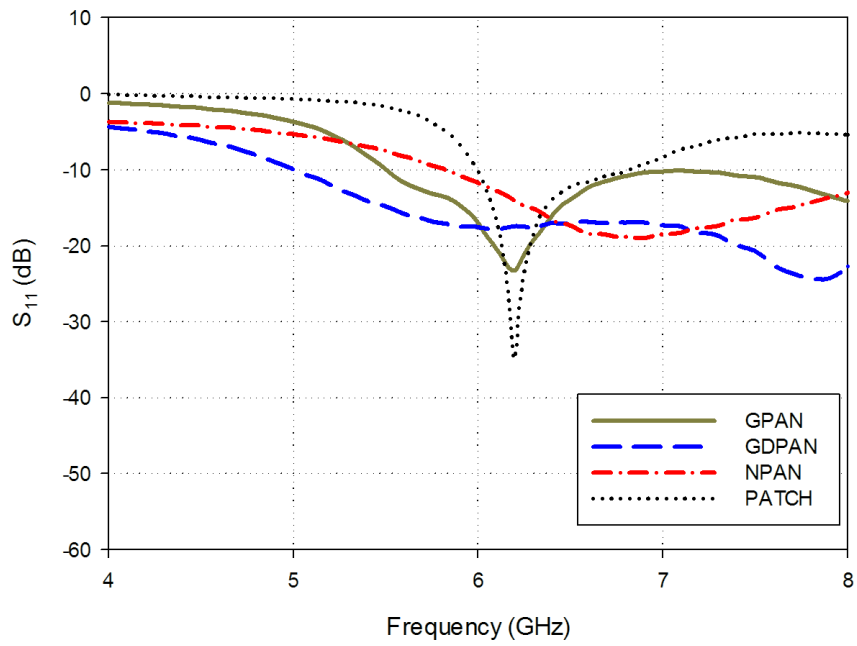


(a) Real part of permittivity

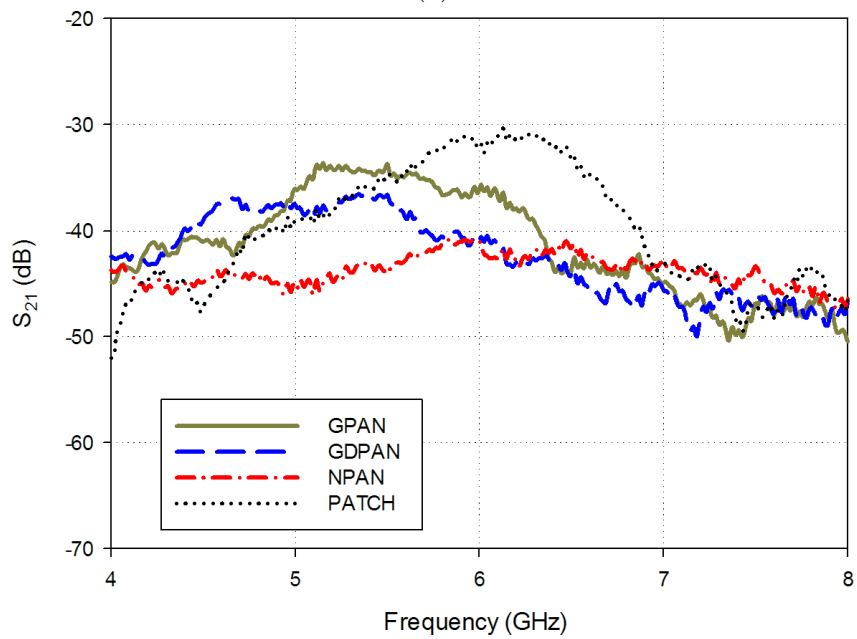


(b) Imaginary part of permittivity

Figure 3.29: Microwave frequency complex permittivity of GPAN, GDPAN and NPAN at C band



(a)



(b)

Figure 3.30: Comparison of S parameters measured for pellet antenna and other forms

3.3.2 Summary

PANi-Graphene composite was synthesized using gelatin as dispersion stabilizer. The FTIR spectrum of the composite was studied which indicated the differences induced by the doping and dedoping of PANi in the composite. The XRD analysis indicates the crystallinity and composition of the material. The SEM images confirm the polymerization of the conducting polymer on graphene sheets. The composite was tested for its microwave material properties at C band and its impedance analysis was done for 20Hz-2MHz band. The composite was used to fabricate a microstrip line fed polymer antenna to evaluate the radiation performance. The S_{11} and S_{21} of the synthesized composite with CSA doping and dedoping was compared to that of normal PANi antenna and to a patch antenna of the same dimensions. The new synthesis routine could make water dispersible PANi-Graphene composites of fairly good conductivity without using GO reduction step. Thus the synthesized PANi-Graphene composite has improved processibility. Yet it proves to be a good absorber than a very high conductor to replace metals. Typical use for this material thus would be as tunable conductivity materials for non-resonant absorption of microwave energy.

Chapter 4

PRINTABLE NON-RESONANT ABSORBERS USING POLYANILINE-GRAPHENE COMPOSITES

This chapter introduces the various techniques used in the realization of wideband absorbers through a brief literature review. It is followed by the design of wideband absorber using polyaniline-graphene composites. The design is based on non-resonant absorption of microwave energy by conductivity graded layered attenuator structure. This offers good impedance matching and with broadband absorption of microwave power within small thickness. The structure has the potential of 3D printability as the entire system uses only polymers to absorb incident microwave. The fabrication, measurement and analysis of the absorber are described in this chapter.

Contents

4.1 Radar absorbers	94
4.2 Choice of absorbant material	100

4.3 Design of the proposed wideband non-resonant absorber	105
4.4 Results and Discussions	107
4.4.1 Parametrics	109
4.4.2 Angular variation	110
4.4.3 Field distribution and Power loss	112
4.4.4 Bistatic RCS analysis	115
4.5 Conclusion	117

4.1 Radar absorbers

Radar absorbing materials (RAM) are electromagnetic structures used to absorb the incident electromagnetic waves so that the reflected power is reduced to a great extent[158, 159]. Some of its applications are radar cross section (RCS) reduction[160], electromagnetic interference (EMI) shielding[161], stealth technology[162, 163] etc. These are very demanding fields as contemporary times are more demanding, in the sense of reduced thickness[164], optical transparency[165], wide bandwidth[166, 167], polarization insensitiveness[168, 169] and ease of fabrication[170, 171]. Radar absorbers can be broadly classified into Resonant absorbers[172] and Non-resonant absorbers[173].

- **Resonant absorbers**

These are absorbers that utilize resonance phenomena and absorb the energy in the resonant mode. Traditionally radar absorption is achieved using Salisbury screens[174] (Figure.4.1) in which a resistive sheet of surface impedance equal to 377Ω at the frequency of operation is kept at a distance of quarter wavelength from the target metal surface. This will offer a TEM wave with a matched load and the energy is dissipated in the resistive medium. Although it is a perfectly good absorber, the bandwidth of absorption is very less.

It is often possible that the radars can adaptively switch to other frequencies differing from that the absorber is designed. This can make the target vulnerable to detection. Hence for wide band coverage, multiple

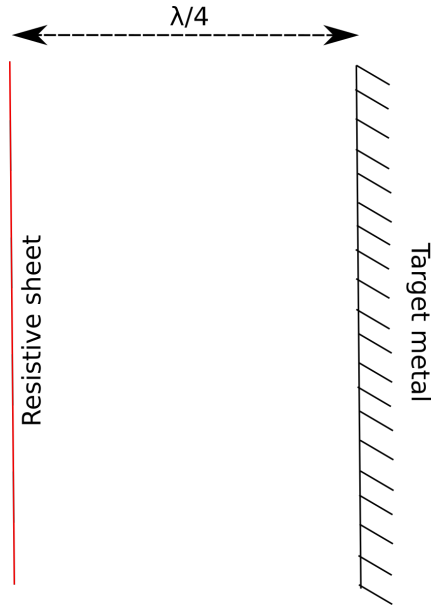


Figure 4.1: A salisbury screen

layered resistive sheets, each for different centre frequencies are designed, with the lowest frequency absorber determining the final thickness of the structure. Such absorbers are called Jaumann absorbers[175] (Figure.4.2). This poses the thickness problem, especially if the target is airborne. When trying to reduce RCS of the target, a substantial increase in thickness is never going to be beneficial. Hence for reducing thickness, dielectrics can be introduced in between the resistive sheets and the metallic backside resulting in reduced physical thickness owing to the higher dielectric constant of the material.

Dallenbach layer absorber (Figure.4.3) uses a loss imparting dielectric instead of a resistive sheet on top of the target metal. These loss imparting material can be carbonyl iron or ferrite based materials or carbon nano tube derivatives which can cause both electric and magnetic losses to the impinging electromagnetic wave.

Another promising method for the design of resonant absorbers is the circuit analog absorbers[176] (Figure.4.4) wherein conductors are patterned above the ground plane so that the combination acts as a high impedance ground plane (HIGP) which creates a magnetic wall and

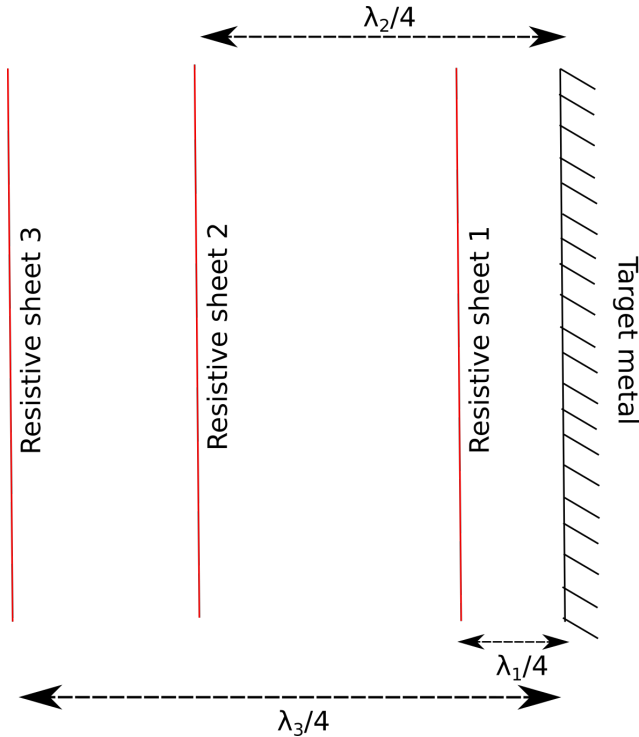


Figure 4.2: A jaumann absorber

hence the maximum electric field intensity at a much lower thickness than quarter wavelength of the frequency of interest. Lumped resistances or patterned resistive films are used to dissipate the resonating microwave energy in the patches. In a similar fashion, there are capacitive circuit absorbers[177] employing low pass square resistive patches instead of bandstop FSS resonators as that in circuit analog absorbers.

- **Non-resonant absorbers**

Non-resonant absorbers do not use resonant elements or structures to absorb microwave energy. It utilizes the materials properties to absorb energy by imparting electric and magnetic losses to the incoming electromagnetic field which is of travelling wave type rather than a resonant standing wave pattern[178]. They are typically broadband in nature and require thicker form factor to absorb a particular wavelength than their resonant counterparts. But the broadband nature outweighs this demerit.

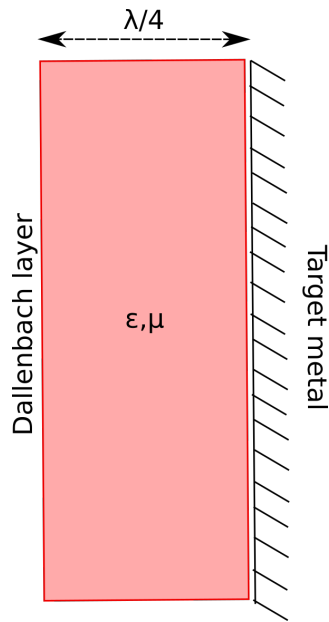


Figure 4.3: A dallenbach absorber

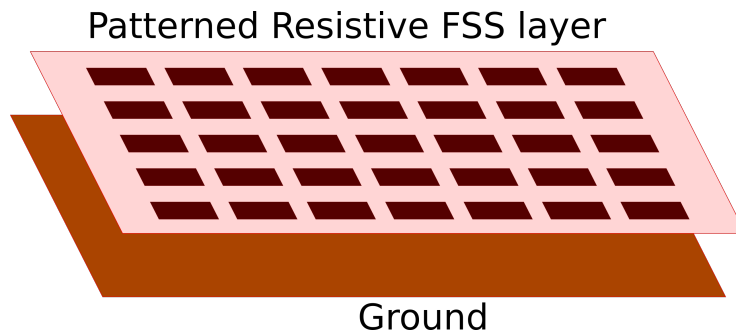


Figure 4.4: A circuit analog absorber

Pyramidal absorbers (Figure.4.5) are non-resonant type which is made from uniformly spaced pyramidal foam absorbers containing carbon black and other microwave absorbing ingredient. Their geometry helps in repeated internal reflections and guiding of incident wave deeper into it until it is completely absorbed. They provide high attenuation with wide frequency and angle range. They can only be used in anechoic chambers due to their large size.

Another type of non-resonant absorber is the tapered loading absorber or graded absorber[179] (Figure.4.6) in which a lossless substrate is loaded

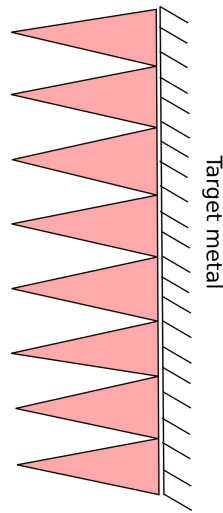


Figure 4.5: A pyramidal absorber

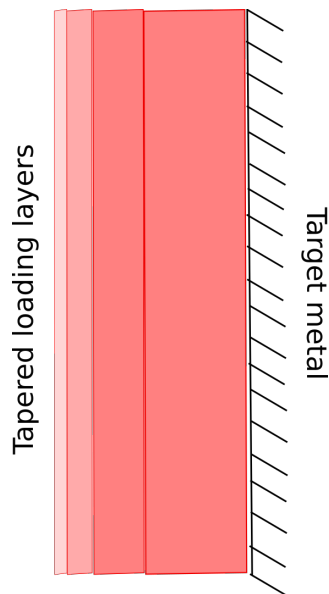


Figure 4.6: A tapered loading absorber

with lossy absorbing component wherein the gradient of lossy components is such a way that it increases from the air interface to the metal interface at the other side of the absorber. Thus in this type, the filler loading is being made incremental from one side to the other side.

A third type of non-resonant absorber called matching layer absorber[180]

(Figure.4.7) exists in which the thickness required for the gradual transition is reduced by an interlayer between the incident and absorbing media. This interlayer has thickness and impedance values that is chosen to match both the absorber and incident media. The idea is to have the combined impedance from the first and second layers be equal to the impedance of the incident medium.

Both these techniques require extensive optimizations and parameter analysis for achieving wideband nature for a higher wavelength to thickness ratio. They might need spacers which can lead to structural complexities that defy the very purpose of RCS reduction in core applications. Moreover it is a highly required attribute for absorbers to be 3D printable to the target conformal specifications, which is seldom addressed[181, 182, 183].

In this work, the absorber is realized with a combination of non resonant and resonant techniques, guiding the incident energy by impedance transformation from that of freespace to that of the metallic ground of the target. The absorber is realized as an all polymer first iteration sierpinski fractal structure without resonating metal patches. It uses graded conductivity polyaniline-graphene composite embedded in a plexiglas substrate to effectively guide the incident wave and attenuate the field as it traverses through the attenuating material. This technique comes under the tapered loading absorber except that they are patterned and that they are made of conducting polymer composites. This can create a periodic surface current pattern on the ground plane, the field of which gets attenuated in the presence of the attenuator pellets. The chemical synthesis and dielectric characterization of the conducting polymer composites used in this work is detailed Chapter 3. The work first discusses the engineering aspects related to the feasible implementation of synthetic conducting composites for RCS reduction. Secondly, it extends the previous work mentioned in Chapter 3 on PANi-graphene composite[184] to the proposed RAM structural design and its performance analysis so as to demonstrate the use of synthetic conducting polymer composites devoid of metals, which is the objective of this work.

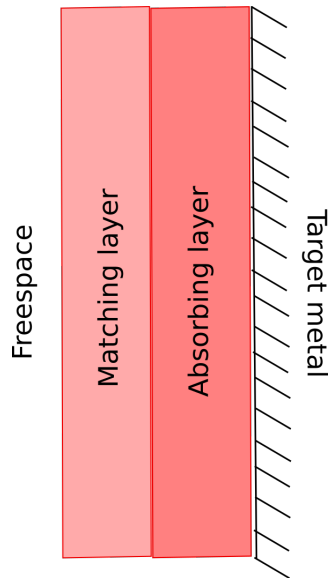


Figure 4.7: A matching layer absorber

4.2 Choice of absorbant material

Conducting polymers are long chain of carbonaceous materials which are formed by polymerization reaction of its monomers under optimum reaction conditions. They are synthetic yet electrically conducting materials whose conductivity can be tuned to suit the required material properties. Of all the conducting polymers available, Polyaniline (PANi) has advantages of environmental stability, availability of cheap monomers and hence many applications propose PANi as a promising candidate. The importance and potential use of PANi in electronics is a broad subject in which microwave applications such as EMI shielding, wearable antenna applications do come often as the stakes are high for a flexible high conductive synthetic material and it is no wonder that quite a large number of material research groups have done impressive contributions in this field[185, 186, 187, 188]. Yet there exists a practical non-viability in the real-world applications of these wonder polymers in microwave. This arises mainly due to the inverse relation between the conductivity of these polymers and their large-scale processibility.

Conducting polymers, which are obtained as powder precipitates in typical reactions, are inherently composed of core shells with metallic conductivity immersed in a pool of dielectric. The chain structure of these polymers are

readily conducting entities with a very high intra-chain conductivity in their doped state. But when considering their inter chain or inter domain electron transport, they have a finite charge tunneling probability and the bulk conductivity is greatly reduced. The conductivity can of course be enhanced by various techniques starting from its altered synthesis routes, secondary doping, mixing with other conducting polymers and stable dispersions in solvents. When a film form of the material is sought, dispersions of PANi in solvents like N-methyl-2-Pyrrolidone, m-cresol, Triton X is made which can be coated onto substrates by spray coating / spin coating / dip coating techniques[189, 190]. These solvents are said to interact with the polymer backbone under the influence of certain dopants based on sulphonic acids, giving rise to conformational stretching or uncoiling of polymer chains so that long range electron transport gets better with a high crystallinity in the bulk material[191]. Highly conducting PANi films are hence obtained by such method whose microwave properties are of great interest as they can act as conductive patches in flexible antennas. But these films need not be a free standing one or the films might deteriorate with ambient conditions and thus practical applications are limited to wafer fabrication, for instance, in sensor applications. If a flexible thick sheet form is required, then PANi can be dispersed in any of the above organic solvents along with conventional polymers such as Natural rubber, Polymethyl methacrylate (PMMA), Polyvinyl chloride (PVC) or Polyethylene terephthalate (PET) and cast into thick sheets[192, 193]. There is an innate loss of conductivity in these blended composites as the matrix polymer hinders charge transport. From an electromagnetic point of view, these composites can be modeled as lossy dielectrics rather than as lossy metals. A yet another approach in making high quality conducting polymer films is by plasma polymerization[194]. For this, the size of the substrate should be very small and is not suitable for RAM/FSS applications albeit their untapped potential in millimeter waves as substrate integrated waveguides and leaky wave structures.

In most of the preparation methods it is highly unlikely to obtain laboratory conductivities during large scale processing in bulk of these polymers. One method to increase the bulk conductivity is by adding conductive fillers like metal nanopowders or carbon nanotubes or graphene or any other conducting polymer of interest[195, 196, 197]. This is done by ex-situ or in-situ

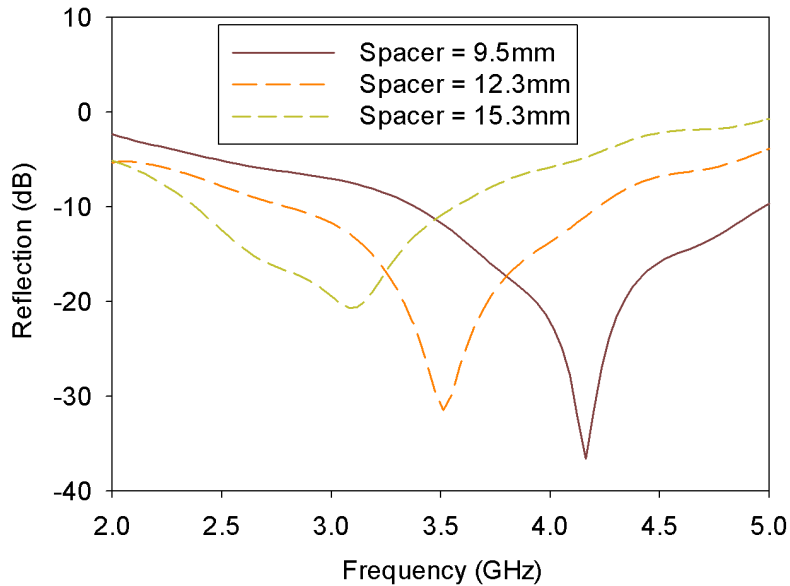


Figure 4.8: Measured reflection from salisbury screen using graphene sheets at different spacer thickness

methods. The first method involves mechanical milling and mixing of the selected conducting filler in the already conducting host matrix. The ratio of the filler to host determines the final product conductivity. The second method is to polymerize the monomers in the presence of fillers. This method has significant impact on conductivity as the material is blended with its filler at a molecular level. The fillers need to act as nucleation sites for the monomers to start reacting into polymers. In the case of Polyaniline-graphene composite, Polyaniline needs a lower pH medium to polymerize, whereas graphene needs a high pH medium. In a lower pH, the graphene layers tend to agglomerate and readily sediments into the bottom of the reaction medium. In standard procedure, graphene is oxidized into graphene oxide, which is stable in low pH and then the PANi monomers are allowed to polymerize on them[198, 199]. This has a downside that, graphene oxide is not a good conductor. So these procedures are eventually followed by a reduction reaction which removes the -OH groups using hydrazine or microwave irradiation or by UV laser, getting back to a reduced graphene oxide form. In the process, the crystallinity of graphene layers is somewhat distorted which is more commonly referred to

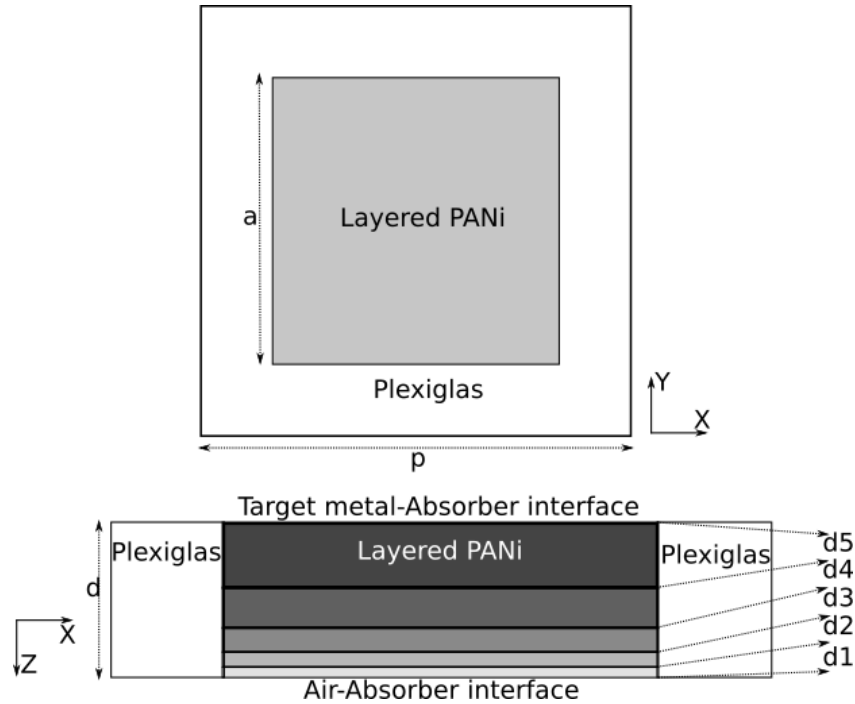


Figure 4.9: Structure of proposed absorber unit cell

as wrinkles in graphene sheet. These distortions can be avoided by using graphene as such with the help of dispersion stabilizers or surfactants. Hence a dispersion stabilizer like Polystyrene sulphonate (PSS) or Gelatin need to be used so that the polymerization can proceed on these well dispersed graphene templates. To add to this stability provided by stabilizers, as the polymerization commences, the interaction of PANi reacting species with graphene also results in dispersion stability.

Graphene is a well acclaimed synthetic conductor which has potential in bandgap and conductivity tuning. The hype around graphene is also followed by such difficulties in obtaining high quality sheets with good mechanical strength at microwave length scales. High quality graphene coatings are obtained on silica or quartz by Chemical vapor deposition (CVD), but on a very small scale. Nevertheless graphene has a promising property of forming very thin stable sheets on certain substrates by mere application of shear stress[200]. This can be done to make ohmic sheets that can act as resistive sheets in Salisbury screens or patterned as resistive metasurfaces in circuit analog absorbers or in FSS. These coatings can be made very thin and conductive

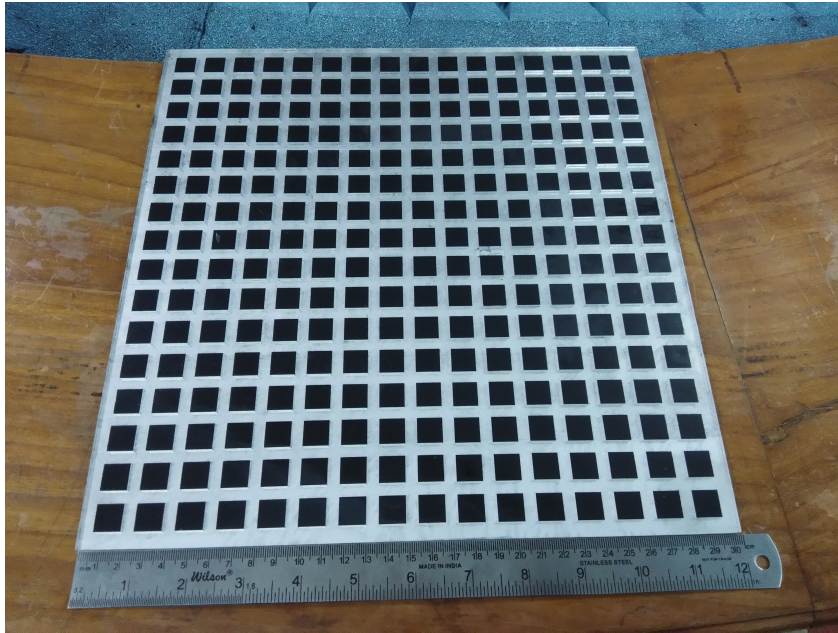


Figure 4.10: Fabricated prototype of the structure

so that the real part of complex permittivity is seldom considered and the coating acts as a lossy metal. A salisbury absorber utilizing microwave exfoliated sulphuric acid intercalated graphene as resistive coating with an average surface resistance of $390 \Omega/\text{square}$ over a Plexiglas substrate (dielectric constant = 3.02 as measured using NRW algorithm) is fabricated at our facility and its measured reflected power for normal incidence is indicated in the Figure. 4.8 for demonstration purpose. Three spacer thicknesses were used and the corresponding resonance shifts in the absorption peaks are clearly observable from the figure. Other complex shapes can be made by laser patterning technique. This demonstration indicates the prospects of synthetic conductors with their tunable intrinsic properties and their constitutive parameters that suit them for microwave applications.

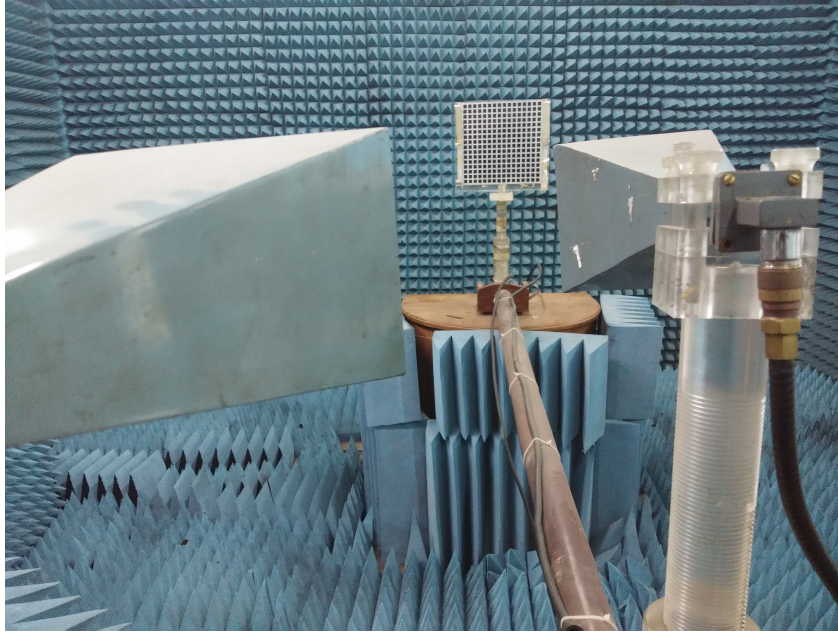


Figure 4.11: Structure mounted for measurement at anechoic chamber

4.3 Design of the proposed wideband non-resonant absorber

In this section, a design schema for the all-polymer microwave absorber is outlined. The absorbing material is pellets of PANi-graphene composite. In a microwave scale of physical lengths, compressed pellet forms of PANi-graphene nano composites offer moderate conductivity and good physical strength. The conductivity modulation can be done using proper acid (for doping) or base (for dedoping) in a controlled nitrogen environment by introducing vapour phase dopants at predetermined concentrations to the powder form of PANi-graphene composites. Thus PANi-graphene composites with graded conductivities can be obtained. These powders can be compressed to make a conductivity graded pellet of varying thickness for each layer. In the current design, a Plexiglas substrate is chosen as it is transparent and easy to 3D print or etch out unwanted regions by instant vaporization using concentrated laser power without any burn-in effects. The substrate thickness is $d = 4.16mm$ with a dielectric constant of 3.6 and electrical conductivity of $0.02Sm^{-1}$. Periodic sierpinski first iteration squares can be etched out from the substrate

into which conductivity graded 5 layered square shaped PANi-graphene pellets are inserted as inclusions. The conductivity of each adjacent layer of the composite varies in the golden ratio with the air interface layer having lowest conductivity and the target interface layer having the highest conductivity. Similarly the ratio of thickness of each adjacent layer is also chosen to be of the golden ratio with the air interface layer being the thinnest. The thickness and conductivity of the layers can be expressed as the following vectors:

Thickness,

$$[d_1 \ d_2 \ d_3 \ d_4 \ d_5] = \left[\frac{1}{377} \ \frac{1}{233} \ \frac{1}{144} \ \frac{1}{89} \ \frac{1}{55} \right] d_{scale} \quad (4.1)$$

Conductivity,

$$[c_1 \ c_2 \ c_3 \ c_4 \ c_5] = [55 \ 89 \ 144 \ 233 \ 377] c_{scale} \quad (4.2)$$

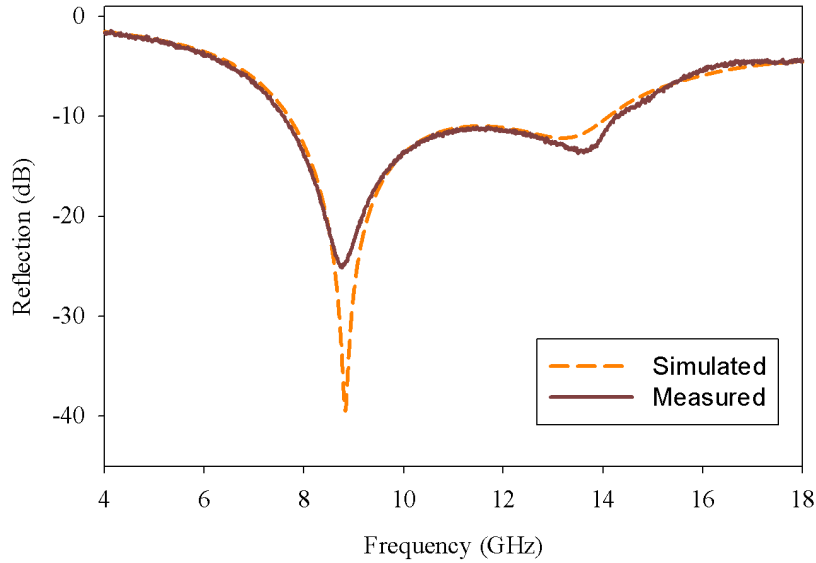


Figure 4.12: Measured and simulated reflection from the designed structure

Where $d_{scale} = 96.07mm$ and $c_{scale} = 0.0447Sm^{-1}$ are scalar parameters estimated by Trust Region optimization algorithm of CST microwave studio and the constants of the right hand side are from fibonacci series, where the ratio of adjacent elements is the golden ratio. The rationale behind the selection of golden ratio is that many naturally occurring systems have logarithmic

structures obtained from designs implementing golden ratio[201, 202]. Hence this ratio has an innate non-resonant nature. The indexes 1 to 5 represent layers from top to bottom.

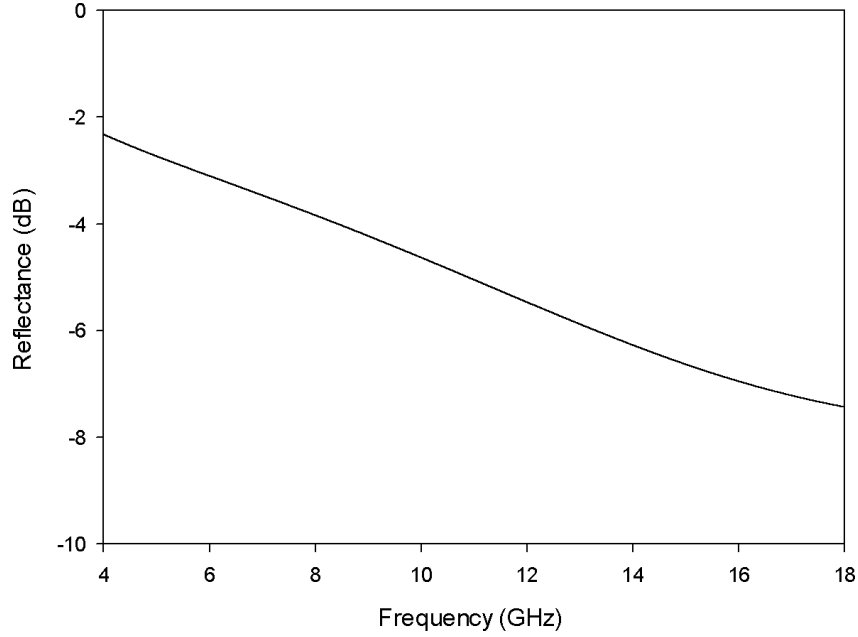


Figure 4.13: The reflection from a continuous sheet of graded absorber

The structure is fabricated out of the same unit cell with 16×16 elements on a Plexiglas substrate of size $304.8mm \times 304.8mm$ as outlined in Figure. 4.9. The final structure is shown in Figure.4.10 and Figure.4.11. The width of the patch $w = 12.39mm$ and the periodicity $p = 18.47mm$ are optimized to suit the design requirements. The pellet can be said to be a combination of geometric transition absorber due to the thickness gradation and tapered loading absorber due to the conductivity gradation. The fact that the pellet behaves non-resonant is evident from the Figure.4.13 where it shows a non-resonant absorption for a wide frequency band.

4.4 Results and Discussions

The unit cell of the absorber was modeled and optimized in CST microwave studio. Polyaniline-graphene pellets are conductivity tuned in a controlled nitrogen atmosphere using Camphor Sulphonic Acid (CSA) as dopant. The

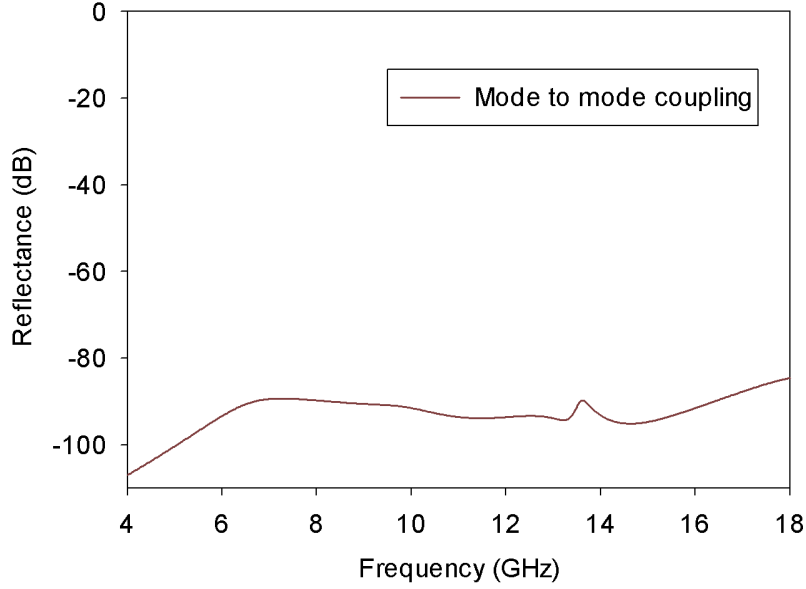


Figure 4.14: Mode to mode coupling

square holes are made in the substrate using laser patterning and the pellets are inserted in the square holes. The reflection is measured in freespace using wideband horn antennas connected to Rohde & Schwarz ZVB20 Vector Network Analyzer calibrated with metal plate of same dimension as that of the test structure in fully shielded anechoic chamber. The reflection (Figure.4.12) shows a 10 dB reduction ranging between 7.8 GHz and 14 GHz, as measured. It can be seen that the measured curve is similar to that of the full EM simulated results from CST Microwave studio although it registers some slight variations from simulation. This can be attributed to the fabrication irregularities involved in the prototype. As defined elsewhere[181], the parameter $\Delta\lambda/d$ in this case is found to be 4.27 where $\Delta\lambda = \lambda_{max} - \lambda_{min}$. The structure thickness in terms of multiple of wavelength is listed for comparison for different recent designs in Table 4.1. The mode to mode couplings (Figure.4.14) indicate that the phenomenon is absorptive and it is not a case of polarization rotated reflection.

Table 4.1: Comparison of structure thickness in terms of wavelengths

Reference	Lower frequency	Upper frequency	Thickness(λ)
[170]	3.5 GHz	24.0 GHz	15.51mm(0.47λ)
[171]	16.3 GHz	54.3 GHz	2.70mm(0.27λ)
[203]	8.4 GHz	21.0 GHz	3.65mm(0.16λ)
[204]	10.0 GHz	70.0 GHz	4.50mm(0.40λ)
[205]	7.0 GHz	37.4 GHz	3.80mm(0.20λ)
Proposed	7.8 GHz	14.0 GHz	4.16mm(0.14λ)

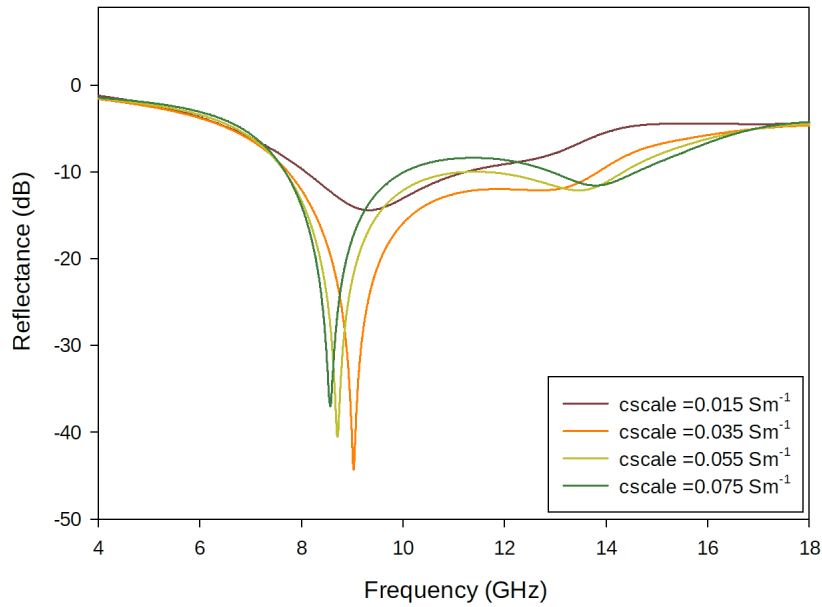


Figure 4.15: Variation of reflectance with layer conductivity

4.4.1 Parametrics

It is found that, rather than a dependence on the width of the resistive square as that in the case of circuit analog absorbers, the band of operation is significantly determined by the thickness of the structure manifested in the factor ‘dscale’ (Figure.4.16). There exists a dependence of band of operation and matching on parameters cscale, w and p as shown in Figure.4.15, Figure.4.17,

Figure.4.18 respectively. Any increase in the width and the spacing of the square patch beyond half wavelength results in the entire structure becoming an electromagnetic scatterer for higher frequencies in the operating band. It can be inferred that the absorption mechanism is due to $\lambda/4$ resonance of the structure thickness at lower frequencies and due to edge diffraction at higher frequencies.

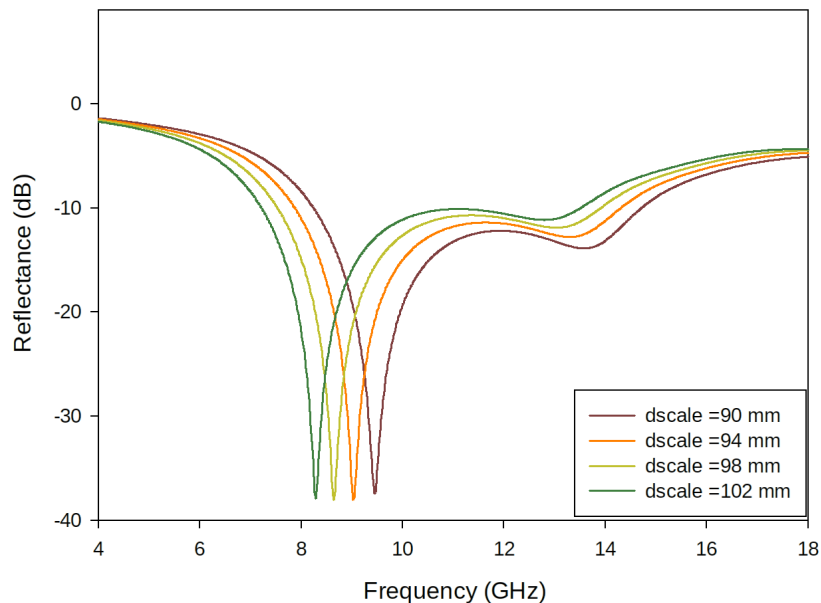


Figure 4.16: Variation of reflectance with structure thickness

4.4.2 Angular variation

Due to the four fold rotation symmetry of the structure, both TE and TM polarizations have the same response upon normal incidence. As evident from Figure.4.19, the angular variation of reflected power for TE mode satisfies a variation upto 30° incident angle after which the response deteriorates within X band. With the angular variation, the TE mode absorption deteriorates whereas the TM mode (Figure.4.20) shows good absorption at wider angles. This is to be expected as the coupling of TM modes are different from that of TE at oblique angles of incidence. In graded non-resonant absorbers, the TM modes refract into the medium which gives rise to the wideband absorption of

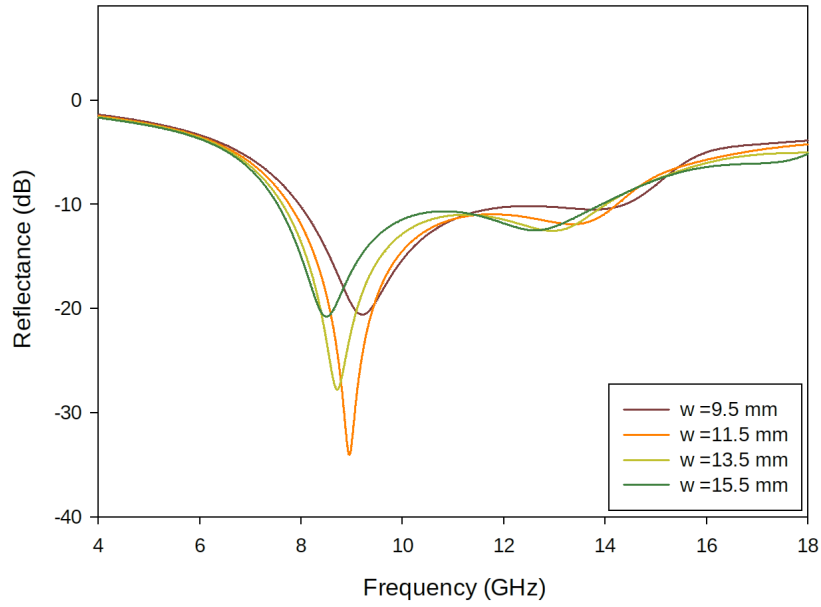


Figure 4.17: Variation of reflectance with square pellet width

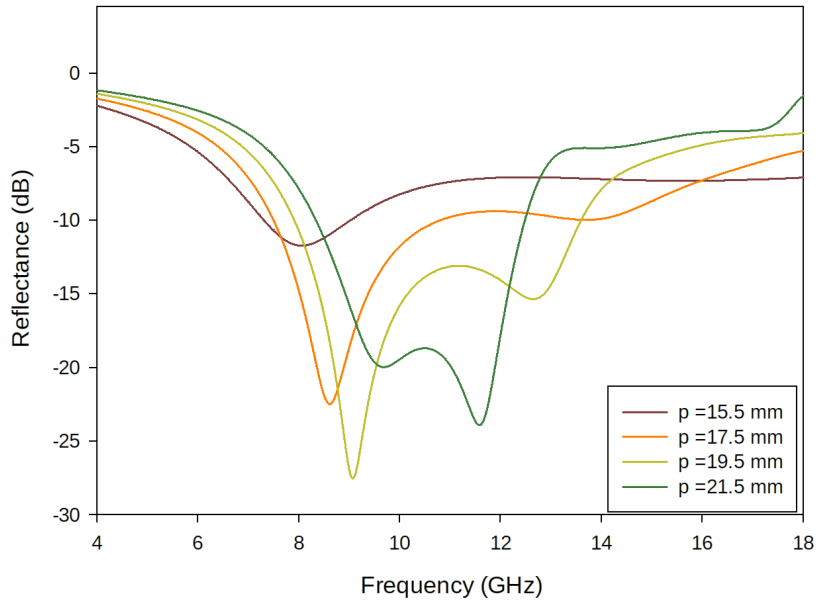


Figure 4.18: Variation of reflectance with unit cell periodicity

those modes at oblique angle of incidence. There exists an angle of incidence at each frequency for which the reflection is minimum in the case of TM modes. This is typical of lossy dielectrics and this angle of incidence is called the Pseudo Brewster angle for the composite structure[206, 207]. The variation of reflectance with angle of incidence for both TE and TM at 11 GHz from the Figure.4.21 indicates the standard lossy dielectric behavior. This is not seen in TE modes as their absorption continues to deteriorate with obliqueness. From the Figure.4.21, the Pseudo Brewster angle for the structure is found to be 46.5° .

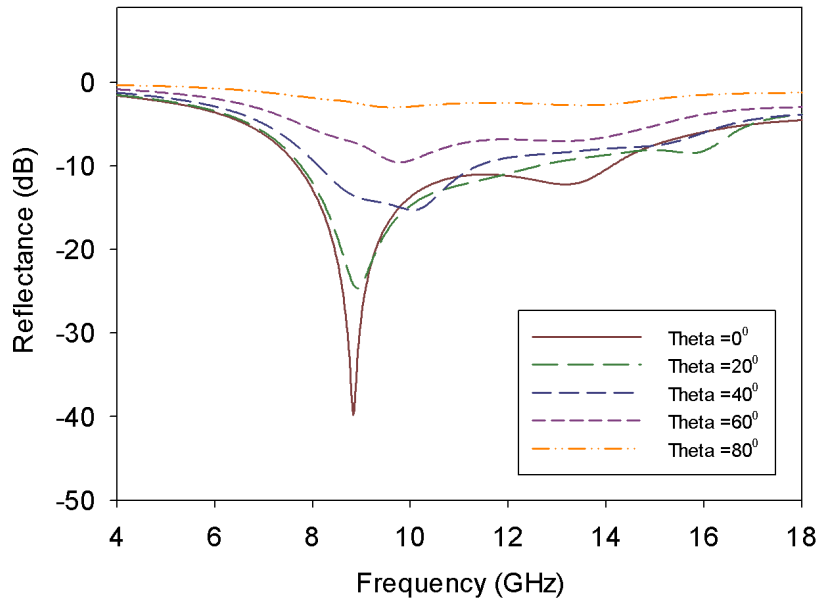


Figure 4.19: Reflectance variation of TE modes with incident angle

4.4.3 Field distribution and Power loss

The power loss density distribution in the structure as shown in Figure.4.22 indicates the strong coupling of incident waves into the structure. It can be seen in the structure that significant power loss happens in PANi as compared to the surrounding Plexiglas substrate. The incident power is heavily dissipated in the top layers and there exists a loss gradient from top to bottom inside the pellet as is indicative from the figure. It is also found that a power

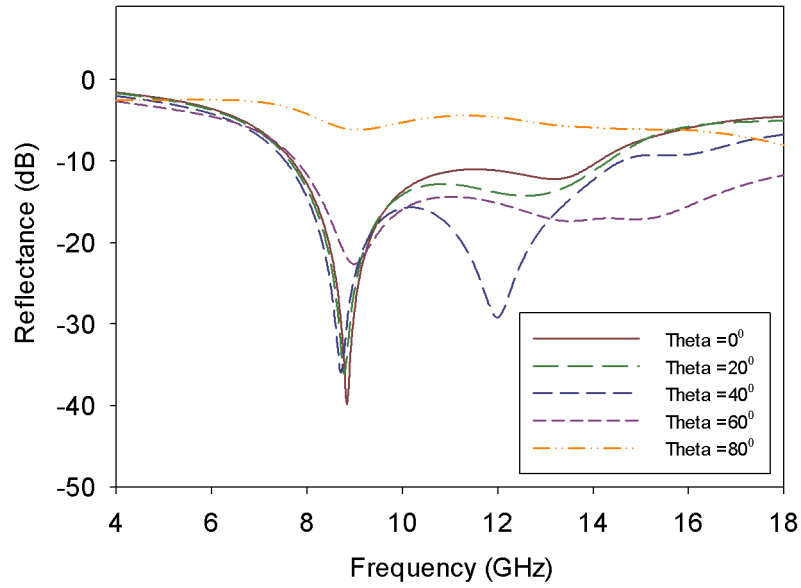


Figure 4.20: Reflectance variation of TM modes with incident angle

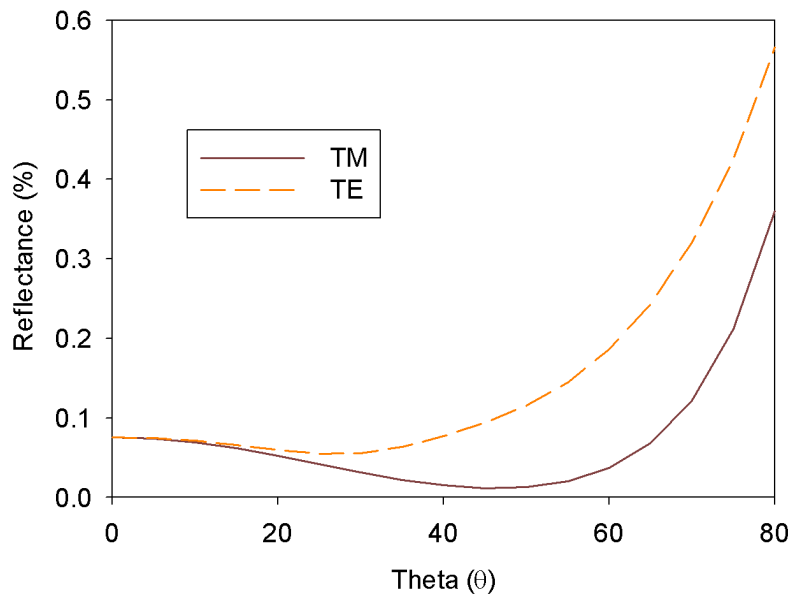


Figure 4.21: Reflectance variation of TE and TM modes at 11 GHz

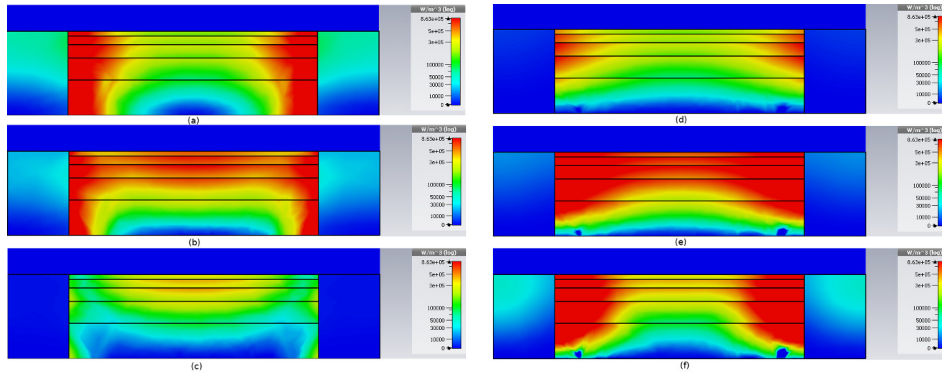


Figure 4.22: Power loss density distribution of the structure at (a)TM-8GHz, (b)TM-11GHz, (c)TM-14GHz, (d)TE-8GHz, (e)TE-11GHz, (f)TE-14GHz

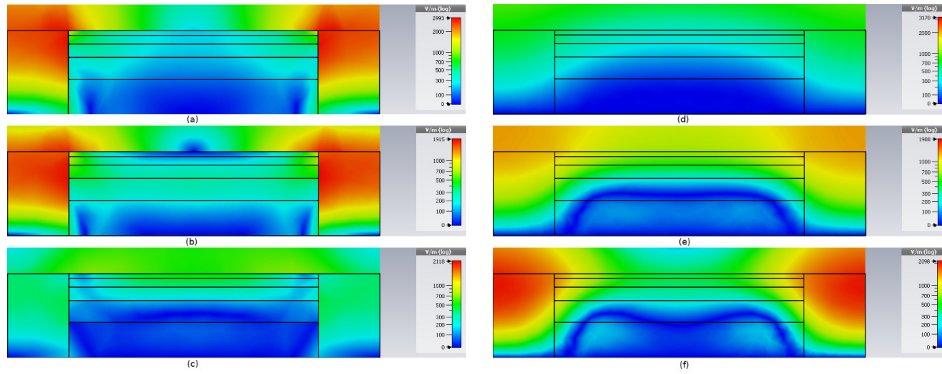


Figure 4.23: E-field distribution of the structure at (a)TM-8GHz, (b)TM-11GHz, (c)TM-14GHz, (d)TE-8GHz, (e)TE-11GHz, (f)TE-14GHz

loss gradient exists in each layer which is very high at the edges of the PANi pellet when compared to the central regions. This has a strong dependence on the polarization of incident wave. The PANi-Plexiglas edges where the electric fields are found to be normal exerts high power loss compared to the perpendicular edge. It can be seen that the loss is slightly higher just below the interface between two PANi layers than that it is just above the interface. This effect is due to the fact that any adjacent bottom layer is having a higher conductivity than the top layer. Hence the ohmic loss encountered by the field will be slightly more in the bottom layer near the interface than above the interface.

The electric and magnetic field distributions are shown in the Figure.4.23

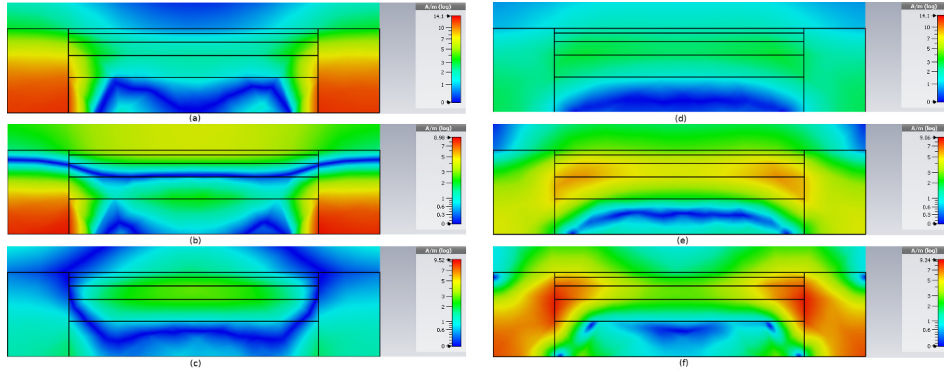


Figure 4.24: H-field distribution of the structure at (a)TM-8GHz, (b)TM-11GHz, (c)TM-14GHz, (d)TE-8GHz, (e)TE-11GHz, (f)TE-14GHz

and Figure.4.24 respectively which shows that there exist a region near the metal where both electric and magnetic fields exist at their minimal value. This is due to the decrease in electric field amplitude as the field attenuates in the pellet gradually. As the field traverses through the pellet, it is subjected to electric losses which are more in the central portion of the pellet hence the surface currents generated on the ground are minimal below the pellet than that it is at the metal under the Plexiglas region. The magnetic field strength is high under the lossless portion of the absorber. As shown in Figure.4.25, this creates a periodic current pattern with constant phase in the ground.

4.4.4 Bistatic RCS analysis

The RCS reduction in the main lobe is about 11.42 dB. Both vertical polarization ($\theta=0^\circ$, $\phi=0^\circ$) and horizontal polarization ($\theta=0^\circ$, $\phi=90^\circ$) for the center frequency (11 GHz) have been plotted in Figure.4.26 and Figure.4.27. It can be seen that at $\theta=\pm 90^\circ$, the PEC has a very low RCS whereas the absorber shows more RCS compared to PEC which can be attributed to evanescent waves propagating along the target metal-absorber interface. In practical applications, this mode can be seldom considered as it is parallel to the absorber. At all the frequencies in the band, the main lobe power is reduced by the absorption mechanism as there is no increase in side lobe power or cross-polar power which indicates the absence of scattering.

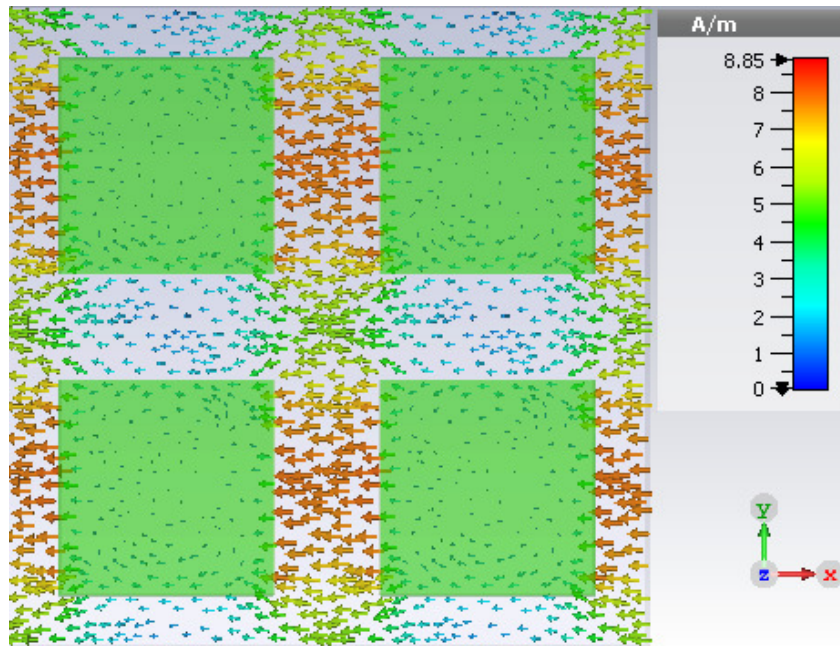


Figure 4.25: Surface current distribution on the target at 11GHz

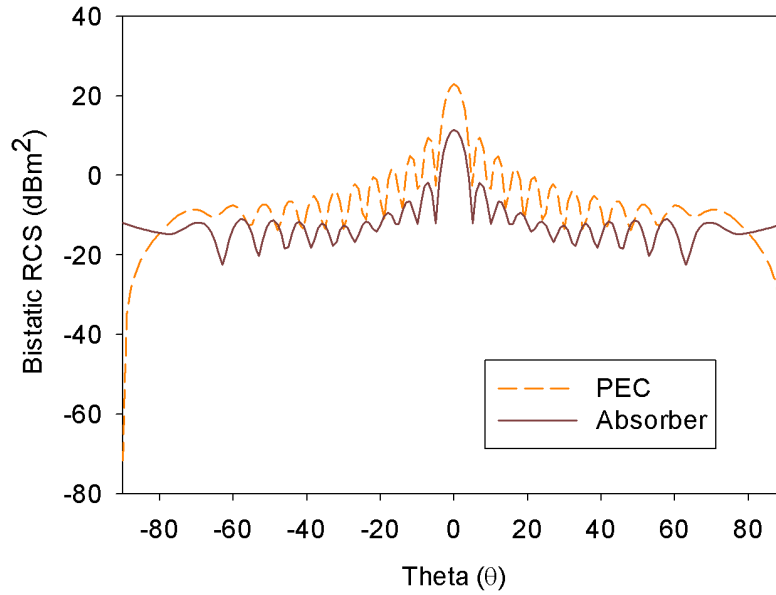


Figure 4.26: RCS Vertical polarization at 11GHz

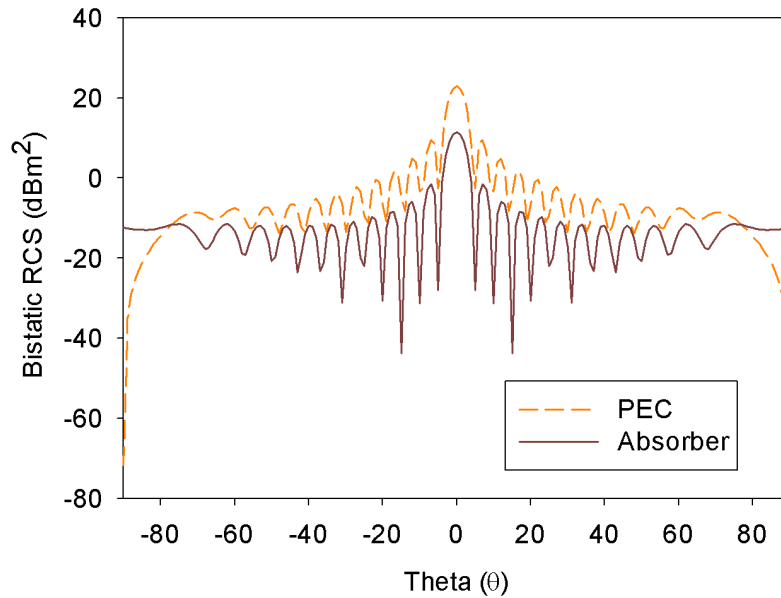


Figure 4.27: RCS Horizontal polarization at 11GHz

4.5 Conclusion

An all-polymer non-resonant wideband absorber with a potential of 3D printing is designed and fabricated. The structure made of Plexiglas contains PANi-Graphene composite with graded conductivity which acts as an impedance transformer to guide the incident electromagnetic fields and attenuate them. The five layered PANi pellet has graded conductivity and thickness based on golden ratio. The parameters have been optimized and the structure absorbs X band and the lower part of Ku band. Its microwave absorptive characteristics have been quantified in terms of reflection loss, bistatic RCS, angular stability and power loss density and field distribution. Conducting polymer composites have a lot of applications especially in the microwave absorption regime as it exhibits good absorption of microwave power. As demonstrated in this work, conducting polymers can be tuned to fabricate wideband absorbers with advantages in fabrication techniques.

Chapter 5

PRINTABLE ANTENNAS BASED ON GRAPHITE DERIVATIVES

The essence of this chapter is the design of UWB antennas on any substrate of choice. After a brief review of literature, the chapter begins with UWB antennas of very small sizes designed on standard FR4 substrate with considerations on the wide bandwidth, portability and circuit integration as outlined by FCC specifications. The metallic regions of the optimized structure was replaced with expanded graphite based material so that the pattern can be created on any substrate. The pilot study was done on FR4 substrate. Later on, the fabrication of the structure on transparent substrate like Poly Methyl Metha Acrylate (PMMA) is done.

Contents

5.1	UWB communication and antennas	120
5.2	Design of compact pentagonal Ultra Wideband monopole antenna with microstrip feed	122
5.2.1	Antenna Geometry	124
5.2.2	Results and discussions	124
5.2.3	Summary	126

5.3	Design of compact planar UWB bevelled monopole antenna with CPW feed	127
5.3.1	Antenna Design and Evolution	127
5.3.2	Results and discussions	130
5.3.3	Summary	132
5.4	Design of CPW fed Band-notched Antenna for Portable UWB Applications	132
5.4.1	Antenna design and discussion	133
5.4.2	Results and discussions	134
5.4.3	Summary	138
5.5	Design of printable UWB antenna made of expanded graphite	139
5.5.1	Antenna design and discussion	140
5.5.2	Results and discussion	141
5.5.3	Summary	145

5.1 UWB communication and antennas

On February 14, 2002, the Federal Communications Commission (FCC) of the United States adopted the First Report and Order that permitted the commercial operation of ultrawideband (UWB) technology[208]. Ultra-wideband communication is a promising wireless communication technology with the allocation of the 3.1 - 10.6GHz bandwidth and has been regarded as one of the most promising wireless technologies that promises to revolutionize high data rate transmission and enables the personal area networking industry leading to new innovations and greater quality of services to the end users. High data rate pulsed communication at power levels below the noise floor and co-existence with other communication systems are the key features of the UWB operations. In the current proposals, UWB is supposed to show its mark in places such as portable devices, wireless USB, BAN, Microwave Imaging etc. to name a few[209]. The wide bandwidth offered by UWB technology is utilized using narrow pulses that are fourth order gaussian in nature.

The virtues of this technology come with many design challenges. One of the major challenges in the transmission of narrow pulses is in the design of the antenna, since a comparable propagation delay and retardation time of the pulse in the antenna with its rise time or duration can result in significant undulations. Apart from the circuit intricacies with its trivial complex algorithm and signal processing expected, the channel interface design that includes an antenna is an integral part of UWB systems and acts as an impedance transformer to efficiently couple the signal into the channel from the circuit and vice versa. Traditionally, broad band antennas fall under the category of traveling wave antennas with their characteristic gradual transitions in impedance from the feed line to that of free space at the antenna edges. However such geometries are relatively large in dimension. In addition, they introduce distortion in their time domain response as a result of displacement of antenna phase center over the wide frequencies of operation. The antenna should be Ultra-Wideband which is usually realized by perturbing multiple resonances in the radiating structure. Multiple resonances can be detrimental to baseband pulses, but the effects are minimized in small element antennas, where surface currents are always in phase unison[210]. Pattern degradation at higher frequencies is minimized in these antennas enabling superior pulse handling capabilities. However, as the size of the antenna shrinks, creating multiple resonances to match and achieve UWB becomes difficult[211, 212, 213].

The current research interest in this field is in its integration with portable systems[214]. For small portable devices, the UWB radiators in planar form are the choice due to their minimal space requisites. The major challenge in designing such antennas is achieving the wide impedance bandwidth within the constrained volume specifications. This rules out the traditional broadband antennas of large size. Hence, in the case of impulse type UWB communications, small sized antennas with wide enough impedance bandwidth help to reduced pulse distortions.

In relation to modernization, printable electronics is a must go solution to many one-time use applications such as paper-based electronic devices, flexible polymer electronics, or in high density charge storage. In its current form, polymer based synthetic conductors are a good choice to be used as precursor materials for microwave radiators in such scenarios where low radiated power and wideband applications are sought. Especially the UWB stands a high chance due to its virtues and that additionally they do have lesser surface

current densities when compared to patch antennas or any other resonant antennas in this regard. Hence the ohmic loss (I^2R loss) suffered in UWB antennas will be much lesser and graphite based UWB antennas are very good option available on the table.

5.2 Design of compact pentagonal Ultra Wide-band monopole antenna with microstrip feed

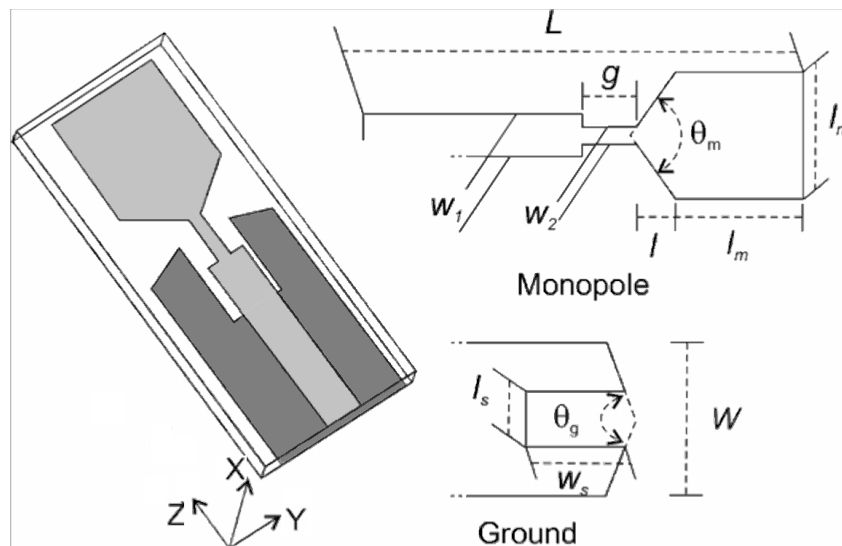


Figure 5.1: Design of the proposed antenna

In this work, we propose the design of a compact pentagonal monopole antenna for use in space constrained applications such as a wireless dongle. UWB antennas designed by employing pentagonal monopoles have been reported widely in the literature[215, 216]. In the present work, multiple matching techniques are incorporated in a pentagonal monopole to realize an ultra compact UWB antenna.

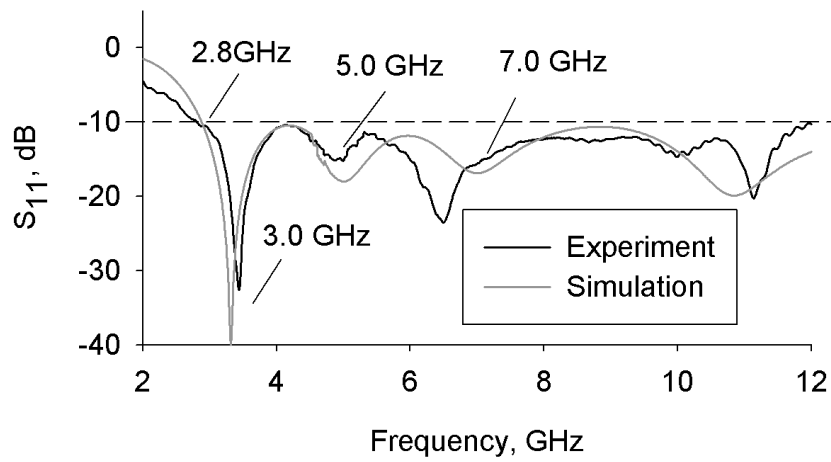


Figure 5.2: Measured and simulated S_{11}

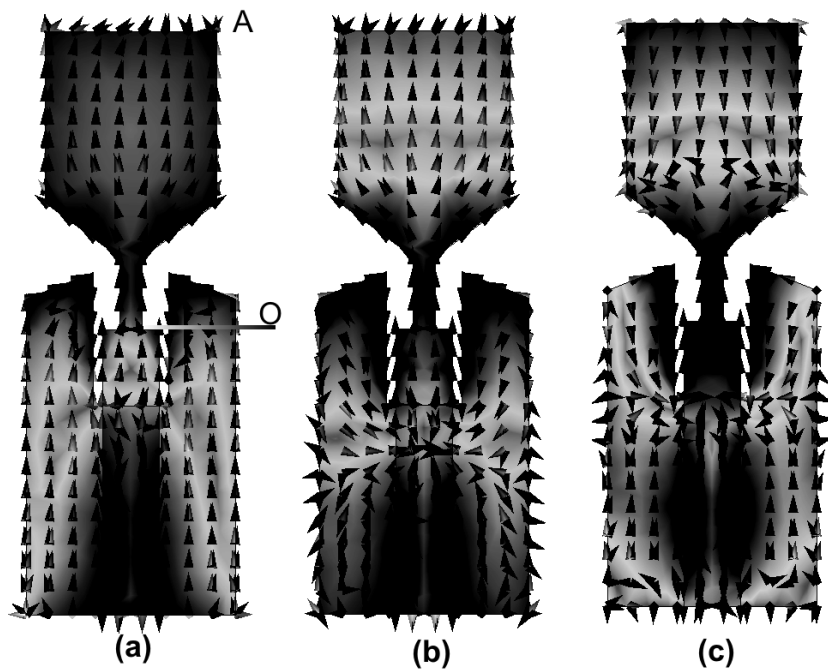


Figure 5.3: Electric field (intensity) and surface current (vector) distributions (dark shade indicates high field intensity) at the three resonances:(a) 3.0 GHz, (b) 5.0 GHz, and (c) 7.0 GHz

Feed	Ground
$L=30\text{mm}$	$W=11\text{mm}$
$l_m=9.0\text{mm}$	$\theta_g=130^\circ$
$l=2.9\text{mm}$	$l_s=4.0\text{mm}$
$\theta_m=106^\circ$	$w_s=7.0\text{mm}$
$w_1=3\text{mm}$	
$w_2=1.2\text{mm}$	
$g=3.8\text{mm}$	

Table 5.1: Optimized parameter values of the design

5.2.1 Antenna Geometry

Figure.5.1 depicts the configuration of the proposed antenna fabricated on FR4 substrate ($\epsilon_r = 4.4$, $h = 1.6\text{mm}$). A 50Ω microstrip line excites the pentagon shaped monopole element as shown. The ground plane of the antenna has a rectangular cut beneath the feed and has flared sides. These along with the pentagonal monopole element perturb multiple resonances in the antenna. Compactness while ultra wide impedance bandwidth is ensured when the cut parameters l_s and w_s , flare parameters θ_m and θ_g and the microstrip width w_2 are properly optimized. On FR4, with optimal geometric parameters, size of the antenna is restricted to $11 \times 30\text{mm}^2$. The optimized parameters are listed in Table.5.1.

5.2.2 Results and discussions

A prototype of the proposed antenna with optimal geometric parameters was fabricated and tested using Rohde & Schwarz ZVB20 Vector Network Analyzer (VNA). Measured and simulated return losses of the antenna are in good agreement as shown in Figure.5.2. The measured -10dB impedance bandwidth is from 2.8-12.0 GHz. The effect of the cut in the ground plane is on the lower band edge and on the overall impedance bandwidth. The first resonance of the antenna can be approximately quantified to a quarter wave variation OA as shown in Figure.5.3, which shows the vector distribution of currents in the antenna. An empirically connected relation to the physical parameters of

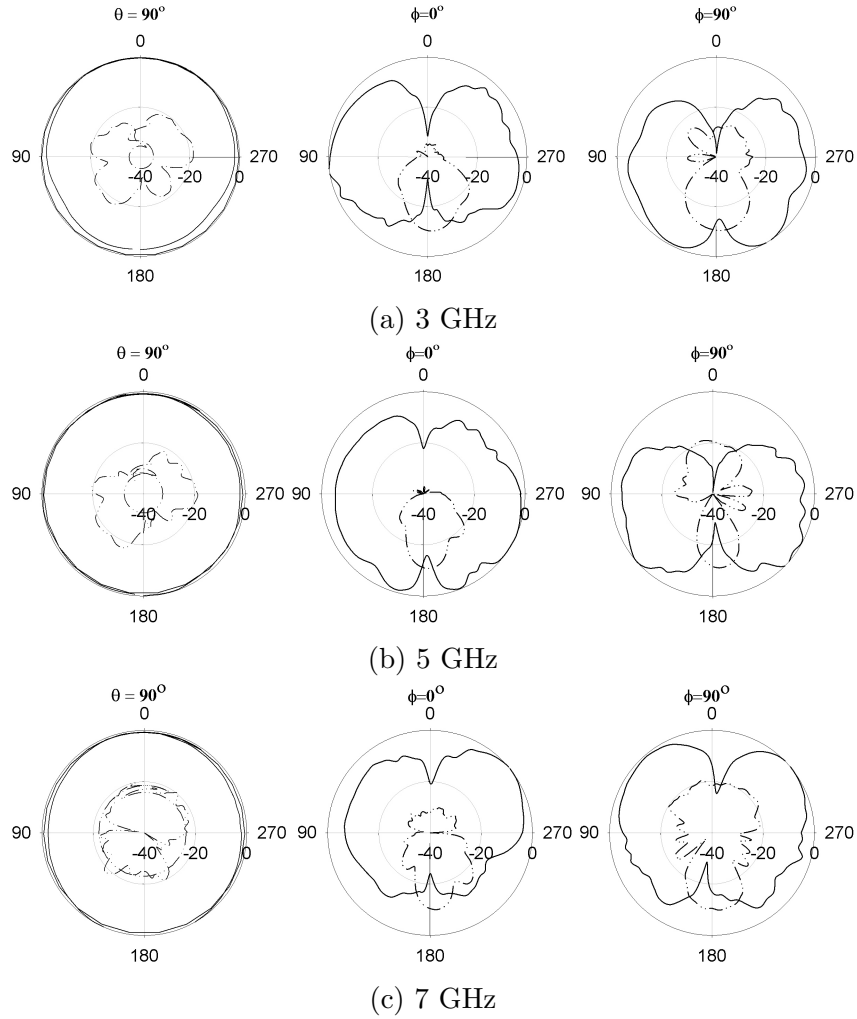


Figure 5.4: Radiation patterns at three resonances

the antenna can be used to relate with the first resonance as in the following equation.

$$f_1(GHz) = \frac{75}{\sqrt{(\epsilon_{\text{eff}} \times OA)}} \quad (5.1)$$

Occurrence of the higher resonances can be attributed to the lower edges of the monopole element and the modified ground plane as seen in Figure.5.3.

The Co-polar and Cross-polar radiation patterns of the antenna at the three resonances in all the three planes and are shown in Figure.5.4. The patterns remain omni-directional in the H-plane (x-z plane) and bi-directional

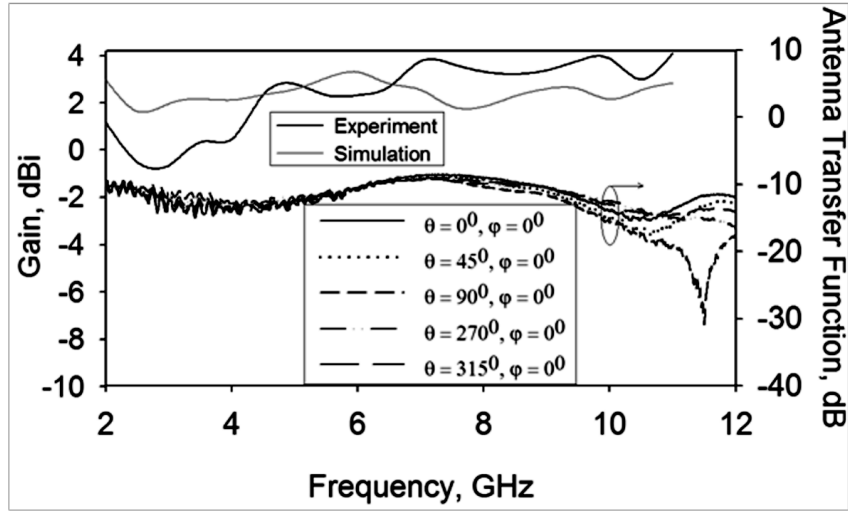


Figure 5.5: Measured gain of the antenna

in the other two planes (x-y, y-z). Antenna polarization is in the y-direction throughout the band as is evident from the current distribution in Figure.5.3. Measured gain of the antenna is shown in Figure.5.5 and the average gain is found to be 2.84 dBi. The antenna transfer function computed as in reported literature[217], remains flat with variation within 10 dB in the entire operational band as shown in Figure.5.5, which is highly desirable for deployment in Discrete Spread UWB systems. Fidelity of a transmitted fourth order Gaussian pulse in the broad side direction is found to be 89% when $\theta = 0^\circ$, $\phi = 0^\circ$ and 88% when $\theta = 90^\circ/270^\circ$, $\phi = 0^\circ$. Unlike in many antennas, fidelity is almost a constant indicating towards superior pulse handling capabilities of this antenna.

5.2.3 Summary

A planar ultra compact antenna occupying an area of $11 \times 30\text{mm}^2$ is proposed for UWB systems. The impedance bandwidth encompasses the FCC specification for UWB applications and more from 2.8-12.0 GHz. Small element size of the antenna results in stable radiation patterns at all frequencies with reasonable gain and excellent pulse handling capabilities. These achievements make the proposed design a good candidate for space constraint UWB applications such as USB dongle and PDA systems.

5.3 Design of compact planar UWB bevelled monopole antenna with CPW feed

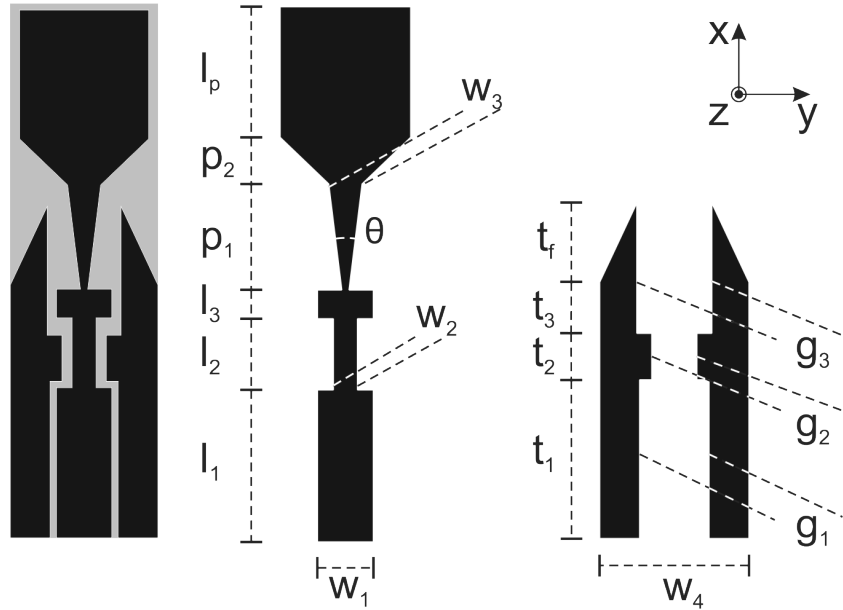


Figure 5.6: Design of the proposed antenna

In this work, the design of a very compact coplanar-fed wideband antenna suitable for portable UWB systems is presented[218]. The antenna offers a bandwidth from 3.0GHz to 11.4GHz. The radiation patterns at different frequencies in the band as well as the gain and efficiency of the antenna are measured. The parameters defining the wide impedance bandwidth are identified and characterized.

5.3.1 Antenna Design and Evolution

Square monopole antenna and its derivatives have been reported widely in literature for UWB operations[211, 213]. The proposed design was evolved keeping in mind the constraint on the space occupied by the radiating element. For easy integration and reduced spatial congestion with the popular USB plug footprint of Type-A, it is desirable to have the device size be equal to or smaller than 12mm at least along one dimension[219]. Hence, the target was to reduce the antenna width to 8mm with a 2mm guard space on either side.

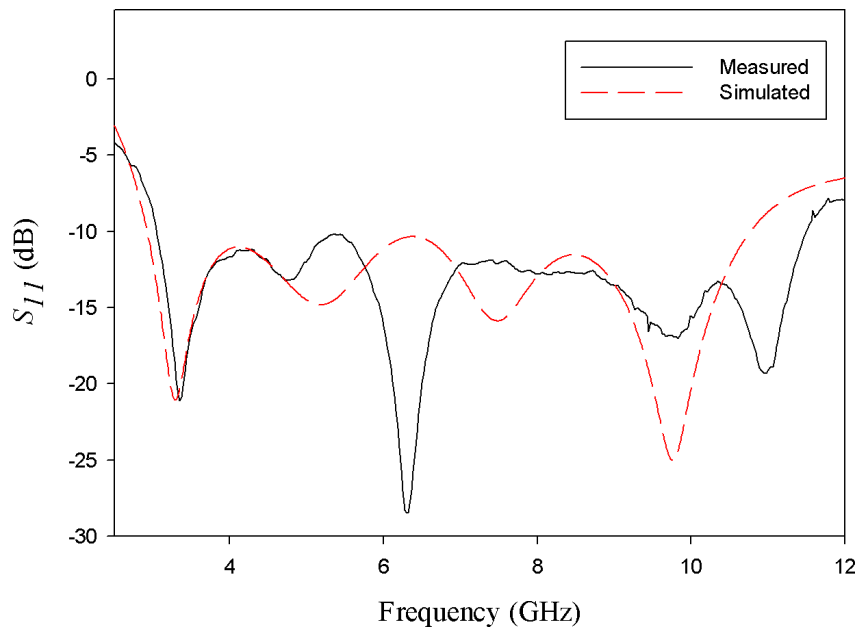
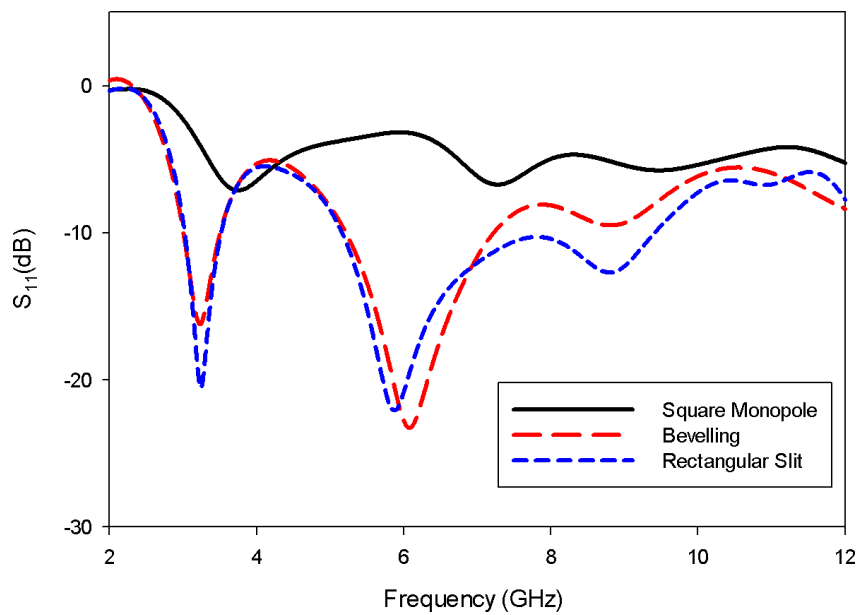
Figure 5.7: Measured and simulated S_{11} 

Figure 5.8: Improvement in S parameter by beveling

The proposed antenna is designed on 1.6mm thick FR4 substrate and fed by a 50Ω coplanar line. The single sided design on the substrate enables easy

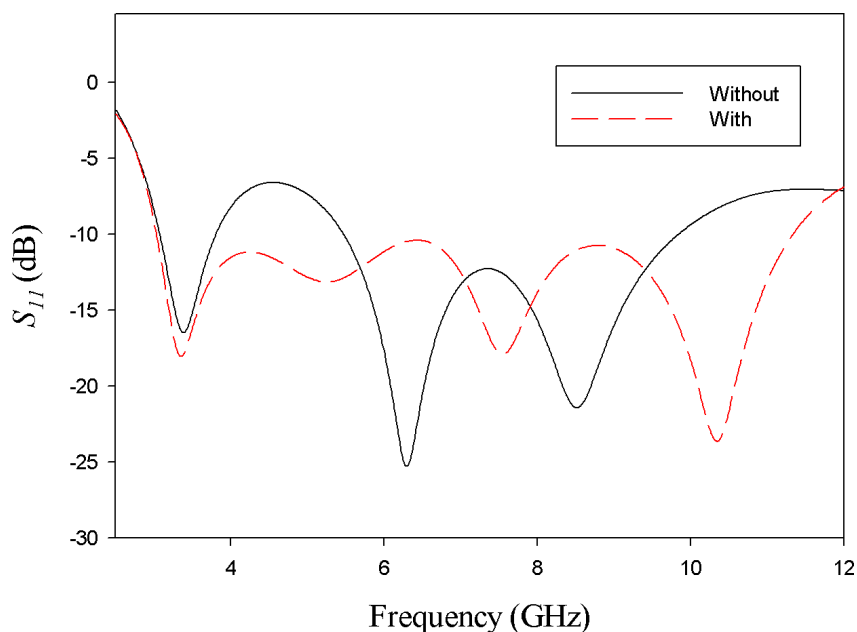


Figure 5.9: Improvement in S parameter by impedance transformer

integration with electronic circuits. The antenna is derived from a square monopole patch of size $7 \times 7 \text{ mm}^2$. The monopole size is compact but is not optimized for impedance matching over the desired band. Hence following steps were carried out to optimize the antenna design for UWB operation. Beveling has been a widely reported technique for achieving broadband performance in case of planar antennas[220, 216]. So, first the monopole and ground plane edges were beveled to improve the impedance bandwidth. A rectangular slit in the ground plane, is also incorporated just beneath the feed monopole transition for further improvement. Figure.5.8 shows the improvement achieved via beveling and rectangular slit[221]. However, these modifications are observed to be not enough for the desired compact UWB operation. It is with the proposed impedance transformer along the feed line that a significant improvement in the antenna bandwidth is achieved. The contribution of impedance transformer is evident from the Figure.5.9.

The antenna geometry is depicted in Figure.5.6 with the optimized parameters tabulated in Table.5.2. The simulation studies on the proposed antenna design were done in CST Microwave Studio and the measurements were taken using Rohde & Schwarz ZVB20 VNA.

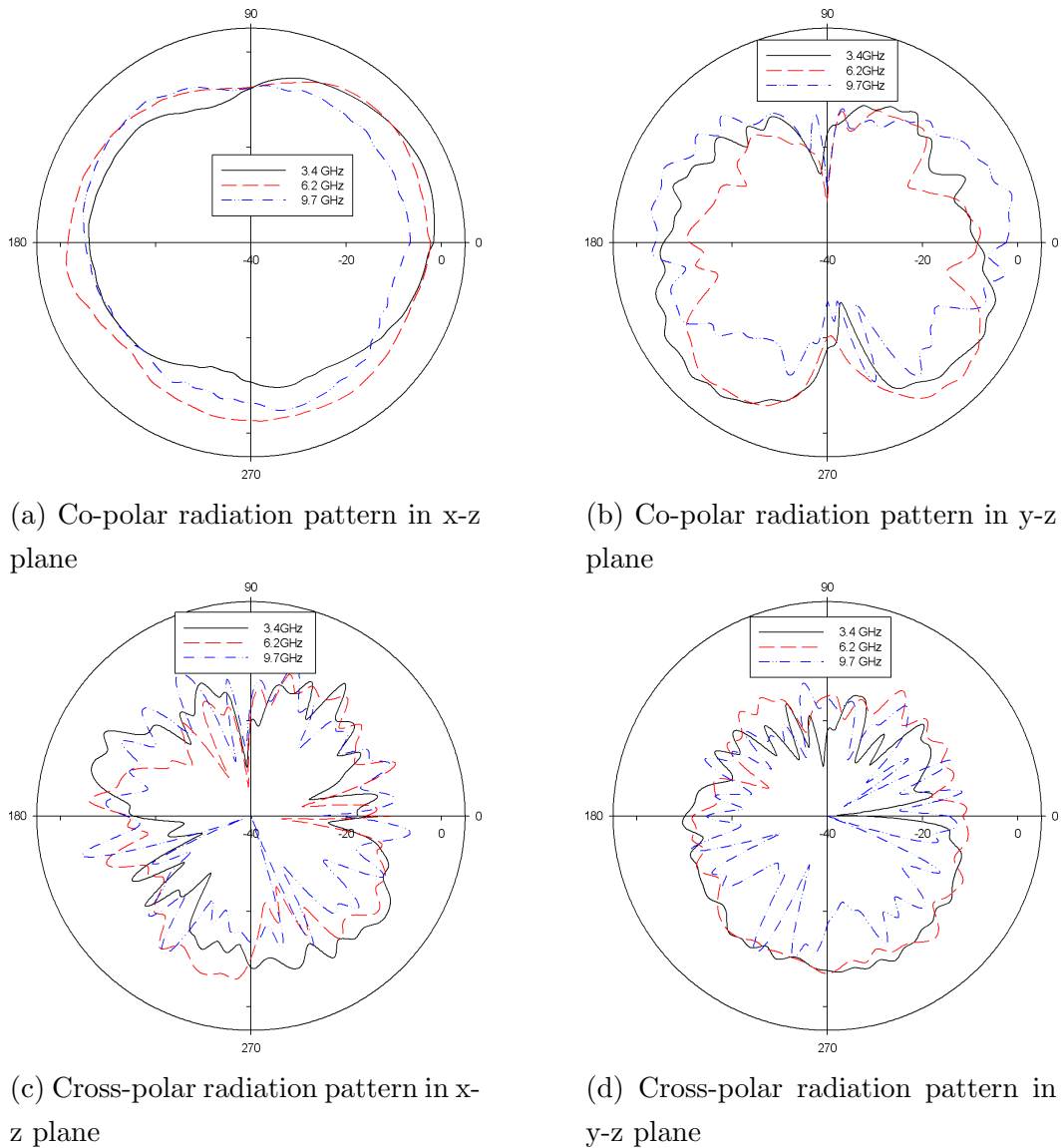


Figure 5.10: Radiation patterns at three resonances

5.3.2 Results and discussions

Results shown in Figure.5.7 indicate that the structure is impedance matched over a wide band with four resonances at 3.4GHz, 5.2GHz, 7.5GHz and 10.4GHz. The start frequency of the operating band can be fixed with the first resonance using the following empirical relationship between antenna pa-

Feed	Ground
$l_1=9.4\text{mm}$	$t_1=9.8\text{mm}$
$l_2=3.8\text{mm}$	$t_2=2.5\text{mm}$
$l_3=1.6\text{mm}$	$t_3=2.7\text{mm}$
$p_1=5.7\text{mm}$	$t_4=4.3\text{mm}$
$p_2=2.5\text{mm}$	$g_1=3.7\text{mm}$
$l_p=7.0\text{mm}$	$g_2=2.4\text{mm}$
$w_1=3.0\text{mm}$	$g_3=4.0\text{mm}$
$w_2=1.3\text{mm}$	$w_4=8.0\text{mm}$
$w_3=1.0\text{mm}$	
$\theta=140^\circ$	

Table 5.2: Optimized parameter values of the design

rameters:

$$f_1(\text{GHz}) = \frac{300}{4(p_1 + p_2 + l_p) \sqrt{\epsilon_{eff}}} \quad (5.2)$$

where the dimensions of p_1 , p_2 and l_p are in millimetres.

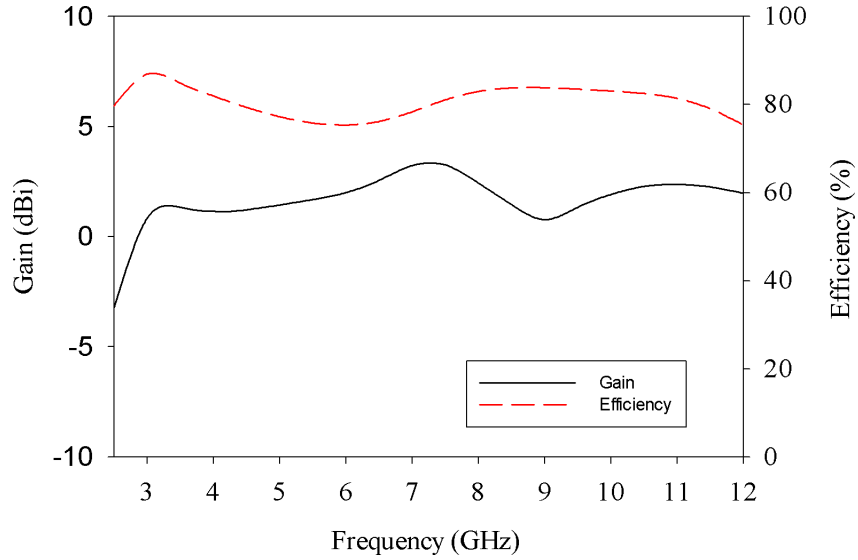


Figure 5.11: Gain and efficiency of the antenna

The wide band operation is then optimized by fine tuning the dimensional

parameters. The radiation patterns in the two orthogonal planes (x-z and y-z) are measured and plotted at the resonant frequencies in Figure.5.10. The measured gain and efficiency of the antenna is shown in Figure.5.11. It is observed that the simulated and measured S_{11} registers a slight disparity at higher frequencies. This effect can be attributed to the finite ground width. The ground currents are observed to be sensitive to the length and the distance of the feeding point and needs to be examined in detail to ensure ground plane isolation during integration.

5.3.3 Summary

A novel compact planar ultra wideband beveled monopole for portable UWB systems is designed. This configuration gives ultra wideband operation under the constraint of a significantly reduced antenna size. The antenna parameters such as return loss, radiation pattern, gain and efficiency are measured. The antenna is suitable for single sided constructions due to its CPW feed and hence avoid constructional complexities arising in microstrip UWB antennas.

5.4 Design of CPW fed Band-notched Antenna for Portable UWB Applications

With all the advantages the UWB systems provide, it is to be noted that the IEEE 802.11a technology (WLAN: 5.1-5.8GHz) which is so ubiquitous, shares a portion of the spectrum allocated for UWB. Hence mutual interference between these two signals is a serious issue. This is usually handled by using a notch filter designed to attenuate WLAN spectrum explicitly between the UWB system and the antenna[222]. As this extra filter usually increases system requirements, this can be incorporated into the antenna itself. In this work, the design of a very compact coplanar-fed wideband antenna with an intrinsic WLAN notch filter suitable for portable UWB systems is presented. The antenna offers a bandwidth from 3.0GHz to 11.4GHz with a notch filter designed for center frequency equal to 5.45GHz. The band is effectively split up into two so that the antenna can communicate in the lower UWB (3.1-5.1GHz) and the upper UWB (5.8-10.6GHz) modes of operation. The

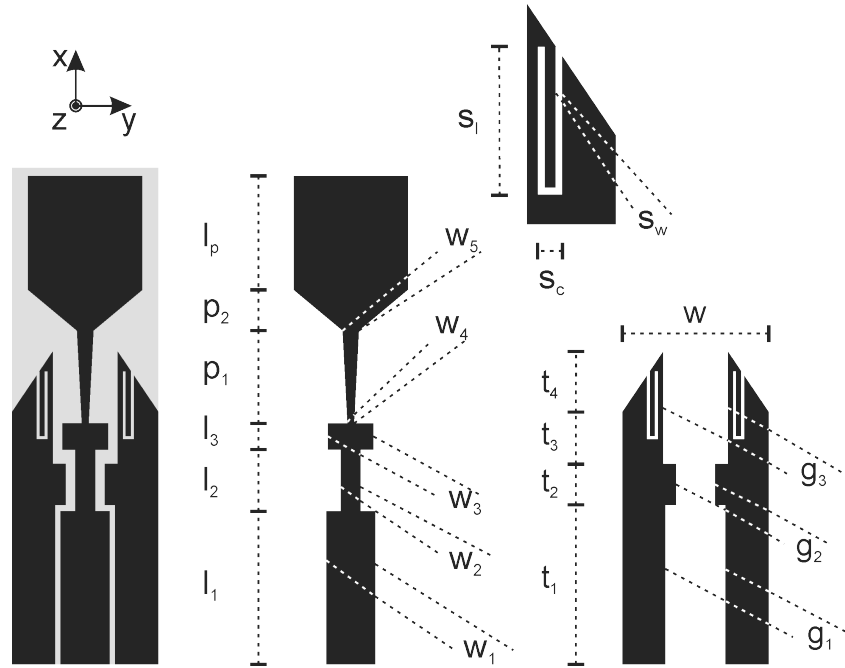


Figure 5.12: Structure of the proposed antenna with notch

radiation patterns at different frequencies in the band as well as the gain and efficiency of the antenna are measured.

5.4.1 Antenna design and discussion

The popularity of USB communication in modern gadgets spawns the possibility of UWB dongles for short ranged, high data rate communication. The integration of UWB radiators in such dongles demand severe spatial congestion alongside other support circuitry onboard. Hence in this study, the spatial constraints occupied by the UWB radiator were accentuated. Generally USB plug footprint of Type-A is regarded as the principal physical specification that USB dongle vendors prefer to connect their devices directly to a host or to the downstream port of a hub and is the most popular type of USB port supported by modern portable computing and multimedia systems. For easy integration and reduced spatial congestion compliant with this specification, it is desirable to have physical size of the USB device equal to or less than 12mm along any dimension. Hence, the design challenge was to reduce the

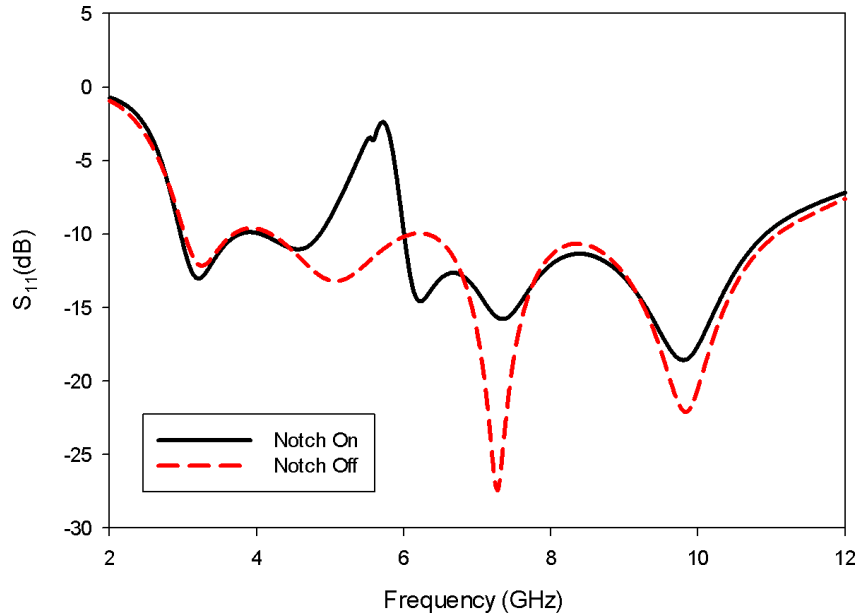


Figure 5.13: S_{11} of the antenna with and without notch action

antenna width with enough guard space on either side without compromising the UWB specifications.

The single sided designs of antenna on substrate enable better conformal integration with electronic circuits. Hence the proposed antenna was designed on FR4 substrate ($h = 1.6\text{mm}$, $\epsilon_r = 4.4$) fed by a 50Ω coplanar feed. Widespread literature can be found regarding the candidature of square monopole antenna and its alterations for achieving UWB operation. Thus as a template design, a square monopole antenna of size $7 \times 7\text{mm}^2$ was chosen.

5.4.2 Results and discussions

Although the square monopole size was compact it was not optimized for impedance matching over the desired band. A series of alterations were made to achieve the target. One way of enhancing the bandwidth of planar antennas is by a technique called beveling. Beveling of ground plane or the monopole edges can significantly enhance the broadband nature by gradual transition of wave impedance from the line to that of free space which has been a widely reported technique. So, first the monopole and ground plane edges were beveled to improve the impedance bandwidth. It was found that beveling significantly

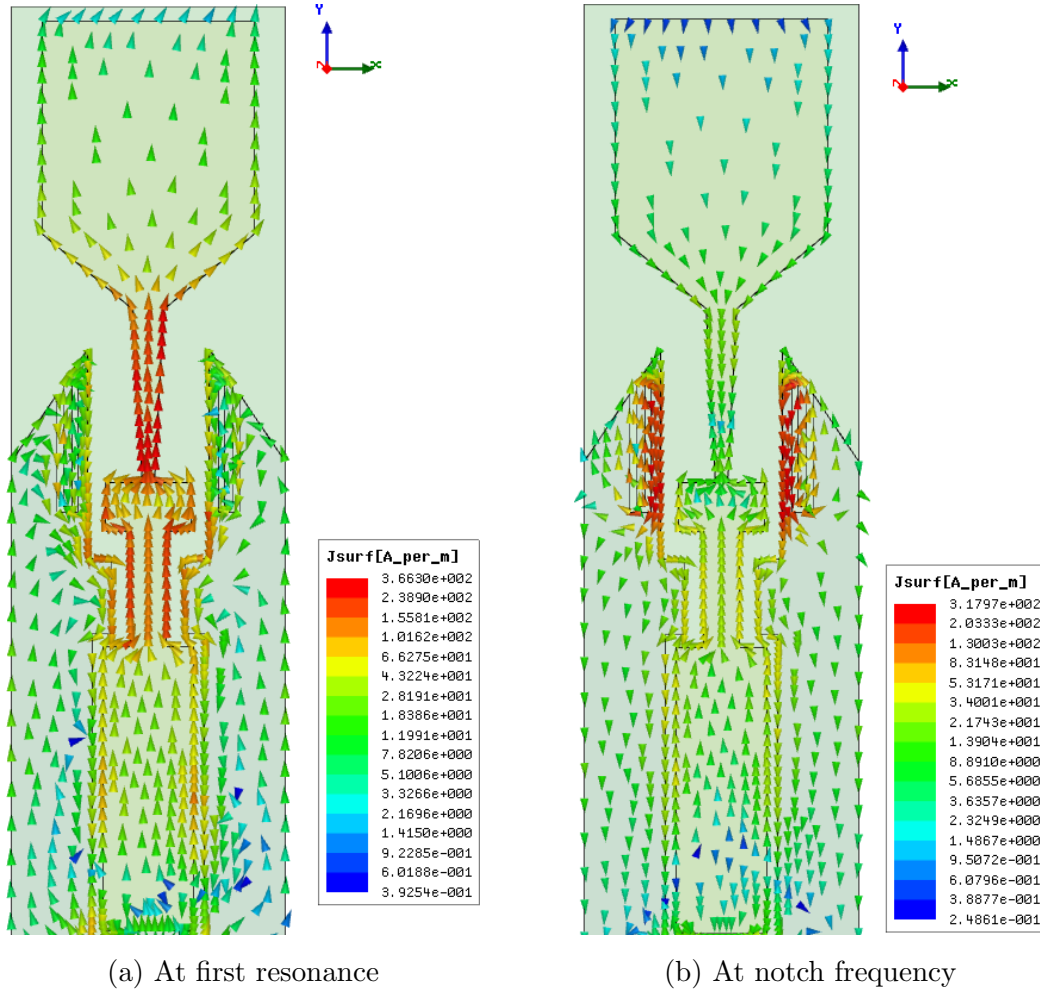


Figure 5.14: Surface current distribution on the antenna

mended the return loss characteristics by introducing a resonance at 6GHz. The entire spectrum was split into a lower band and an upper band. Further improvement over the impedance bandwidth was done by a rectangular slit in the ground plane just beneath the feed to monopole transition. The rectangular slit could give the structure a better response at higher frequencies. The upper bandwidth was effectively increased by this modification. The complete UWB bandwidth was brought into the antenna by a new impedance transformer (w_2 , w_3 , g_2) along the feed line. This impedance transformer could make the peaks at 4GHz and at the high frequency in return loss to come under -10dB. The resonance at 6GHz was found to be shifted to the lower fre-

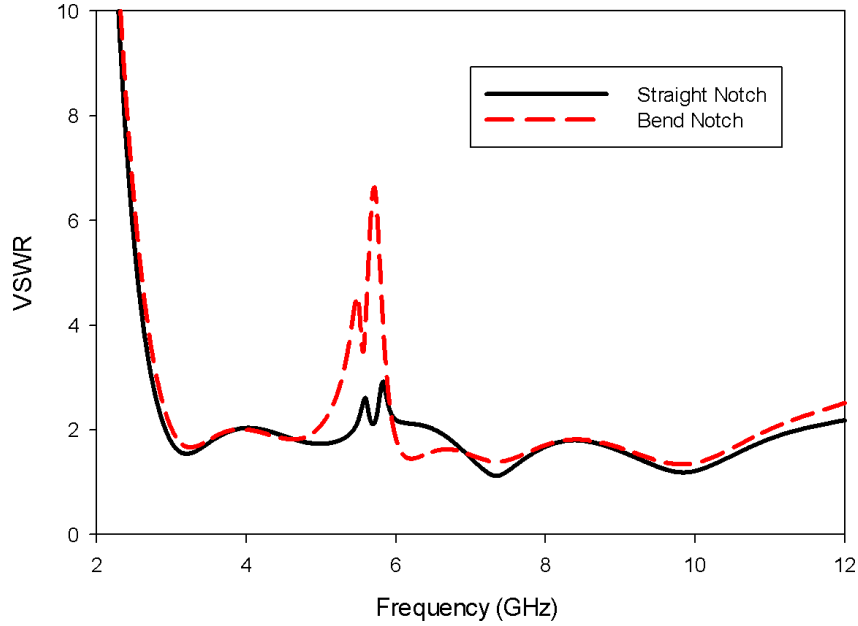


Figure 5.15: VSWR of the antenna for straight notch and for bend notch

quency and two new resonances were found at 7.25GHz and 9.9GHz. These resonances neatly merged the VSWR less than 2 bands of lower and upper bands forming a continuous band from 2.9GHz to 11.04GHz satisfying the FCC specification. This can be seen in Figure.5.13.

The first resonance (f_1) in the band of operation was found to be depended on the parameters p_1 , p_2 and l_p through the following equation:

$$f_1(\text{GHz}) = \frac{75}{(p_1 + p_2 + l_p) \times \sqrt{\epsilon_{eff}}} \quad (5.3)$$

Where ϵ_{eff} = effective dielectric constant of FR4 with air as the second dielectric. The modifications up to this point were done with the complete UWB spectrum under consideration. In order to avoid interference with WLAN, it was worth seeking a filter centred at this band. The idea of quarter wavelength slits for band notching the undesired frequencies can be traced in literature[223]. Similar quarter wavelength slits designed at centre frequency=5.45GHz for notching out 5.1-5.8 GHz regime were realized alongside the antenna structure by introducing two straight symmetric quarter wavelength slits on the ground plane of the antenna. But the VSWR in the band due to the straight slits were very low. It was by a bent configuration of the

Feed	Ground
$l_1=9.4\text{mm}$	$t_1=9.8\text{mm}$
$l_2=3.8\text{mm}$	$t_2=2.5\text{mm}$
$l_3=1.6\text{mm}$	$t_3=3.2\text{mm}$
$p_1=5.7\text{mm}$	$t_4=3.7\text{mm}$
$p_2=2.5\text{mm}$	$g_1=3.7\text{mm}$
$l_p=7.0\text{mm}$	$g_2=2.4\text{mm}$
$w_1=3.0\text{mm}$	$g_3=4.0\text{mm}$
$w_2=1.2\text{mm}$	$w=9.0\text{mm}$
$w_3=2.8\text{mm}$	$s_c=0.7\text{mm}$
$w_4=0.4\text{mm}$	$s_w=0.2\text{mm}$
$w_5=1.0\text{mm}$	$s_l=3.98\text{mm}$

Table 5.3: Optimized parameter values of the design

slits that a very good VSWR was obtained. The comparison is shown in the VSWR plot of Figure 4. Although the tunability of the notch bandwidth is limited by the physical dimensions of the antenna, the bandwidth is dependent on the width (s_w) of the slit. The slits were also found to be inactive when the openings of the slits were short circuited. This makes the slits electronically switchable. The slit parameters (s_w , s_l , s_c) and the notch frequency (f_n) of the filter are related by the following equation:

$$f_n(\text{GHz}) = \frac{75}{(2 \times (s_l - s_w) + s_c) \times \sqrt{\epsilon_{eff}}} \quad (5.4)$$

The final antenna geometry is best described by Figure.5.12 with the optimized parameters in Table.5.3. The simulation studies on the proposed antenna design were done in Ansoft HFSS and the measurements were taken using Rohde & Schwarz ZVB20 VNA. The gain of the antenna with notch and without notch is plotted in Figure.5.16. The dip in gain when the notch is turned on is clearly seen. The average efficiency of the antenna is around 81%. The 3D radiation patterns of the antenna at three frequencies can be seen in Figure.5.17 to be omni-directional.

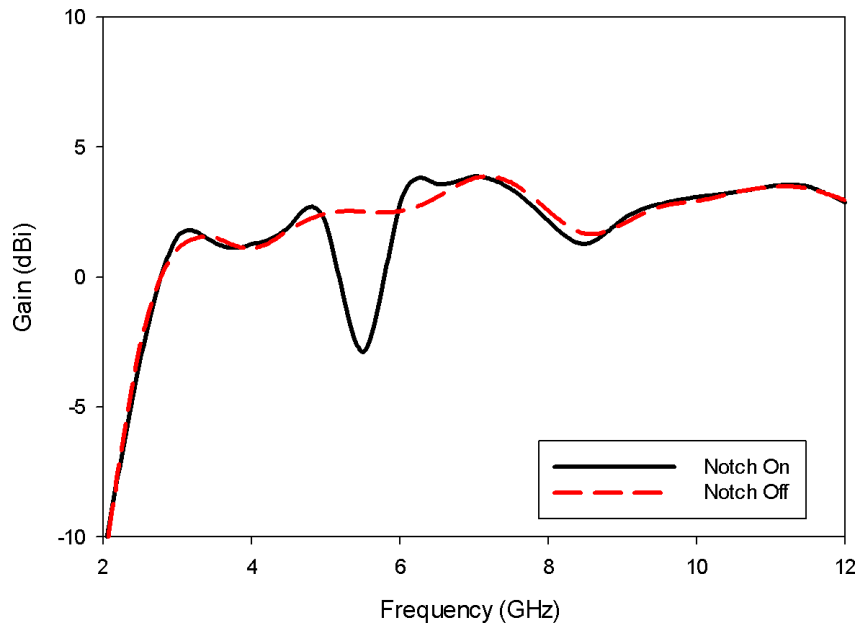


Figure 5.16: Gain of the antenna with notch on and with notch off states

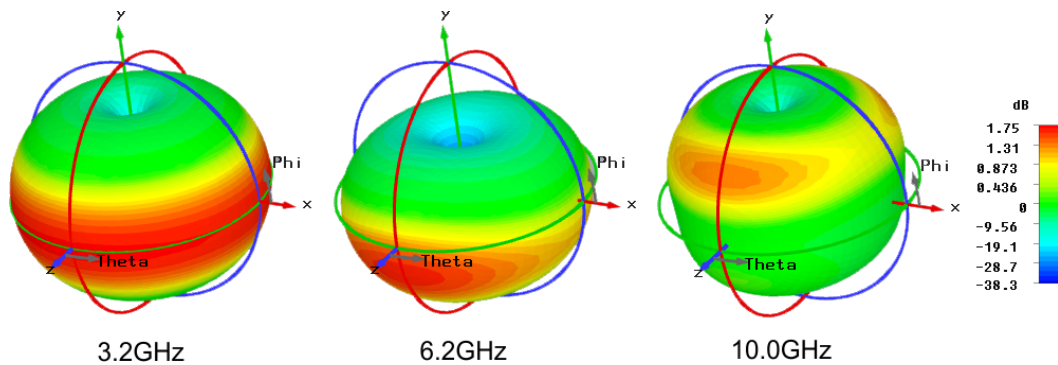


Figure 5.17: Radiation pattern at three frequencies

5.4.3 Summary

A band-notched UWB antenna for portable USB devices is proposed. An exhaustive study to optimize the design parameters was performed. The return loss, gain, efficiency and radiation pattern of the antenna are reported. The design frequency of the notch and first resonance is found to be tunable. The antenna proves to be a good choice with the impedance bandwidth, small size and most importantly, the notch characteristics suitable for UWB applications coexistent with WLAN link.

5.5 Design of printable UWB antenna made of expanded graphite

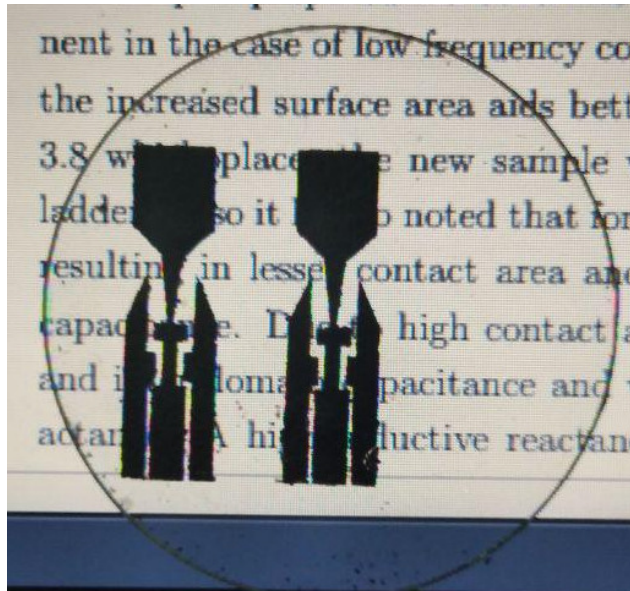


Figure 5.18: Graphene antenna patterned on PMMA substrate

This section outlines the method to fabricate UWB antenna on any substrate of choice using expanded graphite. Preferably, the CPW fed single sided designs are easily printable onto such substrates enabling low fabrication cost and complexity with the possibility of roll to roll production[224]. It also has advantages in terms of absence of via holes, shorting pins, low radiation loss, good impedance match, enhanced bandwidth. Hence in this study, the bevelled square monopole UWB with CPW feed was chosen. In the fabrication of antennas there are two methods to pattern the conducting composite onto the substrate. One is by screen printing and the other is by laser/chemical etching. The latter technique uses more material as the entire substrate is first coated with the material before patterning. But this is more precise as the patterning is done using laser or chemicals. The following is a discussion on the fabrication and performance characterization of graphene based antennas patterned onto FR4 and PMMA substrates (Figure.5.18). The expanded graphite is a good candidate for use as lossy metal. This can act as the metallic areas in a conventional copper based UWB antenna. The rationale behind

the fabrication of UWB antenna using these synthetic materials is owing to the low power and wide bandwidth that UWB uses to communicate.

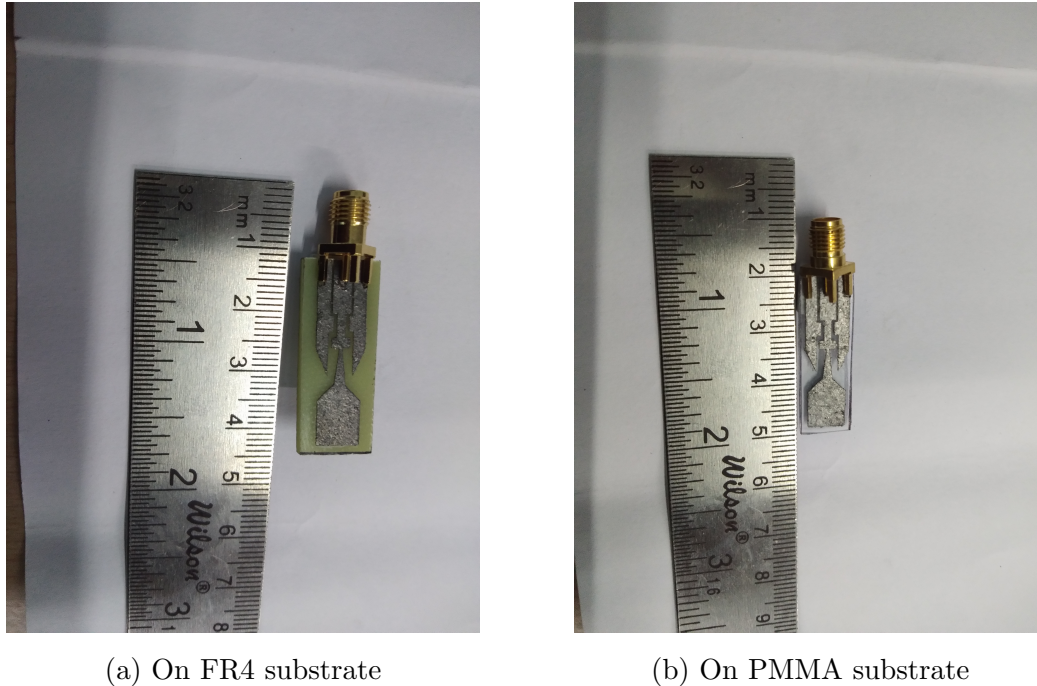


Figure 5.19: Graphene based antenna

5.5.1 Antenna design and discussion

The antennas were patterned on FR4 substrate ($\epsilon_r = 4.4$, $h = 1.6mm$, $s = 0.35mm$, $w = 3mm$) and PMMA substrate ($\epsilon_r = 3.2$, $h = 0.85mm$, $s = 0.2mm$, $w = 3mm$) using pressure sensitive adhesive as the binder and microwave expanded graphite as the conductive filler. In a typical fabrication, a known weight of expanded graphite is spread evenly on the surface of substrate which is already coated with a pressure sensitive adhesive. The substrate is then subjected to high pressure of about $100kg/cm^2$ offered by a hydraulic press for two minutes. The substrate is then taken out of the die and polished using graphite coated cotton to clear the residual debris and to spread a thin layer of continuous graphene platelets over any microscopic defected regions. The coated substrate is then set for patterning. The computer generated pattern is etched onto the graphene layer by laser or CNC milling thereby selectively

removing the unwanted portions. The final structure is cut and polished into required dimensions (Figure.5.19a and Figure.5.19b). The optimized parameters of the FR4 substrate based antenna is already discussed in the previous section. The same dimensions were adopted for the graphene antenna on FR4 substrate. In the case of PMMA substrate, the dimensions of the antenna elements were tuned to suit the required bandwidth. The optimized parameter values of the design are indicated in the Table.5.4.

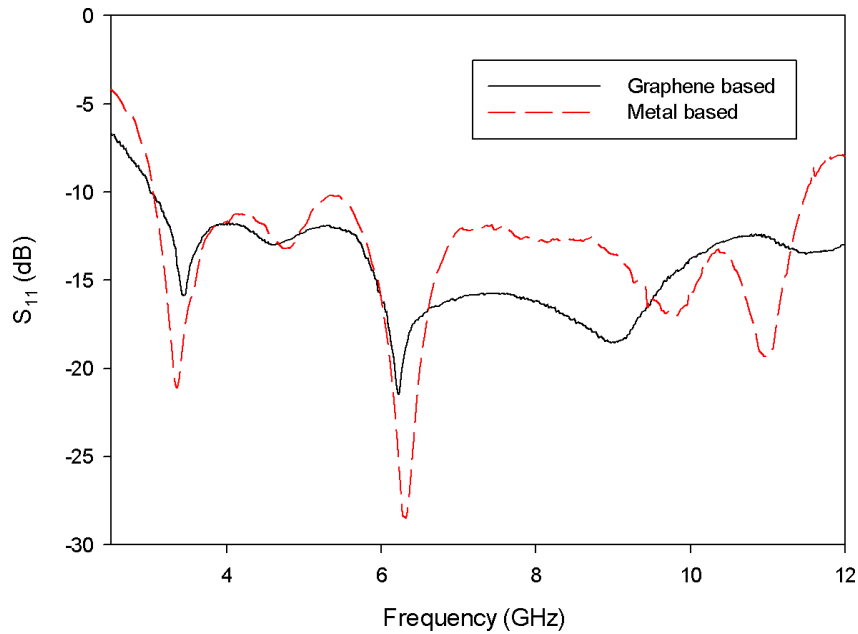


Figure 5.20: Comparison of measured return loss of copper-based and graphene-based antennas on FR4 substrate.

5.5.2 Results and discussion

The antennas were tested for their return loss which is indicated in Figure.5.20 and in Figure.5.21. It can be seen that the FR4 based antenna shows almost the similar return loss as that of the copper based antenna. The PMMA based antenna also expresses congruency with its own simulated results. Both antennas have potential to perform well for use in paper/plastic electronics circuits. The gain and efficiency of FR4 and PMMA substrate antennas are given in Figure.5.23a and Figure.5.23b respectively. As expected, the gain and efficiency of the graphene based antennas are lower than that of copper based

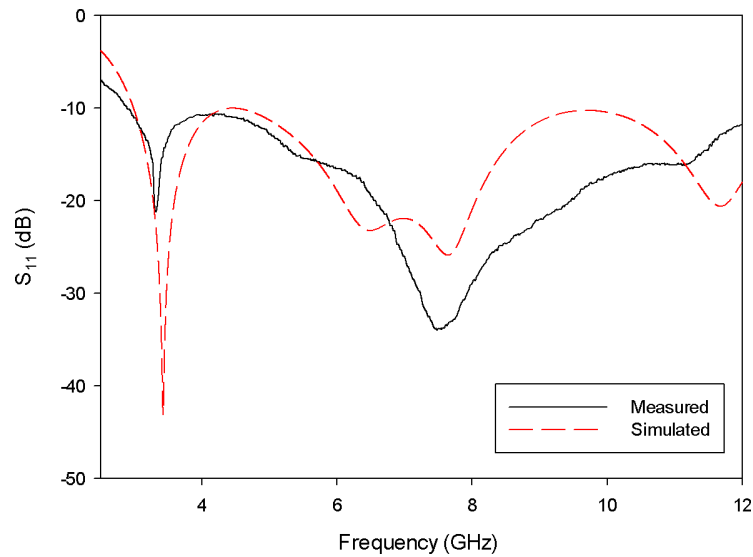


Figure 5.21: Comparison of simulated and measured return loss of graphene-based antenna on PMMA substrate.

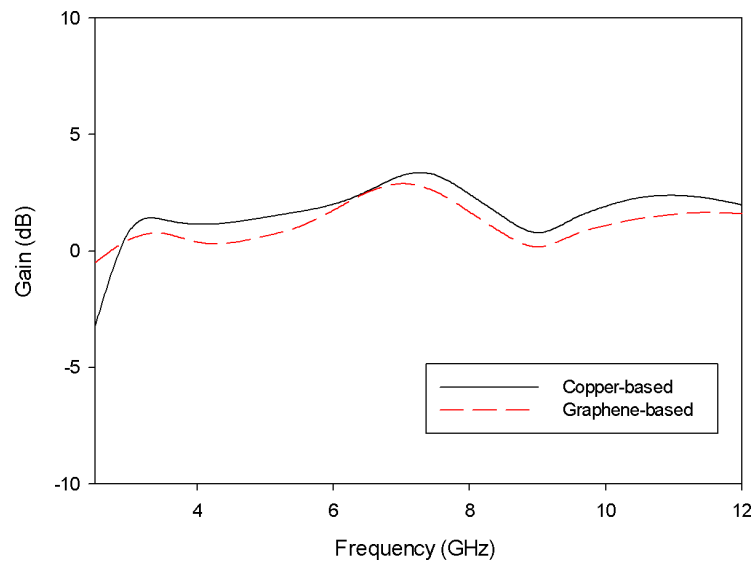
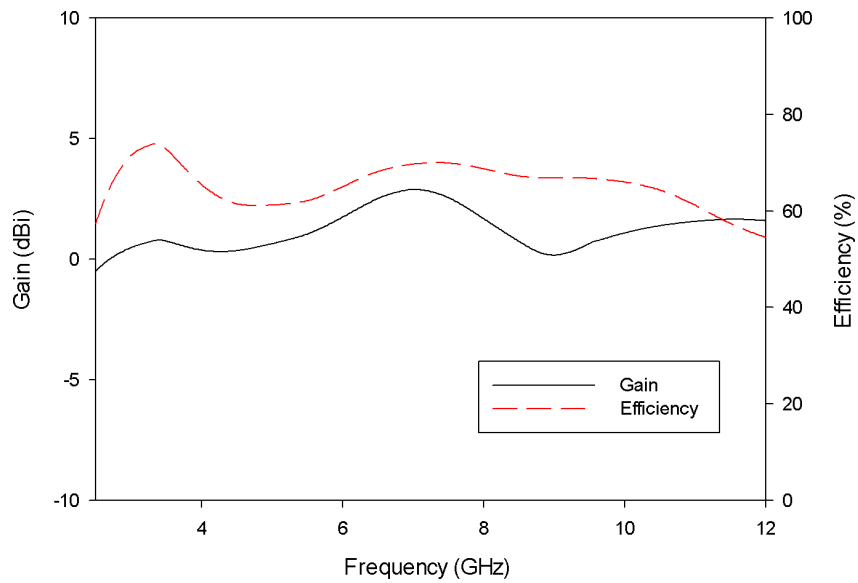
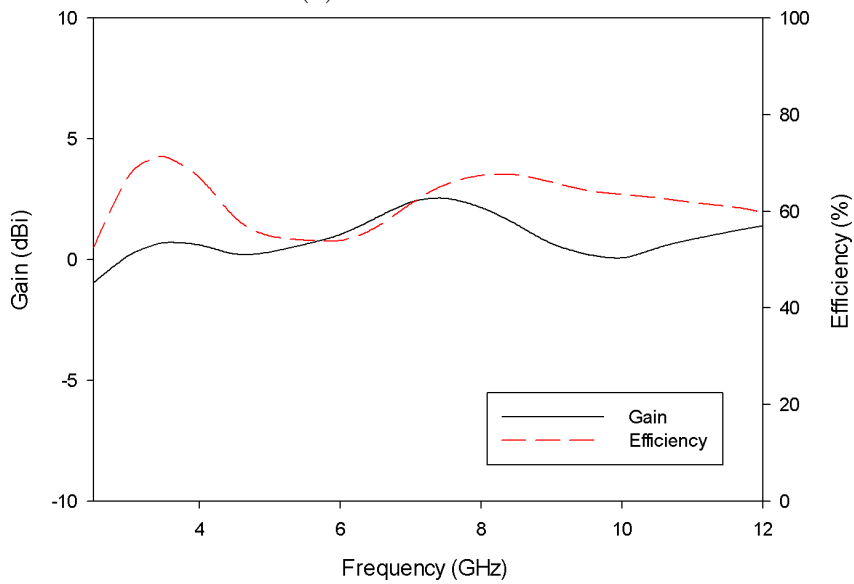


Figure 5.22: Comparison of gain of graphene-based and copper-based antenna on FR4 substrate.

antenna (Figure.5.22). This is due to the presence of small yet finite sheet resistance in lossy metals like graphene. This can be improved by optimizing the electrical properties of the binder, like for instance adding m-cresol



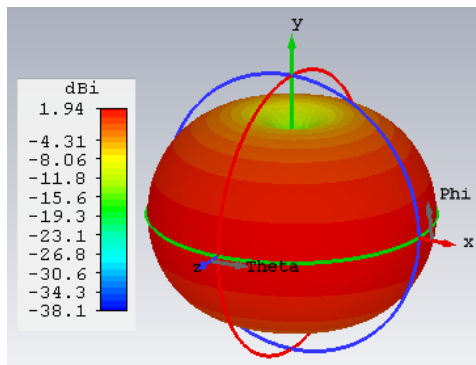
(a) On FR4 substrate



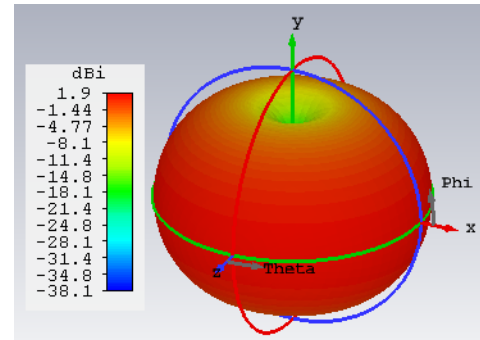
(b) On PMMA substrate

Figure 5.23: Gain and efficiency

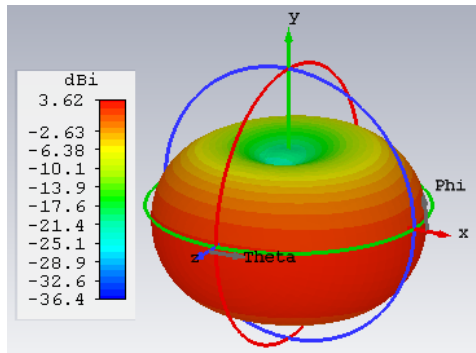
dispersed PANi-CSA as secondary filler in the pressure sensitive binder.



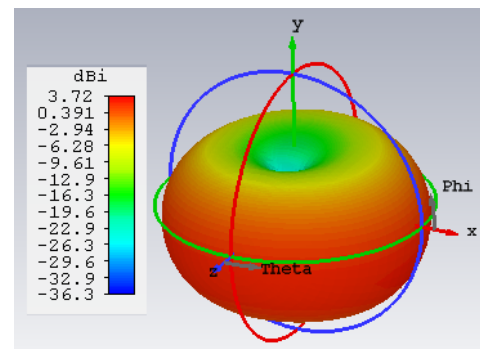
(a) FR4 antenna at 3 GHz



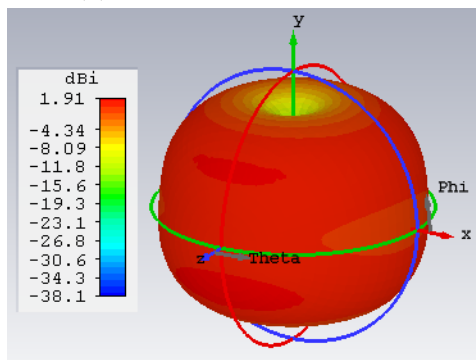
(b) PMMA antenna at 3 GHz



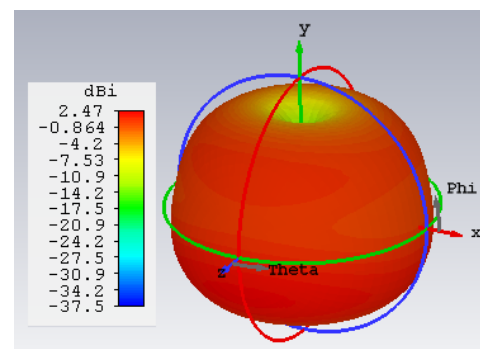
(c) FR4 antenna at 6 GHz



(d) PMMA antenna at 6 GHz



(e) FR4 antenna at 9 GHz



(f) PMMA antenna at 9 GHz

Figure 5.24: Radiation patterns at three resonances

Feed	Ground
$l_1=8.15\text{mm}$	$t_1=8.3\text{mm}$
$l_2=4.0\text{mm}$	$t_2=3.7\text{mm}$
$l_3=1.35\text{mm}$	$t_3=1.73\text{mm}$
$p_1=5.7\text{mm}$	$t_4=4.3\text{mm}$
$p_2=2.5\text{mm}$	$g_1=3.7\text{mm}$
$l_p=7.0\text{mm}$	$g_2=2.4\text{mm}$
$w_1=3.0\text{mm}$	$g_3=4.0\text{mm}$
$w_2=1.3\text{mm}$	$w_4=8.0\text{mm}$
$w_3=1.0\text{mm}$	
$\theta=140^\circ$	

Table 5.4: Optimized parameter values of the design

As for the other antenna properties, such as radiation pattern, both the graphene based antennas show the same characteristics as that of copper antenna as evident from the Figure.5.24. A stable omnidirectional radiation pattern is also seen within the radiation bandwidth.

5.5.3 Summary

This study indicates the feasibility of replacing metals with graphene based patterns. Although the antennas are not flexible, the study hints at the patterning of microwave structures on flexible substrates using the same method. The return loss has been measured and correlated with the simulation results. The gain and efficiency of the antennas were found to be lesser than the copper based antenna owing to the presence of binder. The binder can be made conductive by dispersing conducting secondary fillers in the binder also. The radiation pattern indicates stability throughout the bandwidth. Graphene based antennas are apt candidates as antennas for paper/plastic electronics such as RF-ID circuitry, medical sensors and other one-time or short life-span low profile applications. The antenna has prospects of 3D printing and roll-to-roll processibility which is very advantageous in the sense of production cost and time.

Chapter 6

CONCLUSION AND FUTURE SCOPE

A summarized account of all the works presented in the previous chapters is highlighted in this chapter. The chapter proposes some new directions for future work in this area.

Contents

6.1	Highlights of the current work	148
6.2	Possible future works	150

Non-metallic conductors are futuristic smart materials that is in its young stage of evolution. This field could augment the current technology by integrating more functionalities by virtue of flexibility, reconfigurability, printability, environment sensing, and much more. In the present study Polyaniline which is a low cost conducting polymer and graphene were investigated for their microwave properties. It was found that by properly tuning their crystal structures, very good properties can be obtained. This is done by examining the relation between the end products and the reaction protocol that is adopted for their preparation.

6.1 Highlights of the current work

- Polyaniline was prepared using self stabilized dispersion polymerization without agitation of the reaction mixture. This gave the possibility of having homogeneous nucleation of the oligomeric stage and thus giving rise to good quality polymers. Their enhancement in quality was quantified and compared to that of conventional methods.
- Another significant achievement was the preparation of polyaniline in the presence of gelatin stabilized media where polyaniline polymerizes into water based dispersions. The gelatin stabilizer aided in good water dispersibility for the nanoscale PANi produced by the method.
- A study on the synthesis of graphite derivatives such as graphene oxide, graphite intercalation compounds and expanded graphite was performed as these materials are known to offer remarkable conductivities for use in microwave engineering.
- A composite of expanded graphite with polyaniline was investigated. The samples were prepared with the aid of gelatin stabilized reaction medium. This avoids the requirement for graphene oxide conversion and reduction to reduced graphene oxide as in the conventional methods. As a result, the quality of the samples were better in this case.
- All the synthetic conductors were characterized in microwave frequencies. Their low frequency performance were analyzed. The XRD, SEM and FTIR studies direct on the superior quality of samples due to preparation methods and environment.
- It was found that the losses incurred in polyaniline-graphene pellets are high and thus was used to design microwave absorber. A graded conductivity pellet was designed to match the impedance of freespace to that of the metallic target. The design is an all polymer structure with PMMA frame acting as the mechanical support. It could absorb a wide band of frequencies using this technique. The structure was characterized around its reflection properties, polarization rotation, angular stability, electric and magnetic field distributions, power loss density distributions, surface current distribution, and far field RCS. The structure

opens possibilities towards 3D printing of microwave absorbers based on synthetic conductors.

- The conductivity of expanded graphite offers a way to create resistive coatings on flexible substrates. A resistive coating on flexible substrate on top of a grounded dielectric can act as salisbury screens which is demonstrated using the synthesized expanded graphite.
- The expanded graphite also paves way to have low profile antennas suitable for one time applications as that in the case of paper or plastic based flexible electronics. Especially when the surface currents are less, these antennas tend to lose lesser conduction losses due to I^2R heating. Thus low power UWB antennas are a good start to choose from. As a preliminary study, a microstrip fed UWB antenna was designed and fabricated. Its parameters were identified and optimized.
- As it is easier to have single side patterning especially in the case of flexible antennas, another UWB antenna based on CPW feeding was designed and fabricated after optimization. The structure was very compact and the single side design was particularly useful for flexible antenna fabrication.
- A special case of the CPW fed UWB antenna was designed to notch out coexistent WLAN band at 5.45GHz. This helps to avoid interference with WLAN signals. The notch parameters were identified and optimized.
- The CPW fed UWB antenna was fabricated on FR4 and PMMA substrates by replacing copper with expanded graphite. Commercially available pressure sensitive adhesive was used as the binder and this could be attached to PET substrates as well. The antenna scattering parameters were measured which shows good matching and performance although with lesser gain but with the added advantage of flexibility and printability using laser.

6.2 Possible future works

This pilot study on the applications of synthetic conductors offers a lot of engineering possibilities and design challenges. Some of which are listed here in this section.

- A good application design has its roots in the underlying material used for the end product. Hence significant research is to be done in the synthesis of synthetic conductors. Apart from polyaniline and graphene, there are other conducting families of materials with additional properties such as PEDOT-PSS, CNT, and others. These materials are to be investigated and their composites are potential candidates for microwave engineering.
- The characterization techniques have their own limitations or specifications. If the limits are pushed, then the calibration and measurement techniques are to be revised and modified for faster and more accurate automated measurement with lesser sample quantities.
- Although the applications of microwave absorbers and antennas are illustrated in this thesis, these materials have very good prospectives in substrate integrated waveguides, electrically controllable phase shifters, metamaterial cloaking etc.
- Post processing of synthetic conductors are most often a field which require special attention. Especially the processibility of these materials and scalability of manufacture are areas to be investigated. Large scale production of powder form, sheet form or fibre form of these materials are in high demand due to their application in BAN, flexible and moldable electronics. Often a roll to roll manufacturing of these materials is a technology mostly sought after.
- Patterning technology is something important in the field of microwave technology. Each material can be patterned based on their physical and chemical properties. Hence some can be spray coated onto substrates via masks, some can be printed using custom printers, some can be etched out using lasers or chemicals. Whichever method is to be adopted is a choice made on the basis of such feasibility studies on these techniques.

- Often a less pronounced study on these materials is in their environmental impact, and half life under ambient conditions. When flexible and paper electronics come into consumer electronics, there is the surety of a huge amount of e-waste being generated. Hence the impact of these wonder materials should be emphasized.
- Apart from direct applications in microwave, due to the wide properties exhibited by these materials, hybrid applications can be sought for. An example would be an energy harvesting system which can be used as a reconfigurable antenna also. These materials are already used in LEDs, solar panels, etc. In case of such combined applications, there arises integrated solutions. Graphene intercalation compounds are considered as exhibitors of thermoelectricity and Peltier effect. One can even imagine a synthetic conductor based radar absorbing surface which can cool its internal surface temperature via Peltier effect. Such applications require extensive studies.
- synthetic conductors are principal components in energy storage systems such as supercapacitors. When graphene can offer electrical double layer capacitance, polyaniline can offer pseudo capacitance and both can work in tandem to have high density energy storage medium.
- The flexibility offered by these materials often proclaim their candidature in bio-medical applications such as tissue integrated antennas, sensors, neural scaffolds and electrodes.

Thus the applications of synthetic conductors are the driving force behind the fundamental research related to it. It is worth noting the fact that synthetic conductors are not here to replace silicon based electronics. Its potential here is to augment exotic functionalities and even correct the deficits of silicon electronics. In the next decade, conducting polymers will percolate into our consumer technology in an unprecedented way and it is our choice to be in the frontiers of this technology.

Bibliography

- [1] S. Herculano-Houzel, “The remarkable, yet not extraordinary, human brain as a scaled-up primate brain and its associated cost,” *Proceedings of the National Academy of Sciences*, vol. 109, no. Supplement 1, pp. 10 661–10 668, 2012. [Online]. Available: https://www.pnas.org/content/109/Supplement_1/10661
- [2] Y. Harari, *Sapiens: A Brief History of Humankind*. Random House, 2014. [Online]. Available: <https://books.google.co.in/books?id=1EiJAwAAQBAJ>
- [3] J. Bryant, “The first century of microwaves-1886 to 1986,” *IEEE Trans. Microw. Theory Tech.*, vol. 36, no. 5, pp. 830–858, 1988.
- [4] C. E. Shannon, “A mathematical theory of communication,” *Bell System Technical Journal*, vol. 27, no. 3, pp. 379–423, 1948. [Online]. Available: <https://onlinelibrary.wiley.com/doi/abs/10.1002/j.1538-7305.1948.tb01338.x>
- [5] J. Maxwell and T. Torrance, *A Dynamical Theory of the Electromagnetic Field*, ser. Torrance Collection. Wipf & Stock, 1996. [Online]. Available: <https://books.google.co.in/books?id=p1pKAwAAQBAJ>
- [6] W. Mayer, M. C. Dartiailh, J. Yuan, K. S. Wickramasinghe, A. Matos-Abiague, I. Žutić, and J. Shabani, “Phase signature of topological transition in Josephson Junctions,” *arXiv e-prints*, p. arXiv:1906.01179, Jun 2019.
- [7] K. Cui and B. L. Wardle, “Breakdown of native oxide enables multifunctional, free-form carbon nanotube–metal hierarchical architectures,”

- ACS Applied Materials & Interfaces*, vol. 0, no. 0, p. null, 0, PMID: 31514497. [Online]. Available: <https://doi.org/10.1021/acsami.9b08290>
- [8] S. Fenichell, *Plastic: The Making of a Synthetic Century*. HarperBusiness, 1996. [Online]. Available: <https://books.google.co.in/books?id=4hjcAAAAMAAJ>
- [9] A. Andrady, *Plastics and the Environment*. Wiley, 2003. [Online]. Available: <https://books.google.co.in/books?id=KZCNJ8qSWKYC>
- [10] N. Mills, *Plastics: Microstructure and Engineering Applications*, ser. Metallurgy and materials science. Edward Arnold, 1993. [Online]. Available: <https://books.google.co.in/books?id=NO1TAAAAMAAJ>
- [11] V. Sastri, *Plastics in Medical Devices: Properties, Requirements and Applications*, ser. Plastics Design Library. Elsevier Science, 2010. [Online]. Available: <https://books.google.co.in/books?id=WX4MW1GU3bMC>
- [12] M. Biron, *Industrial Applications of Renewable Plastics: Environmental, Technological, and Economic Advances*, ser. Plastics Design Library. Elsevier Science, 2016. [Online]. Available: <https://books.google.co.in/books?id=K1arDAAAQBAJ>
- [13] S. Kabasci and C. Stevens, *Bio-Based Plastics: Materials and Applications*, ser. Wiley Series in Renewable Resource. Wiley, 2013. [Online]. Available: <https://books.google.co.in/books?id=qZszAQAAQBAJ>
- [14] G. Inzelt, *Conducting Polymers: A New Era in Electrochemistry*, ser. Monographs in Electrochemistry. Springer Berlin Heidelberg, 2012. [Online]. Available: <https://books.google.co.in/books?id=ruYwnJ7FzGQC>
- [15] T. Skotheim, *Handbook of Conducting Polymers, Second Edition*, ser. Handbook of Conducting Polymers, Third Edition. Taylor & Francis, 1997. [Online]. Available: https://books.google.co.in/books?id=6GRovXHas_MC
- [16] K. Tanaka and S. Iijima, *Carbon Nanotubes and Graphene*. Elsevier Science, 2014. [Online]. Available: <https://books.google.co.in/books?id=YRwAfQr23vMC>

-
- [17] A. Mishra, *Carbon Nanotubes: Synthesis and Properties*, ser. Nanotechnology Science and Technology. Nova Science Publishers, Incorporated, 2012. [Online]. Available: <https://books.google.co.in/books?id=OJ3vugAACAAJ>
- [18] J. Warner, F. Schaffel, M. Rummeli, and A. Bachmatiuk, *Graphene: Fundamentals and emergent applications*. Elsevier Science, 2012. [Online]. Available: <https://books.google.co.in/books?id=RqOUuIWTZAIC>
- [19] J. Ferraro and J. Williams, *Introduction to synthetic electrical conductors*. Academic Press, 1987. [Online]. Available: <https://books.google.co.in/books?id=BTtRAAAAMAAJ>
- [20] Millman, *Microelectronics*. McGraw-Hill Education (India) Pvt Limited, 2001. [Online]. Available: <https://books.google.co.in/books?id=OedeoaQJKFAC>
- [21] H. Shirakawa, “The discovery of polyacetylene film: The dawning of an era of conducting polymers (nobel lecture),” *Angewandte Chemie International Edition*, vol. 40, no. 14, pp. 2574–2580, 2001. [Online]. Available: <https://onlinelibrary.wiley.com/doi/abs/10.1002/1521-3773%2820010716%2940%3A14%3C2574%3A%3AAID-ANIE2574%3E3.0.CO%3B2-N>
- [22] T. P. Kaloni, P. K. Giesbrecht, G. Schreckenbach, and M. S. Freund, “Polythiophene: From fundamental perspectives to applications,” *Chemistry of Materials*, vol. 29, no. 24, pp. 10 248–10 283, 2017. [Online]. Available: <https://doi.org/10.1021/acs.chemmater.7b03035>
- [23] A. Elschner, S. Kirchmeyer, W. Lovenich, U. Merker, and K. Reuter, *PEDOT: Principles and Applications of an Intrinsically Conductive Polymer*. CRC Press, 2010. [Online]. Available: <https://books.google.co.in/books?id=e12gOPc4IWAC>
- [24] S. Rasmussen, “Early history of polypyrrole: The first conducting organic polymer,” *Bulletin for the history of chemistry / Division of the History of Chemistry of the American Chemical Society*, vol. 40, pp. 45–55, 09 2015.

- [25] W. Zhou and J. Xu, “Progress in conjugated polyindoles: Synthesis, polymerization mechanisms, properties, and applications,” *Polymer Reviews*, vol. 57, no. 2, pp. 248–275, 2017. [Online]. Available: <https://doi.org/10.1080/15583724.2016.1223130>
- [26] S. Rasmussen, “The early history of polyaniline: Discovery and origins,” *Substantia*, vol. 1, pp. 99–109, 10 2017.
- [27] F. Goppelsröder, “On electrolytic aniline black,” *Comptes Rendus Hebdomadaires des Séances de l’Académie des Sciences*, vol. 82, pp. 331–333, 1876.
- [28] H. Kurosu, “Chapter 16 - electrically-conducting polymers,” in *Solid State NMR of Polymers*, ser. Studies in Physical and Theoretical Chemistry, I. Ando and T. Asakura, Eds. Elsevier, 1998, vol. 84, pp. 589 – 611. [Online]. Available: <http://www.sciencedirect.com/science/article/pii/S0167688198800244>
- [29] C. Chiang, “The bromine doping of polyacetylene,” *Physica A: Statistical Mechanics and its Applications*, vol. 321, no. 1, pp. 139 – 151, 2003, statphys-Taiwan-2002: Lattice Models and Complex Systems. [Online]. Available: <http://www.sciencedirect.com/science/article/pii/S0378437102017545>
- [30] A. J. Heeger, “Semiconducting and metallic polymers: The fourth generation of polymeric materials,” *The Journal of Physical Chemistry B*, vol. 105, no. 36, pp. 8475–8491, 2001. [Online]. Available: <https://doi.org/10.1021/jp011611w>
- [31] H. Liu, M. Dong, W. Huang, J. Gao, K. Dai, J. Guo, G. Zheng, C. Liu, C. Shen, and Z. Guo, “Lightweight conductive graphene/thermoplastic polyurethane foams with ultrahigh compressibility for piezoresistive sensing,” *J. Mater. Chem. C*, vol. 5, pp. 73–83, 2017. [Online]. Available: <http://dx.doi.org/10.1039/C6TC03713E>
- [32] P. P. Deshpande, N. G. Jadhav, V. J. Gelling, and D. Sazou, “Conducting polymers for corrosion protection: a review,” *Journal of Coatings Technology and Research*, vol. 11, no. 4, pp. 473–494, Jul 2014. [Online]. Available: <https://doi.org/10.1007/s11998-014-9586-7>

-
- [33] W. Zhao, I. I. Nugay, B. Yalcin, and M. Cakmak, “Flexible, stretchable, transparent and electrically conductive polymer films via a hybrid electrospinning and solution casting process: In-plane anisotropic conductivity for electro-optical applications,” *Displays*, vol. 45, pp. 48 – 57, 2016. [Online]. Available: <http://www.sciencedirect.com/science/article/pii/S0141938216300026>
- [34] X. Jia, Y. Ge, L. Shao, C. Wang, and G. G. Wallace, “Tunable conducting polymers: Toward sustainable and versatile batteries,” *ACS Sustainable Chemistry & Engineering*, vol. 7, no. 17, pp. 14 321–14 340, 2019. [Online]. Available: <https://doi.org/10.1021/acssuschemeng.9b02315>
- [35] T.-H. Le, Y. Kim, and H. Yoon, “Electrical and electrochemical properties of conducting polymers,” *Polymers*, vol. 9, no. 4, 2017. [Online]. Available: <https://www.mdpi.com/2073-4360/9/4/150>
- [36] Y. Wang, C. Zhu, R. Pfattner, H. Yan, L. Jin, S. Chen, F. Molina-Lopez, F. Lissel, J. Liu, N. I. Rabiah, Z. Chen, J. W. Chung, C. Linder, M. F. Toney, B. Murmann, and Z. Bao, “A highly stretchable, transparent, and conductive polymer,” *Science Advances*, vol. 3, no. 3, 2017. [Online]. Available: <https://advances.sciencemag.org/content/3/3/e1602076>
- [37] A. O. Patil, A. J. Heeger, and F. Wudl, “Optical properties of conducting polymers,” *Chemical Reviews*, vol. 88, no. 1, pp. 183–200, 1988. [Online]. Available: <https://doi.org/10.1021/cr00083a009>
- [38] S. He, M. Mukaida, K. Kirihara, L. Lyu, and Q. Wei, “Reversible protonic doping in poly(3,4-ethylenedioxythiophene),” *Polymers*, vol. 10, no. 10, p. 1065, Sep 2018. [Online]. Available: <https://www.ncbi.nlm.nih.gov/pubmed/30960990>
- [39] V. Kumar, T. Yokozeki, T. Goto, T. Takahashi, S. R. Dhakate, and B. P. Singh, “Irreversible tunability of through-thickness electrical conductivity of polyaniline-based cfrp by de-doping,” *Composites Science and Technology*, vol. 152, pp. 20 – 26, 2017. [Online]. Available: <http://www.sciencedirect.com/science/article/pii/S0266353817318031>

- [40] M. F. Shakir, A. N. Khan, R. Khan, S. Javed, A. Tariq, M. Azeem, A. Riaz, A. Shafqat, H. M. Cheema, M. A. Akram, I. Ahmad, and R. Jan, "Emi shielding properties of polymer blends with inclusion of graphene nano platelets," *Results in Physics*, vol. 14, p. 102365, 2019. [Online]. Available: <http://www.sciencedirect.com/science/article/pii/S2211379719309362>
- [41] R. Rosner, "Conductive materials for esd applications: An overview," *Device and Materials Reliability, IEEE Transactions on*, vol. 1, pp. 9 – 16, 04 2001.
- [42] M. Angelopoulos, J. M. Shaw, K.-L. Lee, W.-S. Huang, M.-A. Lecorre, and M. Tissier, "Conducting polymers as lithographic materials," *Polymer Engineering & Science*, vol. 32, no. 20, pp. 1535–1540, 1992. [Online]. Available: <https://onlinelibrary.wiley.com/doi/abs/10.1002/pen.760322016>
- [43] M. Angelopoulos, "Conducting polymers in microelectronics," *IBM Journal of Research and Development*, vol. 45, pp. 57 – 75, 02 2001.
- [44] T. Ohtsuka, "Corrosion protection of steels by conducting polymer coating," *International Journal of Corrosion*, vol. 2012, 05 2012.
- [45] B. H. Lee, J. Lee, Y. Kahng, N. Kim, Y. Kim, J. Lee, T. Lee, and K. Lee, "Graphene-conducting polymer hybrid transparent electrodes for efficient organic optoelectronic devices," *Advanced Functional Materials*, vol. 24, 04 2014.
- [46] Z. Yi, L. G. Bettini, G. Tomasello, P. Kumar, P. Piseri, I. Valitova, P. Milani, F. Soavi, and F. Cicoira, "Flexible conducting polymer transistors with supercapacitor function," *Journal of Polymer Science Part B: Polymer Physics*, vol. 55, no. 1, pp. 96–103, 2017. [Online]. Available: <https://onlinelibrary.wiley.com/doi/abs/10.1002/polb.24244>
- [47] Y. Han and L. Dai, "Conducting polymers for flexible supercapacitors," *Macromolecular Chemistry and Physics*, vol. 220, no. 3, p. 1800355, 2019. [Online]. Available: <https://onlinelibrary.wiley.com/doi/abs/10.1002/macp.201800355>

- [48] C.-J. Yao, H.-L. Zhang, and Q. Zhang, “Recent progress in thermoelectric materials based on conjugated polymers,” *Polymers*, vol. 11, p. 107, 01 2019.
- [49] H. Anno, K. Yamaguchi, T. Nakabayashi, H. Kurokawa, F. Akagi, M. Hojo, and N. Toshima, “Thermoelectric properties of conducting polyaniline/BaTiO₃nanoparticle composite films,” *IOP Conference Series: Materials Science and Engineering*, vol. 18, no. 14, p. 142003, may 2011. [Online]. Available: <https://doi.org/10.1088%2F1757-899x%2F18%2F14%2F142003>
- [50] D. Luo, Q. Chen, B. Liu, and Y. Qiu, “Emergence of flexible white organic light-emitting diodes,” *Polymers*, vol. 11, no. 2, p. 384, Feb 2019. [Online]. Available: <https://www.ncbi.nlm.nih.gov/pubmed/30960368>
- [51] J. Kawakita, Y. H. Shinoda, T. Shuto, and T. Chikyow, “Conductive polymer/metal composites for interconnect of flexible devices,” *Japanese Journal of Applied Physics*, vol. 54, no. 6S1, p. 06FJ12, apr 2015. [Online]. Available: <https://doi.org/10.7567%2Fjjap.54.06fj12>
- [52] Y. Chen, L. Zhou, J. Wei, C. Mei, S. Jiang, M. Pan, and C. Xu, “Direct ink writing of flexible electronics on paper substrate with graphene/polypyrrole/carbon black ink,” *Journal of Electronic Materials*, vol. 48, no. 5, pp. 3157–3168, May 2019. [Online]. Available: <https://doi.org/10.1007/s11664-019-07085-x>
- [53] Y. Park, J. Jung, and M. Chang, “Research progress on conducting polymer-based biomedical applications,” *Applied Sciences*, vol. 9, no. 6, 2019. [Online]. Available: <https://www.mdpi.com/2076-3417/9/6/1070>
- [54] J. Sołoducho and J. Cabaj, “Conducting polymers in sensor design,” in *Conducting Polymers*, F. Yilmaz, Ed. Rijeka: IntechOpen, 2016, ch. 2. [Online]. Available: <https://doi.org/10.5772/63227>
- [55] D. Evans, “A bird’s eye view of the synthesis and practical application of conducting polymers,” *Polymer International*, vol. 67, no. 4, pp. 351–355, 2018. [Online]. Available: <https://onlinelibrary.wiley.com/doi/abs/10.1002/pi.5531>

- [56] Y. Cao, V. Fatemi, S. Fang, K. Watanabe, T. Taniguchi, E. Kaxiras, and P. Jarillo-Herrero, “Unconventional superconductivity in magic-angle graphene superlattices,” *Nature*, vol. 556, pp. 43 EP –, Mar 2018, article. [Online]. Available: <https://doi.org/10.1038/nature26160>
- [57] H. A. Mizes and E. M. Conwell, “Stability of polarons in conducting polymers,” *Phys. Rev. Lett.*, vol. 70, pp. 1505–1508, Mar 1993. [Online]. Available: <https://link.aps.org/doi/10.1103/PhysRevLett.70.1505>
- [58] T.-H. Le, Y. Kim, and H. Yoon, “Electrical and electrochemical properties of conducting polymers,” *Polymers*, vol. 9, no. 12, p. 150, Apr 2017. [Online]. Available: <http://dx.doi.org/10.3390/polym9040150>
- [59] W. P. Su, J. R. Schrieffer, and A. J. Heeger, “Solitons in polyacetylene,” *Phys. Rev. Lett.*, vol. 42, pp. 1698–1701, Jun 1979. [Online]. Available: <https://link.aps.org/doi/10.1103/PhysRevLett.42.1698>
- [60] K. Lee, S. Cho, S. Heum Park, A. J. Heeger, C.-W. Lee, and S.-H. Lee, “Metallic transport in polyaniline,” *Nature*, vol. 441, no. 7089, pp. 65–68, 2006. [Online]. Available: <https://doi.org/10.1038/nature04705>
- [61] B. Wessling, *Conductive Polymers as Organic Nanometals*. Academic Press, 01 2000, pp. 501 – 575.
- [62] M. M. Ramos and A. Stoneham, “Mesoscopic modelling of charge evolution in conducting polymers,” *Computational Materials Science*, vol. 17, no. 2, pp. 260 – 264, 2000. [Online]. Available: <http://www.sciencedirect.com/science/article/pii/S0927025600000355>
- [63] R. M. Hill, “Variable-range hopping,” *physica status solidi (a)*, vol. 34, no. 2, pp. 601–613, 1976. [Online]. Available: <https://onlinelibrary.wiley.com/doi/abs/10.1002/pssa.2210340223>
- [64] S. Capaccioli, M. Lucchesi, D. Prevosto, and P. Rolla, “Interchain and intra-chain hopping transport in conducting polymers,” *Physica Status Solidi (c)*, vol. 1, pp. 148–151, 01 2004.
- [65] J. Reynolds, B. Thompson, and T. Skotheim, *Conjugated Polymers: Properties, Processing, and Applications*. CRC Press, 2019. [Online]. Available: <https://books.google.co.in/books?id=0vaODwAAQBAJ>

-
- [66] J. Franck and E. G. Dymond, “Elementary processes of photochemical reactions,” *Trans. Faraday Soc.*, vol. 21, pp. 536–542, 1926. [Online]. Available: <http://dx.doi.org/10.1039/TF9262100536>
- [67] E. Condon, “A theory of intensity distribution in band systems,” *Phys. Rev.*, vol. 28, pp. 1182–1201, Dec 1926. [Online]. Available: <https://link.aps.org/doi/10.1103/PhysRev.28.1182>
- [68] J. L. Bredas and G. B. Street, “Polarons, bipolarons, and solitons in conducting polymers,” *Accounts of Chemical Research*, vol. 18, no. 10, pp. 309–315, 1985. [Online]. Available: <https://doi.org/10.1021/ar00118a005>
- [69] R. R. Chance, D. S. Boudreaux, J. L. Brédas, and R. Silbey, “Neutral and charged soliton defects in polyacetylene,” *Phys. Rev. B*, vol. 27, pp. 1440–1442, Jan 1983. [Online]. Available: <https://link.aps.org/doi/10.1103/PhysRevB.27.1440>
- [70] M. M. Ramos and A. Stoneham, “Mesoscopic modelling of charge evolution in conducting polymers,” *Computational Materials Science*, vol. 17, no. 2, pp. 260 – 264, 2000. [Online]. Available: <http://www.sciencedirect.com/science/article/pii/S0927025600000355>
- [71] Y. Geng, X. Jing, and F. Wang, “Solution properties of doped polyaniline,” *Journal of Macromolecular Science, Part B*, vol. 36, no. 1, pp. 125–135, 1997. [Online]. Available: <https://doi.org/10.1080/00222349708220419>
- [72] E. Knott, J. Schaeffer, and M. Tulley, *Radar Cross Section*, ser. Electromagnetics and Radar Series. Institution of Engineering and Technology, 2004. [Online]. Available: <https://books.google.co.in/books?id=j7hdXhgwsw4C>
- [73] H. Singh and R. Jha, *Active Radar Cross Section Reduction*. Cambridge University Press, 2015. [Online]. Available: <https://books.google.co.in/books?id=oqqwBgAAQBAJ>
- [74] R. Marqués, F. Martín, and M. Sorolla, *Metamaterials with Negative Parameters: Theory, Design, and Microwave Applications*, ser. Wiley

- Series in Microwave and Optical Engineering. Wiley, 2011. [Online]. Available: <https://books.google.co.in/books?id=LItxc5Oenr4C>
- [75] C. Caloz and T. Itoh, *Electromagnetic Metamaterials: Transmission Line Theory and Microwave Applications*, ser. Wiley - IEEE. Wiley, 2005. [Online]. Available: <https://books.google.co.in/books?id=ICPI2XDxOacC>
- [76] N. Engheta and R. Ziolkowski, *Metamaterials: Physics and Engineering Explorations*. Wiley, 2006. [Online]. Available: <https://books.google.co.in/books?id=51e0UkEuBP4C>
- [77] D. Sievenpiper, Lijun Zhang, R. F. J. Broas, N. G. Alexopolous, and E. Yablonovitch, "High-impedance electromagnetic surfaces with a forbidden frequency band," *IEEE Transactions on Microwave Theory and Techniques*, vol. 47, no. 11, pp. 2059–2074, Nov 1999.
- [78] M. Maasch, *Tunable Microwave Metamaterial Structures*, ser. Springer Theses. Springer International Publishing, 2016. [Online]. Available: https://books.google.co.in/books?id=_sxyCwAAQBAJ
- [79] C. Shannon and W. Weaver, *The Mathematical Theory of Communication*. University of Illinois Press, 1998. [Online]. Available: <https://books.google.co.in/books?id=IZ77BwAAQBAJ>
- [80] M. Di Benedetto, *UWB Communication Systems: A Comprehensive Overview*, ser. EURASIP book series on Signal Processing and Communications: European Association for Speech, Signal and Image Processing. Hindawi Publishing Corporation, 2006. [Online]. Available: <https://books.google.co.in/books?id=3KVHnkXnMDEC>
- [81] D. Valderas, *Ultrawideband Antennas: Design and Applications*, ser. Knovel Library. Imperial College Press, 2011. [Online]. Available: <https://books.google.co.in/books?id=lniHgSohdGkC>
- [82] Y. Singh, "Electrical resistivity measurements: a review," *International Journal of Modern Physics Conference Series*, vol. 22, pp. 745–756, 01 2013.

-
- [83] L. J. van der PAUW, *A METHOD OF MEASURING SPECIFIC RESISTIVITY AND HALL EFFECT OF DISCS OF ARBITRARY SHAPE*, pp. 174–182. [Online]. Available: https://www.worldscientific.com/doi/abs/10.1142/9789814503464_0017
- [84] A. Fattoum, M. Arous, F. Gmati, W. Dhaoui, and A. Mohamed, “Influence of dopant on dielectric properties of polyaniline weakly doped with dichloro and trichloroacetic acids,” *Journal of Physics D: Applied Physics*, vol. 40, p. 4347, 06 2007.
- [85] K. T. Mathew, *Perturbation Theory*. American Cancer Society, 2005. [Online]. Available: <https://onlinelibrary.wiley.com/doi/abs/10.1002/0471654507.eme309>
- [86] M. Lin and M. Afsar, “A new cavity perturbation technique for accurate measurement of dielectric parameters,” 07 2006, pp. 1630 – 1633.
- [87] W. B. Weir, “Automatic measurement of complex dielectric constant and permeability at microwave frequencies,” *Proceedings of the IEEE*, vol. 62, no. 1, pp. 33–36, Jan 1974.
- [88] O. Luukkonen, S. Maslovski, and S. Tretyakov, “A stepwise nicolson–ross–weir-based material parameter extraction method,” *IEEE Antennas and Wireless Propagation Letters - IEEE ANTENN WIREL PROPAG LETT*, vol. 10, pp. 1295–1298, 12 2011.
- [89] *CST MW Studio*. [Online]. Available: <http://www.cst.com>
- [90] S. Mayekar, M. Bansode, and S. Rathod, “An automated antenna pattern measurement system,” 06 2017, pp. 1–4.
- [91] G. Edric, A. Arousian, K. Arshak, and O. Korostynska, “ph sensitivity of novel pani/pvb/ps3 composite films,” *Sensors*, vol. 7, 12 2007.
- [92] R. Khan and M. Dhayal, “Chitosan/polyaniline hybrid conducting biopolymer base impedimetric immunosensor to detect ochratoxin-a,” *Biosensors & bioelectronics*, vol. 24, pp. 1700–5, 10 2008.
- [93] B. Arun D., “Poly(aniline-co-o-anisidine): A conducting copolymer as a anion-exchange resin,” *Journal of Chemical and Pharmaceutical Research*, vol. 4, pp. 2081–2086, 2012.

- [94] L. J. Pan, H. Qiu, C. Dou, Y. Li, L. Pu, J. Xu, and Y. Shi, "Conducting polymer nanostructures: Template synthesis and applications in energy storage," *International journal of molecular sciences*, vol. 11, pp. 2636–57, 07 2010.
- [95] J. de Albuquerque, L. Mattoso, R. Faria, J. Masters, and A. MacDiarmid, "Study of the interconversion of polyaniline oxidation states by optical absorption spectroscopy," *Synthetic Metals*, vol. 146, no. 1, pp. 1 – 10, 2004. [Online]. Available: <http://www.sciencedirect.com/science/article/pii/S0379677904002437>
- [96] A. Rashidian, D. Klymyshyn, M. Tayfeh, M. Börner, and J. Mohr, "Development of polymer-based dielectric resonator antennas for millimeter-wave applications," *Progress in Electromagnetics Research C (PIER C)*, vol. 13, pp. 203–216, 01 2010.
- [97] R. Menon M. R., R. Thomas, H. John, R. Joseph, and T. Mathew, "Polyaniline as an automatic beam steering material," *Microwave and Optical Technology Letters*, vol. 50, 02 2008.
- [98] I. Sapurina, N. Kazantseva, N. Ryvkina, J. Prokeš, P. Saha, and J. Stejskal, "Electromagnetic radiation shielding by composites of conducting polymers and wood," *Journal of Applied Polymer Science*, vol. 95, pp. 807 – 814, 12 2004.
- [99] N. Kirsch, N. Vacirca, E. Plowman, T. Kurzweg, A. Fontecchio, and K. Dandekar, "Optically transparent conductive polymer rfid meandering dipole antenna," 05 2009, pp. 278 – 282.
- [100] J. Stejskal, I. Sapurina, and M. Trchová, "Cheminform abstract: Polyaniline nanostructures and the role of aniline oligomers in their formation," *Progress in Polymer Science - PROG POLYM SCI*, vol. 35, pp. 1420–1481, 12 2010.
- [101] A. G. Macdiarmid and A. J. Epstein, "Secondary doping: A new concept in conducting polymers," *Macromolecular Symposia*, vol. 98, no. 1, pp. 835–842, 1995. [Online]. Available: <https://onlinelibrary.wiley.com/doi/abs/10.1002/masy.19950980170>

-
- [102] B. Wessling, “New insight into organic metal polyaniline morphology and structure,” *Polymers*, 12 2010.
- [103] K. P. Neeraj, T. Paulbert, J. Honey, A. C. K., and T. Tessamma, “Conducting polymers for microwave applications,” *International Journal of Emerging Technologies and Innovative Research*, vol. 5, no. 9, pp. 510–527, 2018.
- [104] I. Sapurina and S. Fedorova, “Surface polymerization and precipitation polymerization of aniline in the presence of sodium tungstate,” *Langmuir*, vol. 19, 07 2003.
- [105] H. Adly, M. Mohy Eldin, A. Elsyed, A. Elazm, Abo, E. Younes, and H. Motaweh, “Synthesis and properties of polyaniline/ferrites nanocomposites,” *International journal of electrochemical science*, vol. 6, pp. 1887–1897, 01 2011.
- [106] E. Detsri and S. Dubas, “Interfacial polymerization of water-soluble polyaniline and its assembly using the layer-by-layer technique,” *J. Met. Mater. Miner.*, vol. 19, 01 2009.
- [107] J. Stejskal, “Polyaniline. preparation of a conducting polymer,” *Pure Appl. Chem.*, vol. 74, pp. 8547–8867, 01 2002.
- [108] C. Baker, B. Shedd, P. Innis, P. Whitten, G. Spinks, G. Wallace, and R. Kaner, “Monolithic actuators from flash-welded polyaniline nanofibers,” *Advanced Materials*, vol. 20, pp. 155 – 158, 12 2007.
- [109] M. Wan, “A template-free method towards conducting polymer nanostructures,” *Advanced Materials*, vol. 20, pp. 2926 – 2932, 08 2008.
- [110] J. Stejskal and I. Sapurina, “Polyaniline: Thin films and colloidal dispersions (iupac technical report),” *Pure and Applied Chemistry - PURE APPL CHEM*, vol. 77, pp. 815–826, 01 2005.
- [111] J. Huang, “Syntheses and applications of conducting polymer polyaniline nanofibers,” *Pure Appl. Chem*, vol. 78, pp. 15–27, 01 2006.
- [112] S. Bhadra, D. Khastgir, N. Singha, and J. Lee, “Progress in preparation, processing and applications of polyaniline,” *Progress in Polymer Science*, vol. 34, pp. 783–810, 08 2009.

- [113] D. Li and R. Kaner, “Shape and aggregation control of nanoparticles: Not shaken, not stirred,” *Journal of the American Chemical Society*, vol. 128, pp. 968–75, 02 2006.
- [114] —, “How nucleation affects the aggregation of nanoparticles,” *Journal of Materials Chemistry - J MATER CHEM*, vol. 17, 06 2007.
- [115] S.-H. Lee, J. Lee, K. Lee, and C.-W. Lee, “High-performance polyaniline prepared via polymerization in a self-stabilized dispersion,” *Advanced Functional Materials*, vol. 15, pp. 1495 – 1500, 09 2005.
- [116] H. Rmili, J.-L. Miane, H. Zangar, and T. Olinga, “Microwave conductivity measurements of high conductive polyaniline films,” <http://dx.doi.org/10.1051/epjap:2004208>, vol. 9, 01 2005.
- [117] M. Popis, J. Krupka, I. Wielgus, and M. Zagórska, “Measurements of microwave conductivity of conjugated polymers and their blends,” *Ferroelectrics*, vol. 388, pp. 5–9, 09 2009.
- [118] E. Ozkazanc, S. Zor, H. Ozkazanc, H. Y. Guney, and U. Abaci, “Synthesis, characterization and dielectric behavior of (es)-form polyaniline/cerium(iii)-nitrate-hexahydrate composites,” *Materials Chemistry and Physics*, vol. 133, no. 1, pp. 356 – 362, 2012. [Online]. Available: <http://www.sciencedirect.com/science/article/pii/S025405841200051X>
- [119] M. Ali and T. Hirai, “Relationship between electrode polarization and electrical actuation of dielectric pvc gel actuators,” *Soft Matter*, vol. 8, pp. 3694–3699, 2012. [Online]. Available: <http://dx.doi.org/10.1039/C2SM07273D>
- [120] H. Sanabria and J. H. Miller, “Relaxation processes due to the electrode-electrolyte interface in ionic solutions,” *Phys. Rev. E*, vol. 74, p. 051505, Nov 2006. [Online]. Available: <https://link.aps.org/doi/10.1103/PhysRevE.74.051505>
- [121] P. Ishai, M. Talary, A. Caduff, E. Levy, and Y. Feldman, “Topical review electrode polarization in dielectric measurements: a review,” *Measurement Science and Technology*, vol. 24, pp. 102001–21, 10 2013.

-
- [122] T. Y. Kim, C.-H. Park, and N. Marzari, “The electronic thermal conductivity of graphene,” *Nano Letters*, vol. 16, no. 4, pp. 2439–2443, 2016, pMID: 26907524. [Online]. Available: <https://doi.org/10.1021/acs.nanolett.5b05288>
- [123] D. Li, Z. Yang, D. Jia, D. Wu, Q. Zhu, B. Liang, S. Wang, and y. Zhou, “Microstructure, oxidation and thermal shock resistance of graphene reinforced siben ceramics,” *Ceramics International*, vol. 42, 11 2015.
- [124] D. G. Papageorgiou, I. A. Kinloch, and R. J. Young, “Mechanical properties of graphene and graphene-based nanocomposites,” *Progress in Materials Science*, vol. 90, pp. 75 – 127, 2017. [Online]. Available: <http://www.sciencedirect.com/science/article/pii/S0079642517300968>
- [125] D. Yoon, Y.-W. Son, and H. Cheong, “Negative thermal expansion coefficient of graphene measured by raman spectroscopy,” *Nano Letters*, vol. 11, no. 8, pp. 3227–3231, 2011, pMID: 21728349. [Online]. Available: <https://doi.org/10.1021/nl201488g>
- [126] D. Berman, A. Erdemir, and A. V. Sumant, “Graphene: a new emerging lubricant,” *Materials Today*, vol. 17, no. 1, pp. 31 – 42, 2014. [Online]. Available: <http://www.sciencedirect.com/science/article/pii/S1369702113004574>
- [127] S. Zhou, Y. Wu, W. Zhao, J. Yu, F. Jiang, and L. Ma, “Comparative corrosion resistance of graphene sheets with different structures in waterborne epoxy coatings,” *Colloids and Surfaces A: Physicochemical and Engineering Aspects*, vol. 556, pp. 273 – 283, 2018. [Online]. Available: <http://www.sciencedirect.com/science/article/pii/S0927775718307386>
- [128] N. V. Ponraj, A. Azhagurajan, S. Vettivel, X. S. Shajan, P. Nabhiraj, and M. Sivapragash, “Graphene nanosheet as reinforcement agent in copper matrix composite by using powder metallurgy method,” *Surfaces and Interfaces*, vol. 6, pp. 190 – 196, 2017. [Online]. Available: <http://www.sciencedirect.com/science/article/pii/S246802301730010X>

- [129] P. Mukhopadhyay and R. Gupta, *Graphite, Graphene, and Their Polymer Nanocomposites*. CRC Press, 2012. [Online]. Available: <https://books.google.co.in/books?id=mDXNBQAAQBAJ>
- [130] D. Chung, “Graphite intercalation compounds,” in *Reference Module in Materials Science and Materials Engineering*. Elsevier, 2016. [Online]. Available: <http://www.sciencedirect.com/science/article/pii/B9780128035818023110>
- [131] —, “Graphite intercalation compounds,” in *Encyclopedia of Materials: Science and Technology*, K. J. Buschow, R. W. Cahn, M. C. Flemings, B. Ilschner, E. J. Kramer, S. Mahajan, and P. Veyssi re, Eds. Oxford: Elsevier, 2001, pp. 3641 – 3645. [Online]. Available: <http://www.sciencedirect.com/science/article/pii/B0080431526006495>
- [132] D. D. L. Chung, “A review of exfoliated graphite,” *Journal of Materials Science*, vol. 51, no. 1, pp. 554–568, Jan 2016. [Online]. Available: <https://doi.org/10.1007/s10853-015-9284-6>
- [133] W. S. Hummers and R. E. Offeman, “Preparation of graphitic oxide,” *Journal of the American Chemical Society*, vol. 80, no. 6, pp. 1339–1339, 1958. [Online]. Available: <https://doi.org/10.1021/ja01539a017>
- [134] H. Yu, B. Zhang, C. Bulin, R. Li, and R. Xing, “High-efficient synthesis of graphene oxide based on improved hummers method,” *Scientific Reports*, vol. 6, pp. 36 143 EP –, Nov 2016, article. [Online]. Available: <https://doi.org/10.1038/srep36143>
- [135] D. Dreyer, S. Park, C. Bielawski, and R. Ruoff, “The chemistry of graphene oxide,” *Chem. Soc. Rev.*, vol. 39, 12 2009.
- [136] S. Eigler, “Graphite sulphate - a precursor to graphene,” *Chem. Commun.*, vol. 51, 01 2015.
- [137] M. Matsumoto, Y. Saito, C. Park, T. Fukushima, and T. Aida, “Ultrahigh-throughput exfoliation of graphite into pristine ‘single-layer’ graphene using microwaves and molecularly engineered ionic liquids,” *Nature chemistry*, vol. 7, pp. 730–6, 09 2015.

-
- [138] X. Qiu, V. Bouchiat, D. Colombet, and F. Ayela, “Liquid-phase exfoliation of graphite into graphene nanosheets in a hydrocavitating ‘lab-on-a-chip’,” *RSC Advances*, vol. 9, pp. 3232–3238, 01 2019.
- [139] S. Woltornist, A. Oyer, J.-M. Carrillo, A. Dobrynin, and D. Adamson, “Conductive thin films of pristine graphene by solvent interface trapping,” *ACS nano*, vol. 7, 07 2013.
- [140] W. Wang, Y. Wang, Y. Gao, and Y. Zhao, “Control of number of graphene layers using ultrasound in supercritical co₂ and their application in lithium-ion batteries,” *The Journal of Supercritical Fluids*, vol. 85, 01 2013.
- [141] P. Mandal, M. Naik, and M. Saha, “Room temperature synthesis of graphene nanosheets,” *Crystal Research and Technology*, vol. 53, p. 1700250, 01 2018.
- [142] T. Achee, W. Sun, J. Hope, S. Quitzau, C. Sweeney, S. Shah, T. Habib, and M. Green, “High-yield scalable graphene nanosheet production from compressed graphite using electrochemical exfoliation,” *Scientific Reports*, vol. 8, 12 2018.
- [143] A. M. Dimiev and J. M. Tour, “Mechanism of graphene oxide formation,” *ACS Nano*, vol. 8, no. 3, pp. 3060–3068, 2014, PMID: 24568241. [Online]. Available: <https://doi.org/10.1021/nm500606a>
- [144] *Molyduval tack spray*. [Online]. Available: http://www.molyduval.com/index.php?module=explorer&displayAction=download&downloadFile=datenblaetter_cd/en/tds/tack%20spray.pdf
- [145] W. Choi, I. Lahiri, R. Seelaboyina, and Y. S. Kang, “Synthesis of graphene and its applications: A review,” *Critical Reviews in Solid State and Materials Sciences - CRIT REV SOLID STATE MAT SCI*, vol. 35, pp. 52–71, 02 2010.
- [146] B. H. Nguyen and V. H. Nguyen, “Promising applications of graphene and graphene-based nanostructures,” *Advances in Natural Sciences: Nanoscience and Nanotechnology*, vol. 7, no. 2, p. 023002, apr 2016. [Online]. Available: <https://doi.org/10.1088%2F2043-6262%2F7%2F2%2F023002>

- [147] A. K. Sood, I. Lund, Y. R. Puri, H. Efstathiadis, P. Haldar, N. K. Dhar, J. Lewis, M. Dubey, E. Zakar, P. Wijewarnasuriya, D. L. Polla, and M. Fritze, “Review of graphene technology and its applications for electronic devices,” in *Graphene*, F. Ebrahimi, Ed. Rijeka: IntechOpen, 2015, ch. 3. [Online]. Available: <https://doi.org/10.5772/61316>
- [148] Y. Huang, J. Liang, and Y. Chen, “An overview of the applications of graphene-based materials in supercapacitors,” *Small*, vol. 8, no. 12, pp. 1805–1834, 2012. [Online]. Available: <https://onlinelibrary.wiley.com/doi/abs/10.1002/sml.201102635>
- [149] L. Wan, B. Wang, S. Wang, X. Wang, Z. Guo, H. Xiong, B. Dong, L. Zhao, H. Lu, Z. Xu, X. Zhang, T. Li, and W. Zhou, “Water-soluble polyaniline/graphene prepared by in situ polymerization in graphene dispersions and use as counter-electrode materials for dye-sensitized solar cells,” *Reactive and Functional Polymers*, vol. 79, pp. 47 – 53, 2014. [Online]. Available: <http://www.sciencedirect.com/science/article/pii/S1381514814000650>
- [150] W. Zhang, W. He, and X. Jing, “Preparation of a stable graphene dispersion with high concentration by ultrasound,” *The Journal of Physical Chemistry B*, vol. 114, no. 32, pp. 10 368–10 373, 2010, pMID: 20701371. [Online]. Available: <https://doi.org/10.1021/jp1037443>
- [151] D. Voiry, J. Yang, J. Kupferberg, R. Fullon, C. Lee, H. Y. Jeong, H. Shin, and M. Chhowalla, “High-quality graphene via microwave reduction of solution-exfoliated graphene oxide,” *Science*, vol. 353, pp. 1–6, 09 2016.
- [152] J. Lin, Y. Huang, S. Wang, and G. Chen, “Microwave-assisted rapid exfoliation of graphite into graphene by using ammonium bicarbonate as the intercalation agent,” *Industrial & Engineering Chemistry Research*, vol. 56, no. 33, pp. 9341–9346, 2017. [Online]. Available: <https://doi.org/10.1021/acs.iecr.7b01302>
- [153] W. He, W. Zhang, Y. Li, and X. Jing, “A high concentration graphene dispersion stabilized by polyaniline nanofibers,” *Synthetic Metals*, vol. 162, no. 13, pp. 1107 – 1113, 2012. [Online]. Available: <http://www.sciencedirect.com/science/article/pii/S0379677912001531>

-
- [154] D. W. Johnson, B. P. Dobson, and K. S. Coleman, “A manufacturing perspective on graphene dispersions,” *Current Opinion in Colloid & Interface Science*, vol. 20, no. 5, pp. 367 – 382, 2015. [Online]. Available: <http://www.sciencedirect.com/science/article/pii/S135902941500093X>
- [155] X. Mei and J. Ouyang, “Ultrasonication-assisted ultrafast reduction of graphene oxide by zinc powder at room temperature,” *Carbon*, vol. 49, no. 15, pp. 5389 – 5397, 2011. [Online]. Available: <http://www.sciencedirect.com/science/article/pii/S000862231100666X>
- [156] H. Nassira, A. Sánchez-Ferrer, J. Adamcik, S. Handschin, H. Mahdavi, N. Taheri Qazvini, and R. Mezzenga, “Gelatin–graphene nanocomposites with ultralow electrical percolation threshold,” *Advanced Materials*, vol. 28, no. 32, pp. 6914–6920, 2016. [Online]. Available: <https://onlinelibrary.wiley.com/doi/abs/10.1002/adma.201601115>
- [157] D. C. Marcano, D. V. Kosynkin, J. M. Berlin, A. Sinitskii, Z. Sun, A. Slesarev, L. B. Alemany, W. Lu, and J. M. Tour, “Improved synthesis of graphene oxide,” *ACS Nano*, vol. 4, no. 8, pp. 4806–4814, 2010, pMID: 20731455. [Online]. Available: <https://doi.org/10.1021/nn1006368>
- [158] W. Emerson, “Electromagnetic wave absorbers and anechoic chambers through the years,” *IEEE Transactions on Antennas and Propagation*, vol. 21, no. 4, pp. 484–490, July 1973.
- [159] R. Panwar and J. R. Lee, “Recent advances in thin and broadband layered microwave absorbing and shielding structures for commercial and defense applications,” *Functional Composites and Structures*, vol. 1, no. 3, p. 032001, jul 2019. [Online]. Available: <https://doi.org/10.1088%2F2631-6331%2Fab2863>
- [160] E. Ameri, S. H. Esmaeli, and S. H. Sedighy, “Ultra wideband radar cross section reduction by using polarization conversion metasurfaces,” *Scientific Reports*, vol. 9, no. 1, p. 478, 2019. [Online]. Available: <https://doi.org/10.1038/s41598-018-36542-6>
- [161] V. Shukla, “Review of electromagnetic interference shielding materials fabricated by iron ingredients,” *Nanoscale Adv.*, vol. 1, pp. 1640–1671, 2019. [Online]. Available: <http://dx.doi.org/10.1039/C9NA00108E>

- [162] H. Ahmad, A. Tariq, A. Shehzad, M. S. Faheem, M. Shafiq, I. A. Rashid, A. Afzal, A. Munir, M. T. Riaz, H. T. Haider, A. Afzal, M. B. Qadir, and Z. Khaliq, "Stealth technology: Methods and composite materials—a review," *Polymer Composites*, vol. 0, no. 0. [Online]. Available: <https://onlinelibrary.wiley.com/doi/abs/10.1002/pc.25311>
- [163] Y. Li, J. Huang, S. Hong, Z. Wu, and Z. Liu, "A new assessment method for the comprehensive stealth performance of penetration aircrafts," *Aerospace Science and Technology - AEROSP SCI TECHNOL*, vol. 15, pp. 511–518, 10 2011.
- [164] T. Kollatou, A. Dimitriadis, S. Assimonis, N. Kantartzis, and C. Antonopoulos, "A family of ultra-thin, polarization-insensitive, multi-band, highly absorbing metamaterial structures," *Progress In Electromagnetics Research*, vol. 136, pp. 579–594, 01 2013.
- [165] R. Deng, M. Li, B. Muneer, Q. Zhu, Z. Shi, L. Song, and T. Zhang, "Theoretical analysis and design of ultrathin broadband optically transparent microwave metamaterial absorbers," *Materials*, vol. 11, no. 1, 2018.
- [166] S. Zabri, R. Cahill, and A. Schuchinsky, "Compact fss absorber design using resistively loaded quadruple hexagonal loops for bandwidth enhancement," *Electronics Letters*, vol. 51, pp. 162–164, 01 2015.
- [167] Z. Jianfei, M. Zhaofeng, S. Wujiong, F. D., H. Qiong, Z. Lei, and M. Yungui, "Ultra-broadband terahertz metamaterial absorber," *Appl. Phys. Lett*, vol. 105, no. 021102, pp. 1–4, 2014.
- [168] M. Yoo, H. K. Kim, and S. Lim, "Angular- and polarization-insensitive metamaterial absorber using subwavelength unit cell in multilayer technology," *IEEE Antennas and Wireless Propagation Letters*, vol. 15, pp. 1–1, 01 2015.
- [169] L. Li and Z. Lv, "Ultra-wideband polarization-insensitive and wide-angle thin absorber based on resistive metasurfaces with three resonant modes," *Journal of Applied Physics*, vol. 122, p. 055104, 08 2017.

-
- [170] W. Jiang, L. Yan, H. Ma, Y. Fan, J. Wang, M. Feng, and S. Qu, “Electromagnetic wave absorption and compressive behavior of a three-dimensional metamaterial absorber based on 3d printed honeycomb,” *Scientific Reports*, vol. 8, 12 2018.
- [171] Y. Lu, B. Chi, D. Liu, S. Gao, P. Gao, Y. Huang, J. Yang, Z. Yin, and D. Guangsheng, “Wideband metamaterial absorbers based on conductive plastic with additive manufacturing technology,” *ACS Omega*, vol. 3, pp. 11 144–11 150, 09 2018.
- [172] D. Xie, X. Liu, H. Guo, X. Yang, C. Liu, and L. Zhu, “A wideband absorber with a multiresonant gridded-square fss for antenna rcs reduction,” *IEEE Antennas and Wireless Propagation Letters*, vol. 16, pp. 629–632, 2017.
- [173] B. Threswar, R. Yahiaoui, K. Selemani, and H. Ouslimani, “A dual layer broadband radar absorber to minimize electromagnetic interference in radomes,” *Scientific Reports*, vol. 8, 12 2018.
- [174] R. Fante and M. McCormack, “Reflection properties of salisbury screen,” *Antennas and Propagation, IEEE Transactions on*, vol. 36, pp. 1443 – 1454, 11 1988.
- [175] L. Toit, “Design of jauman absorbers,” *Antennas and Propagation Magazine, IEEE*, vol. 36, pp. 17 – 25, 01 1995.
- [176] B. Munk, P. Munk, and J. Pryor, “On designing jaumann and circuit analog absorbers (ca absorbers) for oblique angle of incidence,” *Antennas and Propagation, IEEE Transactions on*, vol. 55, pp. 186 – 193, 02 2007.
- [177] A. Zadeh and A. Karlsson, “Capacitive circuit method for fast and efficient design of wideband radar absorbers,” *Antennas and Propagation, IEEE Transactions on*, vol. 57, pp. 2307 – 2314, 09 2009.
- [178] K. L. Ford and B. Chambers, “Geometric transition absorber with improved low frequency performance,” in *2006 IEEE Antennas and Propagation Society International Symposium*, July 2006, pp. 1955–1958.

- [179] R. B. Yang, W. F. Liang, C. H. Wu, and C. C. Chen, "Synthesis and microwave absorbing characteristics of functionally graded carbonyl iron/polyurethane composites," *AIP Advances*, vol. 6, no. 5, p. 055910, 2016. [Online]. Available: <https://doi.org/10.1063/1.4943239>
- [180] C. Wei, X. Shen, F. Song, Y. Zhu, and Y. Wang, "Double-layer microwave absorber based on nanocrystalline $\text{Zn}_0.5\text{Ni}_0.5\text{Fe}_2\text{O}_4/\alpha\text{-Fe}$ microfibers," *Materials & Design*, vol. 35, p. 363–368, 03 2012.
- [181] A. Noor and Z. Hu, "Wideband multilayer sierpinski carpet array radar absorber," *Electronics Letters*, vol. 52, 08 2016.
- [182] M. Petroff, J. Appel, K. Rostem, C. Bennett, J. Eimer, T. Marriage, J. Ramirez, and E. Wollack, "A 3d-printed broadband millimeter wave absorber," *Review of Scientific Instruments*, vol. 90, p. 024701, 02 2019.
- [183] J. Ren and J. Y. Yin, "3d-printed low-cost dielectric-resonator-based ultra-broadband microwave absorber using carbon-loaded acrylonitrile butadiene styrene polymer," *Materials*, vol. 11, p. 1249, 07 2018.
- [184] P. Thomas, N. K. Pushkaran, and C. K. Aanandan, "Preparation and microwave characterization of novel polyaniline-graphene composite for antenna applications," in *2017 Progress in Electromagnetics Research Symposium - Fall (PIERS - FALL)*, Nov 2017, pp. 1239–1244.
- [185] H. R. Tantawy, D. E. Aston, J. R. Smith, and J. L. Young, "Comparison of electromagnetic shielding with polyaniline nanopowders produced in solvent-limited conditions," *ACS Applied Materials & Interfaces*, vol. 5, no. 11, pp. 4648–4658, 2013, PMID: 23672188. [Online]. Available: <https://doi.org/10.1021/am401695p>
- [186] Z. Hamouda, W. Jean Luc, A. Pud, L. Koné, S. Bergheul, and T. Lasri, "A flexible uwb organic antenna for wearable technologies application," *IET Microwaves, Antennas & Propagation*, vol. 12, 09 2017.
- [187] S. Pinto and M. Rezende, "Performance prediction of microwave absorbers based on poma/carbon black composites in the frequency range of 8.2 to 20 GHz," *Journal of Aerospace Technology and Management*, vol. 10, 03 2018.

-
- [188] M. Qiu, Y. Zhang, and B. Wen, “Facile synthesis of polyaniline nanostructures with effective electromagnetic interference shielding performance,” *Journal of Materials Science: Materials in Electronics*, 04 2018.
- [189] V. Dutta, “Novel microstructure in spin coated polyaniline thin films,” *Journal of physics. Condensed matter : an Institute of Physics journal*, vol. 19, p. 186212, 05 2007.
- [190] A. Karyakin, M. Vuki, L. Lukachova, E. Karyakina, A. Orlov, G. Karpachova, and J. Wang, “Processible polyaniline as an advanced potentiometric ph transducer. application to biosensors,” *Analytical chemistry*, vol. 71, pp. 2534–40, 08 1999.
- [191] F. Gervais, N. Petit, C. Popon, and P. Buvat, “Doping dependence of infrared conductivity of camphor-sulphonic-acid-doped polyaniline,” *Physics of Condensed Matter*, vol. 31, pp. 47–52, 01 2003.
- [192] S. Lamouri, S. Bendahgane, and A. Oudia, “The preparation and analytical study of conducting polyaniline thin films,” *J Pet Environ Biotechnol*, vol. 5, 01 2014.
- [193] M. Yazid, S. Ghani, A. F. Osman, S. Hajar, and T. Jin, “The effect on poly (ethylene oxide) / poly (vinyl chloride) / polyaniline (pani) films by ethylene dimethacrylate as surface modifier: electrical conductivity and characterization,” *Journal of Physics: Conference Series*, vol. 908, p. 012007, 10 2017.
- [194] D. G. Lakshmi, A. Dhillon, A. Siddiqui, M. Zulfequar, and D. Avasthi, “Rf-plasma polymerization and characterization of polyaniline,” *European Polymer Journal - EUR POLYM J*, vol. 45, pp. 2873–2877, 10 2009.
- [195] A. Kumar, V. Kumar, and K. Awasthi, “Polyaniline-carbon nanotube composites: Preparation methods, properties and applications,” *Polymer-Plastics Technology and Engineering*, vol. 57, 03 2017.
- [196] J. Wu, Q. Zhang, J. Wang, X. Huang, and H. Bai, “A self-assembly route to porous polyaniline/reduced graphene oxide composite materials with molecular-level uniformity for high-performance supercapacitors,” *Energy and Environmental Science*, vol. 11, pp. 1280–1286, 05 2018.

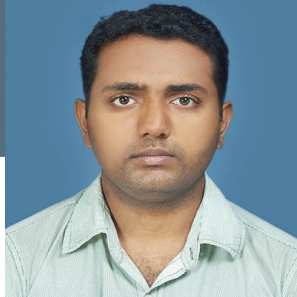
- [197] A. K. Nanjundan, C. Hyun-Jung, Y. Shin, D. w. Chang, L. Dai, and J.-B. Baek, "Polyaniline-grafted reduced graphene oxide for efficient electrochemical supercapacitors," *ACS nano*, vol. 6, pp. 1715–23, 02 2012.
- [198] X. Chen, F. Meng, Z. Zhou, X. Tian, L. Shan, S. Zhu, X. Xu, M. Jiang, L. Wang, D. Hui, Y. Wang, J. Lu, and J. Gou, "One-step synthesis of graphene/polyaniline hybrids by in situ intercalation polymerization and their electromagnetic properties," *Nanoscale*, vol. 6, 05 2014.
- [199] K. Paton, E. Varrla, C. Backes, R. Smith, U. Khan, A. Gallagher, C. Boland, M. Lotya, O. Istrate, P. King, T. Higgins, S. Barwich, P. Puczarski, I. Ahmad, M. Möbius, H. Pettersson, E. Long, J. Coelho, and J. Coleman, "Scalable production of large quantities, defect-free few-layer graphene by shear exfoliation in liquids," *Nature materials*, vol. 13, 04 2014.
- [200] X. Huang, T. Leng, X. Zhang, J. Chen, K. Chang, A. Geim, K. Novoselov, and Z. Hu, "Binder-free highly conductive graphene laminate for low cost printed radio frequency applications," *Applied Physics Letters*, vol. 106, p. 203105, 05 2015.
- [201] Y. Liang, C.-T. Li, Y. Guan, and Y. Hu, "Gait recognition based on the golden ratio," *EURASIP Journal on Image and Video Processing*, vol. 2016, 12 2016.
- [202] E. Unal, F. Dincer, E. Tetik, M. Karaaslan, M. Bakir, and C. Sabah, "Tunable perfect metamaterial absorber design using the golden ratio and energy harvesting and sensor applications," *Journal of Materials Science Materials in Electronics*, vol. 26, 08 2015.
- [203] H. Xiong, J.-S. Hong, C.-M. Luo, and L.-L. Zhong, "An ultrathin and broadband metamaterial absorber using multi-layer structures," *Journal of Applied Physics*, vol. 114, 08 2013.
- [204] J. Sun, L. Liu, G. Dong, and J. Zhou, "An extremely broad band metamaterial absorber based on destructive interference," *Optics express*, vol. 19, pp. 21 155–62, 10 2011.

-
- [205] L. Li and Z. Lv, “Ultra-wideband polarization-insensitive and wide-angle thin absorber based on resistive metasurfaces with three resonant modes,” *Journal of Applied Physics*, vol. 122, p. 055104, 08 2017.
- [206] G. Ohman, “The pseudo-brewster angle,” *Antennas and Propagation, IEEE Transactions on*, vol. 25, pp. 903 – 904, 12 1977.
- [207] M. Akimoto and Y. Gekka, “Brewster and pseudo-brewster angle technique for determination of optical constants,” *Japanese Journal of Applied Physics*, vol. 31, pp. 120–, 01 1992.
- [208] F. C. Commission, “In the matter of revision of part 15 of the commission’s rules regarding ultra-wideband transmission systems,” *First Report And Order, ET Docket 98-153*, 2002. [Online]. Available: <https://ci.nii.ac.jp/naid/10013476121/en/>
- [209] R. Aiello and A. Batra, *Ultra Wideband Systems: Technologies and Applications*, ser. Communications engineering series. Elsevier Science, 2006. [Online]. Available: https://books.google.co.in/books?id=6_XVg-nX9qgC
- [210] K. Siwiak and D. McKeown, *Ultra-wideband Radio Technology*. Wiley, 2005. [Online]. Available: <https://books.google.co.in/books?id=rWtDTeFTwisC>
- [211] J. Jung, H. Lee, and Y. Lim, “Compact band-notched ultra-wideband antenna,” *Electronics Letters*, vol. 44, pp. 391 – 392, 02 2008.
- [212] R. Zaker, C. Ghobadi, and J. Nourinia, “Novel modified uwb planar monopole antenna with variable frequency band-notch function,” *Antennas and Wireless Propagation Letters, IEEE*, vol. 7, pp. 112 – 114, 02 2008.
- [213] Q. Wu, R. Jin, J. Geng, and M. Ding, “Printed omni-directional uwb monopole antenna with very compact size,” *Antennas and Propagation, IEEE Transactions on*, vol. 56, pp. 896 – 899, 04 2008.
- [214] J. Shin, H. Seokjin, and J. Choi, “A compact internal uwb antenna for wireless usb dongle application,” *Microwave and Optical Technology Letters*, vol. 50, 06 2008.

- [215] Z. Low, J. H. Cheong, and C. Law, "Low-cost pcb antennas for uwb applications," *Antennas and Wireless Propagation Letters, IEEE*, vol. 4, pp. 237 – 239, 02 2005.
- [216] Q.-X. Chu and Y.-Y. Yang, "3.5/5.5 ghz dual band-notch ultra-wideband antenna," *Electronics Letters*, vol. 44, pp. 172 – 174, 02 2008.
- [217] Y. Duroc, T.-P. Vuong, and S. Tedjini, "A time/frequency model of ultrawideband antennas," *Antennas and Propagation, IEEE Transactions on*, vol. 55, pp. 2342 – 2350, 09 2007.
- [218] D. D. Krishna, G. Madanan, A. C K, M. Pezholil, and V. Kesavath, "Ultra-wideband slot antenna with band-notch characteristics for wireless usb dongle applications," *Microwave and Optical Technology Letters*, vol. 51, pp. 1500 – 1504, 06 2009.
- [219] *USB serial bus specification, Revision 2.0*, 04 2000. [Online]. Available: http://sdphca.ucsd.edu/lab equip_manuals/usb_20.pdf
- [220] J. Jung, H. Lee, and Y. Lim, "Band notched ultra wideband internal antenna for usb dongle application," *Microwave and Optical Technology Letters*, vol. 50, pp. 1789 – 1793, 07 2008.
- [221] X. Bao and M. Ammann, "Investigation on uwb monopole antenna with rectangular slitted ground plane," *Microwave and Optical Technology Letters*, vol. 49, pp. 1585 – 1587, 07 2007.
- [222] S. Yadav, A. Gautam, and B. Kanaujia, "Design of dual band-notched uwb antenna," 12 2015, pp. 1–2.
- [223] G. Madanan, D. D. Krishna, A. Chandran, and A. C K, "Square monopole antenna for ultra wide band communication applications," *Journal of Electromagnetic Waves and Applications*, vol. 21, pp. 1525–1537, 09 2007.
- [224] H. R. Khaleel, H. M. Al-Rizzo, and A. I. Abbosh, "Design, fabrication, and testing of flexible antennas," in *Advancement in Microstrip Antennas with Recent Applications*, A. Kishk, Ed. Rijeka: IntechOpen, 2013, ch. 15. [Online]. Available: <https://doi.org/10.5772/50841>

LIST OF PUBLICATIONS

1. **Paulbert Thomas**, Neeraj K. Pushkaran, and C. K. Aanandan, Preparation and Microwave Characterization of Novel Polyaniline-graphene Composite for Antenna Applications, PIERS, Singapore, November 2017
2. **Paulbert Thomas**, Neeraj K. Pushkaran and C. K. Aanandan, Microwave characterization of polyaniline prepared via agitation-free self-stabilized dispersion polymerization, Journal of Functional Materials and Biomolecules, 1(2)-2017 pp 64-69
3. **Paulbert Thomas**, Dinesh R., Deepti Das Krishna, Aanandan C. K., Compact CPW fed band-notched antenna for portable UWB applications, International Conference on Advances in Computing and Communications, April 11, 2012
4. **P. Thomas**, D.D. Krishna, M. Gopikrishna, U.G. Kalappura and C.K. Aanandan, Compact planar ultra-wideband beveled monopole for portable UWB systems, ELECTRONICS LETTERS 29th September 2011 Vol. 47 No. 20
5. **Paulbert Thomas**, M. Gopikrishna, C. K. Aanandan, P. Mohanan, and K. Vasudevan, A Compact Pentagonal Monopole Antenna for Portable UWB Systems, Microwave and Optical Technology Letters, Vol 52, Issue 10, pages 2390-2393, 2010
6. Neeraj K. Pushkaran , **Paulbert Thomas** , C. K. Aanandan , Tessamma Thomas, A 6.8 GHz Polyaniline-Graphene Antenna On FR4 Substrate, Materials Today: Proceedings 11 (2019) 980–984
7. Neeraj K. Pushkaran, **Paulbert Thomas**, Honey John, C. K. Aanandan, Tessamma Thomas, Conducting polymers for microwave applications, JETIR September 2018, Volume 5, Issue 9
8. S Sreenath, P Ashkarali, Nair M Sreejith, **Thomas Paulbert** and Chandroth Aanandan, Slot Line Fed Uniplanar Antenna for 2.4/5.8 GHz WLAN Applications, European Journal of Advances in Engineering and Technology, Vol. 2, No. 5, Pages 7-11, 2015
9. Ullas G. Kalappura, **Paulbert Thomas**, Cyriac M. Odackal, K. T. Mathew, Modified Cavity Perturbation Method for Microwave Characterization of Conducting polymers, International Journal of Advanced Materials Science, Vol. 4, No. 1, Pages 7-20, 2013
10. S. Sreenath, P. Ashkarali, **Paulbert Thomas**, R. Dinesh, and C. K Aanandan, Cpw-fed compact bent monopole antenna for uwb applications, Microwave and optical technology letters, Vol. 55, No.1, Pages 56-58, 2013
11. K. Preetha Nair, **Paulbert Thomas**, Rani Joseph, Latex stage blending of multiwalled carbon nanotube in carboxylated acrylonitrile butadiene rubber: Mechanical and electrical properties, Materials and Design, Vol. 41, Pages 23-30, 2012
12. Ullas G. Kalappura, **Paulbert Thomas**, Cyriac M. Odackal and K. T. Mathew, Preparation and Dielectric Characterization of Arrowroot-Chitosan Film for Microwave Phantom Applications, Microwave Review, Vol. 18, No. 2, Pages 17-20, 2012



Paulbert Thomas

Assistant Professor,
Department of Electronics, The Cochin College, Kochi-2
paulbertthomas@gmail.com
+919496827278, +914842511325

Education

- 2009 – Present **Ph.D. Microwave Electronics (Ongoing)**
Dept. of Electronics, CUSAT
Topic: Electro-magnetic applications of conducting polymers
- 2006 – 2008 **M.Sc. Electronics Science**
Dept. of Electronics, CUSAT, Kochi
Year: 2006-08, CGPA: 8.44/10
- 2003 – 2006 **B.Sc. Physics**
Union Christian College, Aluva, Kochi
Percentage: 84.4%

Professional Affiliation

- 2012 – Present **Assistant Professor**, Dept. of Electronics, The Cochin College, Kochi
- 2009 **Project Fellow**, DRDO sponsored project, CUSAT, Kochi
- 2008 – 2009 **Consultant**, Embedded Systems Design & Development Wing, Laxmi Infotek, Kalamassery, Kochi

Technical Experience

Research Interests • Electromagnetics-Antennas, EMI shielding, frequency selective

	<p>surface, RADAR absorbing structures, metamaterials</p> <ul style="list-style-type: none"> • Material research-Conducting polymers, graphene • Embedded Systems • Energy storage/ harvest
Platforms worked	<ul style="list-style-type: none"> • Linux • Windows
Softwares familiar	<ul style="list-style-type: none"> • Proteus, Eagle, Visual Studio, Ansoft HFSS, CST Microwave Studio, IE3D, Comsol Multiphysics, Coventorware, Intellisuite, Moodle
Programming language used	<ul style="list-style-type: none"> • Matlab, C, VB.NET, Embedded C for PIC Microcontrollers, Bash Scripting, Python
Projects done	<ul style="list-style-type: none"> • Developed an Automated 2-D pattern measurement setup for Radar Cross Section and Antenna Pattern Measurement. • Designed software in Matlab to measure and compute the dielectric properties of unknown material using TCP/IP and SCPI interface with Agilent Impedance Analyzer. • Designed and developed an automated setup for Cavity Perturbation Technique. • Designed and developed a Fuel Vending System for Fuel Stations using PIC18F4550 microcontroller. • Designed and developed an Industrial Liquid Level Management System for Wipro Technologies, Infopark using PIC16F873 microcontroller.
Experience	<ul style="list-style-type: none"> • Experience in using Vector Network Analyzers, Impedance analyzers • Experience in characterization tools: Scanning Electron Microscopy (SEM), X-ray diffractometer (XRD), Fourier

Transform Infrared Spectroscopy (FTIR)

- Preparation methods of conducting polymers, graphene
- Microwave characterization of materials by Cavity perturbation, Nicolson-Ross-Weir algorithm, Shielding effectiveness
- Design of Ultra Wideband antennas

Personal Details

Date of birth	November 01, 1985
Nationality	Indian
Address	Kurisingal House, Church Road, Muttinakam, Varapuzha, Kochi, India - 683517

Declaration

I do hereby declare that the above information is true to my knowledge.

Kochi

Paulbert Thomas

